Synthesis of Fischer-Tropsch Catalysts in an Autoclave System

Nina Tung Gynnild

Preface

This thesis was completed after two years as a student at the Norwegian University of Science and Technology, leading to the degree Master in Science (MSc) in Chemical Engineering.

The work and the results that form the basis for this thesis were conducted during the spring semester in 2012. This project was initiated by Statoil in order to investigate the usage of an autoclave continuous stirred tank reactor for catalyst synthesis. The financial support was received from Statoil ASA.

Catalyst synthesis and characterization were performed at Statoil Research Centre at Rotvoll, Trondheim. I would use this opportunity to dedicate thanks to the great people at Rotvoll, who received me with open arms. Special thanks are dedicated to Sigrid Eri, Torild Hulsund Skagseth and Øyvind Borg. Without your guidance in the laboratory and your advices both experimentally and theoretically, it would have been hard for me to finish this thesis. Thanks for your patience and enthusiasm toward my work.

The Fischer-Tropsch synthesis analysis was operated by Andreas Helland Lillebø at the Department of Chemical Engineering at NTNU. I would like to thank Andreas for technical assistance and guidance in connection with the Fischer-Tropsch runs. Special thanks are dedicated to Sindre Håvik. Thank you for your patience and support during the FT analysis. I could not have done it without your help. Sigurd Skarra, thank you for your support, and for making me dinners after a hard day at school.

Finally, I would like to say thanks to my supervisors Prof. Magnus Rønning and Prof. Erling Rytter.

I declare that this is an independent work according to exam regulations at the Norwegian University of Science and Technology.

……………………………

Nina Tung Gynnild   Trondheim, 22.06.2012

Summary

12- or 18 wt.% cobalt and 0.5 wt.% rhenium was impregnated on nickel-aluminate spinel support supplied by Statoil R&D. The catalysts were dried in an autoclave continuous stirred tank reactor with different reactor parameters. Reactor parameters, such as duration, temperature and stirring rate were adjusted in each experiment in order to see how they affect the catalyst preparation. Some of the catalysts were treated in a closed reactor system or a combination of both closed and open reactor system. All catalysts have been characterised by nitrogen adsorption/desorption analysis and hydrogen chemisorption. In addition, a number of catalysts were further run in the Fischer-Tropsch synthesis. These catalysts were also characterised by oxygen titration in order to determine the degree of reduction.

Each experiment was devised on the basis of the result obtained from the previous one. The intention was to dry each catalyst in the reactor for three hours and with a stirring rate of 100 rates per minutes. In most experiment, the stirring rate was adjusted to 200 rates per minutes and duration varied within 30 minutes to three hours. The desired drying or set temperatures were 110, 150 or 270 ^{o}C. It was difficult to maintain a constant set temperature in the experiments. The temperature increased and decreased ongoing in each experiment. In addition, the highest observed temperature during drying for some catalysts was almost 80 ^{o}C higher than the desired drying temperature.

The majority of the catalysts were dry after drying in the autoclave reactor. Some of the catalysts, particular catalysts dried at 110 ^{o}C and catalysts treated in a closed reactor system, had to be further dried in the air furnace. Some of these catalysts had a higher dispersion and surface area compared to the others.

Apparently, a higher drying temperature in the reactor led to a decrease in both surface area and dispersion. A decrease in both surface area and dispersion was found when 18 wt. % was added to the catalyst. However, it was difficult to compare how the results were affected by a particular parameter. It was not only one parameter that affected the catalyst, but the whole system. This made it somewhat difficult to interpret the results.

Two catalysts were dried with exact same drying procedure. The results from the characterisation showed that it was possible to reproduce the same catalyst with same properties.

Five catalysts were run in the Fischer-Tropsch synthesis. The results obtained from the Fischer-Tropsch synthesis shows that all catalysts were active during the synthesis and managed to reach a high C_{5+} selectivity.

There is a potential for making good catalysts at 110 ^{o}C in the reactor, also with treatment in a closed reactor system. Drying and calcination of catalysts in an autoclave reactor at 270 ^{o}C does not seem to be suited.

Sammendrag

Katalysatorer med 12- eller 18 vekt % kobolt og 0,5 vekt % rhenium ble impregnert på nikkel-aluminat spinelbærer gitt av Statoil R&D. Katalysatorene ble tørket i en autoklav CSTR med ulike reaktor parametere. Reaktor parametere som temperatur, varighet og rørehastighet, ble justert i hvert forsøk for å se hvordan disse påvirket katalysatoren. Noen katalysatorer ble behandlet i et lukket reaktor system eller en kombinasjon av lukket og åpent system. Alle katalysatorer har blitt karakterisert ved nitrogen adsorpsjon/desorpsjon analyse eller hydrogen kjemisorpsjon. I tillegg ble noen prøver kjørt i Fischer-Tropsch syntesen. Disse katalysatorene ble også karakterisert med oksygen titrering for å finne reduksjonsgraden.

Hvert forsøk ble lagd på grunnlag av resultatet fra den forrige prøven. Formålet var og tørke hver katalysator i tre timer med en rørehastighet på 100 omdreininger per minutt i reaktoren. I de fleste tilfellene ble rørehastigheten justert til 200 omdreininger per minutt, der varigheten varierte mellom 30 minutt til tre timer. De ønskelige tørke eller set temperaturene var enten 110, 150 eller 270 ^{o}C, og det var vanskelig å holde en konstant temperatur i hvert forsøk. Temperaturen økte og minket om hverandre under hvert forsøk. I tillegg var den høyeste observerte temperaturen for noen katalysatorer nesten 80 ^{o}C høyere enn ønsket set temperatur.

Flertallet av katalysatorene var tørre etter tørkingen i reaktoren. Noen av katalysatorene, spesielt de som var tørket ved 110 ^{o}C og de som ble behandlet i et lukket reaktor system, måtte i tillegg tørkes i tørkeskapet. En høyere dispersjon og overflateareal ble målt for disse katalysatorene sammenlignet med de andre.

Antagelig så førte en høyere tørketemperatur til en reduksjon i både overflateareal og dispersjon. Reduksjon i både overflateareal og dispersjon ble også funnet dersom 18 vekt% kobolt ble tilsatt katalysatoren. Uansett så var det vanskelig å sammenligne hvordan disse resultatene ble påvirket av en bestemt parameter. Det var ikke bare en type parameter som påvirket katalysatoren, men hele systemet. Dette førte til at det ble vanskelig å tolke resultatene.

To katalysatorer ble tørket med eksakt samme betingelser. Resultater fra karakteriseringen viser at det er mulig å reprodusere den samme katalysatoren med de samme egenskapene.

Totalt fem prøver ble kjørt i Fischer-Tropsch syntesen. Resultatet fra syntesen indikerer at alle katalysatorer var aktive under syntesen, og oppnådde en høy C_{5+} selektivitet.

Resultater viser at det er mulig å lage gode katalysatorer ved 110 ^{o}C, spesielt i lukket reaktorsystem. Det ser ikke ut som om tørking og kalsinering av katalysatorer i reaktoren ved 270 ^{o}C egner seg.

Table of contents

List of abbreviations

BET	Brunauer, Emmet and Teller
BJH	Barrett, Joyner, Halenda
Calc.	Calcined
CO	Carbon monoxide
CSTR	Continuous stirred tank reactor
DOR	Degree of reduction
FT(S)	Fischer-Tropsch (synthesis)
FID	Flame ionizing detector
GC	Gas chromatograph
GTL	Gas-to-liquid
Nox	NO and NO_2
MFC	Mass flow controller
Rpm	Revolutions per minute
TCD	Thermal conductivity detector
TOF	Turn over frequency
TOS	Time on stream, given in minutes
Wt.%	Weight percentage
WGS	Water-gas-shift

List of symbols

Symbol	Unit	Description
α	-	Chain growth probability
$\alpha_{i,0}$	-	Mole fraction ratio of component i at the reactor inlet
$\alpha_{i,1}$	-	Mole fraction ratio of component i at the reactor outlet
$\alpha_{j,1}$	-	Mole fraction ratio of a component containing j carbon atoms at the reactor outlet
σ	m^2	Area occupied by one absorbed molecule
ΔH_1^o	kJ/mole	Heat of adsorption of the first layer
ΔH_2^o	kJ/mole	heat of liquefaction of the adsorbate gas
ΔH_0^{298}	kJ/mole	Enthalpy at 1 bar and 25 ^{o}C
a	-	slope
$A_{i,1}$	-	TCD area of component j at the reactor outlet
$A_{i,0}$	-	TCD area of component i at the reactor outlet
$A'_{j,1}$	-	FID area of product containing j carbon atoms at the reactor outlet
b	-	intercept
C	-	BET constant
d	nm	Particle diameter
D	%	Dispersion
E_a	J/mole	Activation energy
E_d	J/mole	Desorption energy
$E_{i,0}$	-	Relative response factor of component i at the reactor inlet
$E_{i,1}$	-	Relative response factor of component i at the reactor outlet
$\varepsilon_{i,1}$	mole i/ area i	Response factor of component i at the reactor inlet
F	-	Stoichiometric coefficient
$F_{i,0}$	mole/s	Flow rate of component i at the reactor inlet
$F_{i,1}$	mole/s	Flow rate of component i at the reactor outlet
$F_{j,1}$	mole/s	Flow rate of a component containing j carbon atoms at the reactor outlet
$F_{tot,0}$	mole/s	Total flow rate at the reactor inlet
$F_{tot,1}$	mole/s	Total flow rate at the reactor outlet

i	-	specie
j	-	Number of carbon atoms
K	-	Equilibrium constant
k	h^{-1}	Adsorption constant
M_w	gram/mole	Molecular weight
m_s	gram	The weight of the sample being impregnated
N_a	$mole^{-1}$	Avogadro's constant
n	-	Number of carbon atoms
N_s	-	Surface metal atoms
N_t	-	Total number of metal atoms
p	Pascal	Equilibrium pressure of adsorbed gas
P_0	Pascal	Saturation pressure of adsorbed gas
P_{co}	Pascal	Partial pressure of CO
P_{H2}	Pascal	Partial pressure of H_2
R	$JK^{-1}mole^{-1}$	Gas constant
$-r_{co}$	$mole_{co}/g*h$	Reaction rate
S_j	%	Selectivity of product containing j carbon atoms
T	K or ^{o}C	Temperature
V_a	m^{-3}	Volume of gas adsorbed at equilibrium pressure
V_m	m^{-3}	Adsorbed at monolayer
$V_{i.g}$	$m^{-3}/mole$	Volume of one mole ideal gas at 1 atm and 0 ^{o}C
V_{O2}	m^{-3}	Cumulative amount given from the oxygen titration instrument
x	-	Weight fraction of metal
$x_{i,0}$	-	Mole fraction of component i at the reactor inlet
$x_{i,1}$	-	Mole fraction of component i at the reactor outlet
$x_{j,1}$	-	Mole fraction ratio of a component containing j carbon atoms at the reactor outlet

Introduction

The world population have just passed seven billion and the energy demand is expected to increase rapidly in the next years. Natural gas represents a huge energy resource and large reservoirs of natural gas could help sustain the energy demand. The Fischer-Tropsch synthesis, part of the Gas-To-Liquid process, is a tool to produce high quality products, such as transportation fuel and chemicals, from natural gas, coal or biomass. In this respect the Fischer-Tropsch synthesis could play an important role in the future.

The synthesis is a catalytic process, where supported cobalt is considered to be the most favourable catalyst for the synthesis of long chain hydrocarbons from natural gas based synthesis gas. Cobalt is favourable because of its high activity, high selectivity to linear paraffins, high resistance toward deactivation and low water-gas-shift activity. The metal is normally dispersed on a high surface area support in order to maximize the exposure of metal to the support. [1] In many studies, cobalt has been applied together with an another metal, essentially from group VIII. Studies have shown that addition of small amounts of rhenium tends to increase the selectivity towards long-chain hydrocarbons during Fischer-Tropsch synthesis[1]

The supported cobalt catalysts are often prepared by means of impregnating a pre-shaped support with an aqueous solution containing nitrate hexahydrate. Impregnation is normally followed by drying and calcination in order to decompose the supported cobalt nitrate hydrate and to obtain the supported cobalt oxide. According to [2] conditions during calcination of impregnated cobalt precursors have a significant influence on the performance of the final catalyst. They observed high cobalt metal surface areas and high catalytic activities when the concentration of nitrogen oxides and water was kept low during calcination.

The effect of drying conditions, and thus the effect of using an autoclave continuous stirred reactor for drying, is not described very extensively in the literature.

The motivation behind this thesis was to investigate the effect of using an autoclave Parr continuous stirred tank reactor for the catalyst synthesis. The reactor was loaded with cobalt and rhenium impregnated on a nickel-aluminate spinel support material supplied by Statoil R&D. Reactor parameters, such as temperature, duration and stirring rate, were adjusted in

each experiment in order to see how they affect the catalyst synthesis. In addition, two different metal loadings were impregnated to the same support, and some catalysts were treated in a closed reactor system, i.e. hydrothermal treatment. All catalysts were characterised by nitrogen adsorption/desorption and hydrogen chemisorption. A number of catalysts were further run in the Fischer-Tropsch synthesis. These were also characterised by oxygen titration in order to determine the degree of reduction. The study was carried out at Statoil R&D Centre in Trondheim and at the Department of Chemical Engineering at NTNU.

1   Literature review

This chapter presents some of the available literature relevant for this study. A full literature review is far beyond the scope of this work, because the main focus of this thesis is of experimental nature. The effect of drying conditions and treatment in the autoclave CSTR on the catalytic behaviour of the cobalt catalyst are not described very extensively in the literature. This section will provide the reader with the most important factors and variables related to this thesis. More information may be found in the given references.

1.1   Catalyst synthesis

Supported catalysts consist of small crystallites of a catalytically active component dispersed in a porous support. Incipient wetness impregnation of a metal oxide support with an aqueous solution of cobalt nitrate hexahydrate is a common way to produce Fischer-Tropsch catalysts. The impregnation method involves three steps. First step is contacting the support with impregnating solution for a certain period of time. Impregnation is then followed by drying of the support to remove the absorbed liquid. The catalysts are then calcined. The calcination step is done in order to decompose the supported cobalt nitrate hydrate and obtain supported cobalt oxide. Each step in the synthesis has a significant impact on the final catalyst.

1.1.1   Impregnation

The catalyst support can be in different forms, for instance in a powdered or a granular form. The impregnation technique can be classified as dry or wet impregnation according to the prior of state of the support. Incipient wetness impregnation, also called capillary impregnation or dry impregnation, is when the metal-containing solution is added to the catalyst support containing the same volume as the volume of solution that was added. It is the capillary action that draws the solution into the pores. Any diffusion transport of the catalyst precursors is superimposed on the convective flow.[3]

In wet impregnation the pore volume of the support is saturated with water before impregnation. Excess solution causes the solution transport to change from capillary action to a diffusion process. The solution can be adsorbed onto the surface of the pore wall as the solute moves into the pore space of the support. In addition, other solutes containing other metal precursors can be added to the impregnation solution. When another solute is added to

the impregnation solution, the metal precursors will compete for the adsorption site on the support surface. This impregnation method is called co-impregnation. [3]

The maximum metal loading is limited by the solubility of the precursors in the solution.

1.1.2   Drying

The drying of the impregnated catalysts is usually performed at temperatures between 50 to 230 ^{o}C. [3] A desired drying process enables the drying to be carried out in order to minimal the drying time and to not destroy the structure of dried material. During drying, the liquid solution is in the first period transported by capillary flow, while diffusion mechanisms dominate in the second period of drying. The moist material will change the physical properties during this process. The precursors may be redistributed by adsorption/desorption phenomenon. When the solvent evaporates, precipitation of the solute occurs as the solution becomes supersaturated.[3, 4]

Several drying models have been presented in the literature to give a better understanding about the thermodynamic during the drying process. More information can be found in the article made by Kowalski [4].

1.1.3   Calcination and pre-calcination

The impregnation of cobalt nitrate hexahydrat on support is normally followed by drying and calcination in order to decompose the supported cobalt nitrate hydrate and obtain supported cobalt oxide. Previous studies show that calcination of impregnated cobalt precursors has a significant influence on the performance of the final catalyst. According to Borg *et al* [5] increasing calcination temperature of γ-Al_2O_3 supported cobalt catalyst decreased the amount of residual nitrate. Results from the hydrogen chemisorption analysis shows that the cobalt dispersion decreased with increasing temperature of calcination. They also observed that in order to obtain high cobalt dispersion, it was necessary to remove the decomposition products as efficiently as possible.

ExxonMobil has written a patent, which involves pre calcination at 160 ^{o}C in oxygen containing water free atmosphere followed by a final calcination at 300 ^{o}C of cobalt support system. This was done in order to enhance the cobalt activity. [6] Another patent from the

same company investigated the cobalt activity by using wet atmosphere storage of the pre calcined support/catalyst before the final calcination. [7] Both patents claim better distribution of cobalt by the described methods.

1.2   Autoclave Parr CSTR

Parr CSTRs are used in many branches of chemical technology. According to the Parr Instrument Company's homepage [8], the reactors are used within catalytic hydrogenation together with catalyst development and testing, polymer development and the vessels have been used extensively in hydrometallurgical applications. The reactor can operate at relative high pressures and temperatures, allowing hydrothermal synthesis. Hydrothermal synthesis is an environmental friendly, low temperature method to crystallize anhydrous materials from aqueous media at elevated temperatures and pressures.[9]

Zhang *et al* [10] have reported that hydrothermal treatment has the potential of modifying both the physical and the chemical properties of the support material. Alumina support was used in this study.

For more reading, an overview of the past, present and future perspective of hydrothermal treatment technology as a tool to fabricate advanced materials has been written by Yoshimura and Byrappa in 2008.[11]

More about the autoclave Parr-reactor is presented in the experimental part.

1.3   Fischer-Tropsch synthesis

1.3.1   Turn over frequency

Turn over frequency (TOF) is a surface specific activity. In this thesis TOF is defined as the number of converted CO molecules per mol exposed cobalt atoms on the catalyst surface. The denomination for TOF is second $^{-1}$. TOF is calculated from experimental measured reaction rate and the gas uptake during selective chemisorption.

The effect of the cobalt size on the activity has been studied by a various authors using different catalysts. Breejen [12] has made an overview over the effect of cobalt particle size obtained from results found in the literature. This overview is presented in Figure 1.
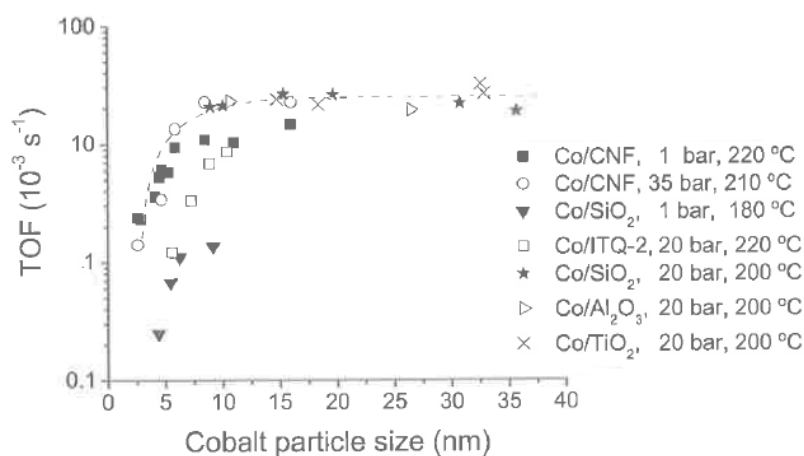
Figure 1: Turn over frequency as a function of cobalt particle size. [12]

The figure shows that the surface-specific activity will be constant for large cobalt particles (>10 nm). However, the absolute TOF value will strongly depend on applied Fischer-Tropsch conditions. A decrease in TOF for decreasing cobalt particle size is observed for smaller cobalt particles (<10 nm).

1.3.2   Selectivity

The Fischer-Tropsch products are a complex multicomponent mixture with variations in carbon number and type. A product mixture includes hydrocarbons ranging up to C_{100}. The product mixture is often divided into C1, C_2- C_4 and C_{5+} hydrocarbons , where the C_{5+} selectivity is often used as a parameter.

Bezemer *et al* [13] studied five catalysts having particle sizes ranging from 2.6 to 16 nm. The C_{5+} selectivity at 35bar is shown in Figure 2.
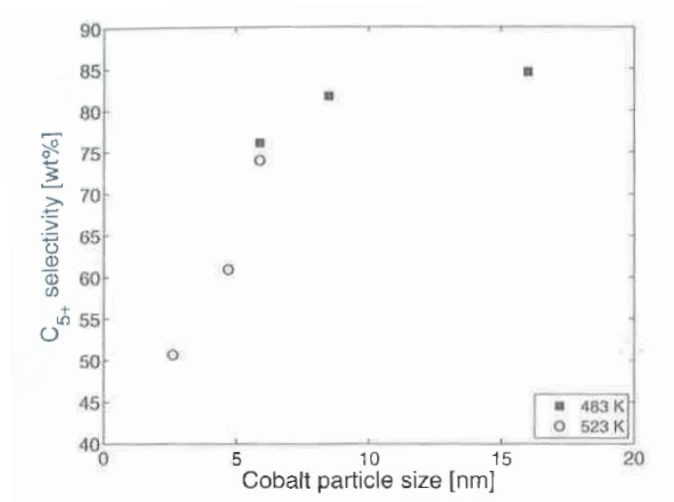
Figure 2: C$_{5+}$ selectivity as a function of cobalt particle size at 35 bar. [14]

The figure shows that the product distribution depends on the cobalt particle size. The C$_{5+}$ selectivity was lower at 250 ^{o}C compare to 210 ^{o}C. It is worth mentioning that the catalysts were prepared using different solvents during the incipient wetness impregnation and contained different cobalt amounts. Bezemer *et al* [13] explained that the variations in selectivity were due to differences in cobalt site density.

1.3.3   Deactivation

Like many other systems, cobalt FTS catalysts lose their activity with time on stream. It is observed that activity decreases rapidly during the first day, followed by a slow steady-state deactivation. Moodley [15] has in his doctoral thesis mentioned several possible deactivation mechanisms, including fouling and sintering. One possible deactivation mechanism is agglomeration. Agglomeration of cobalt nanoparticles during the FTS could lead to loss of active surface area. At low temperatures during the synthesis, production of long chain waxes could happen. This could lead to a build up on the surface and in the catalyst pores of these waxes, inhibiting adsorption and slows down diffusion rates. Another possible deactivation mechanism is that inert carbon phases can be formed during extended runs. This could lead to a blockage of the active phase.

1.3.4   Cobalt loading

The effect of cobalt loading on alumina supported cobalt catalysts was studied by Wang *et al* [16]. They found that the catalytic activity is increased with increasing cobalt loading, where the optimum activity was reached at 12 wt% Cobalt/Al$_2$O$_3$. At low weight percentages, the

activity will decrease, most likely due to the inactivity of $CoAl_2O_4$ to CO hydrogenation. The turn over frequency of all samples were found to be similar at higher metal loadings.

1.3.5   Promoters

A wide variety of promoters have been deliberately added to cobalt based catalysts in order to modify the catalyst properties. A study made by Morales and Weckhuysen [17] discuss this. The following chemical elements have been investigated as promoters: B, Mg, K, Ti, V, Cr, Mn, Ni, Cu, Zr, Nb, Mo, Ru, Rh, Pd, La,Re, Ir, Pt, Ce, Gd and Th. This thesis only includes rhenium as the promoter.

It is generally believed that addition of rhenium to cobalt based catalysts leads to an increase in the Fischer-Tropsch activity, and has been widely studied in cobalt based Fischer-Tropsch catalysis. From the literature, Re is regarded as a structural promoter and has beneficial effect on the cobalt reducibility. The promotion occurs via hydrogen spillover and leads to catalysts with enhanced cobalt dispersion.[17]

Li *et al* [18] observed that the addition of Re to Co/TiO_2 catalysts with 10 wt% Co improves the Fischer-Tropsch activity compared to unpromoted catalysts. Also Storsæter *et al* reported an increase in activity and C_{5+} selectivity for all Re promoted catalysts on alumina, silica and titania supports when compared to the unpromoted catalysts.[19]

However, others claim that Re has no effect on the selectivity. According to Bertole *et al* [20] promotion of Re did not affect the Fischer-Tropsch synthesis selectivity. In this study the Re content in the Co-Re catalysts was approximately 0.1 by weight of the cobalt loading.

1.3.6   Effect of water on cobalt-based catalysts for Fischer-Tropsch synthesis

Water is a product in the Fischer-Tropsch synthesis and will always be present during reaction. The amount of produced water depends on several factors such as the conversion and the reactor system. Presence of water during the synthesis could influence the reaction rate, the product distribution, and the deactivation rate. Several studies have been carried out to gain a better knowledge of the impact of water. [21]

1.3.7 Influence of process conditions

Fischer [22] has made an overview over the influence of experimental conditions on the product distribution in the Fischer-Tropsch synthesis. Table 1 displays this overview.

Table 1: The effects of process conditions on Fischer-Tropsch synthesis [1]

	Temperature	Pressure	H_2/CO	Residence time
CH_4 selectivity	+	-	+	+
Chain growth	-	+	-	≈
Chain branching	+	-	≈	≈
Olefin selectivity	≈	≈	-	-
Oxygenate selectivity	-	+	-	-
Carbon deposition	+	≈	-	≈

---

[1]   +   increase with increasing parameter
         -        decrease with decreasing parameter
         ≈   no clear effect

2 Theory

The Fischer-Tropsch technology has gained interest as a tool for converting natural gas into liquid fuels, and is considered as the chemical heart of the gas-to-liquids technology. The demand for cleaner fuels has risen, and diesel produced from natural gas by the Fischer-Tropsch process offer significant environmental benefits compared to fuels derived from crude oil. This is because the Fischer-Tropsch diesel is free of nitrogen, sulphur, aromatics and metals. This chapter provides information about relevant principles encountered in this work, starting with elementary concepts of the Fischer-Tropsch synthesis. Characterization methods for the support and the different catalysts employed in this work are described in section 3.2.

2.1 Fischer-Tropsch

This section gives an introduction to the Fischer-Tropsch synthesis, chemical reactions related to the process and principles used for determination of conversion levels, selectivity and reaction rates.

2.1.1 History

Catalytic hydrogenation experiments of carbon monoxide were first carried out by P. Sabatier and J.D Senerens in the beginning of the 20th century. In this process carbon monoxide was converted to methane over a reduced nickel catalyst.[14] About 20 years later, Franz Fischer (1877-1947) and Hans Tropsch (1889-1935) reported their study on the production of hydrocarbons from CO, carbon monoxide, and H$_2$, hydrogen, using alkalized iron catalysts. In 1925, Fischer and Tropsch managed to produce higher hydrocarbons at atmospheric pressure over alkalized nickel and cobalt catalysts. The Fischer-Tropsch process has since then passed through a number of periods with varying interest. During the Second World War, Germany and Japan used the Fischer-Tropsch technology to produce substitute fuels. As a result of Allied bombing, Germany's industrial capacity was decimated towards the end of the war. After the Second World War, some countries started to use the Fischer-Tropsch process for producing synthetic fuels, but with high capital and operating costs, environmental concerns and widely available cheap oil prompted all such effort to falter. [23]

Lack of oil resources in the 1970's increased the interest of the Fischer-Tropsch synthesis, especially in South Africa. Years of Fischer-Tropsch development have resulted in better catalysts and better engineering. Sasol, a government owned company in South Africa, uses syngas from coal and natural gas to produce a variety of synthetic petroleum products. Currently, the three Sasol plants are the only indirect coal liquefaction plants producing liquid fuels by the Fischer-Tropsch process.[24]

The Fischer-Tropsch plant in located in Malaysia was built by Shell, and converts remote natural gas into middle distillates over a cobalt based catalyst. The plant has been operating since 1994 and shows that the interest in Fischer-Tropsch is still there.

2.1.2   Principles and technology

The gas-to-liquid process comprises of three main elements as shown in Figure 3.

Natural gas

Reforming

Synthesis gas

Fischer-Tropsch synthesis

Synthetic crude oil
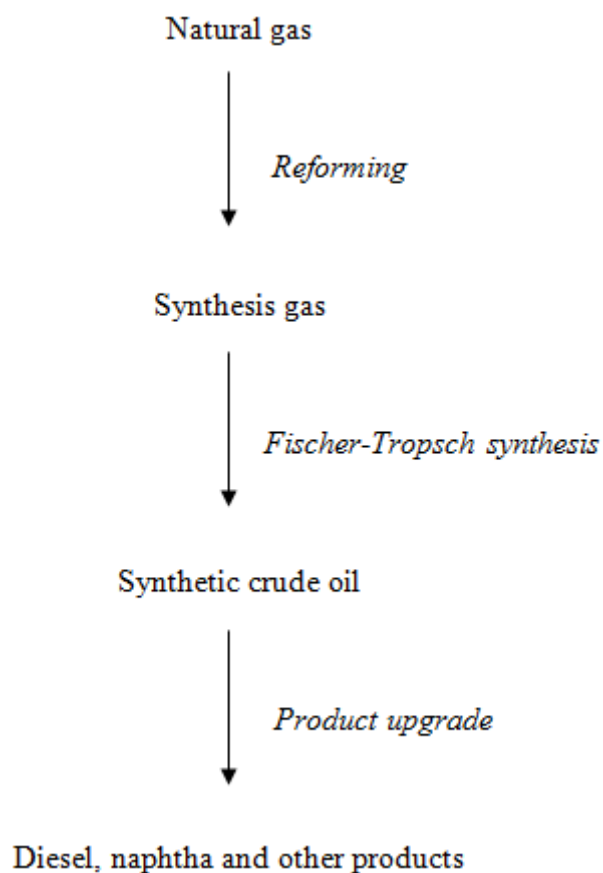
Product upgrade

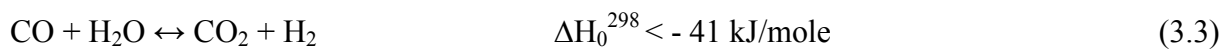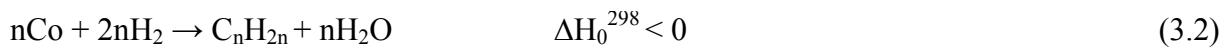Diesel, naphtha and other products

Figure 3: The three main steps in the gas-to-liquid technology. The picture is recreated after Borg's doctorial thesis[14]

Synthesis gas is produced from natural gas in the first stage. Steam reforming, partial oxidation and autothermal reforming are available technologies for synthesis gas production.

In stage two, the synthesis gas is catalytically converted into paraffinic and olefinic hydrocarbons of varying chain lengths. The product distribution ranges from methane to hard wax. The second stage is better known as the Fischer-Tropsch synthesis. The products from the Fischer-Tropsch synthesis are upgraded to gain right properties in the last stage. [14]

Although the chemistry of the Fischer-Tropsch is complex and probably not fully understood, the fundamental aspects can be described by a few generalized equations:

$$nCo + (2n+1)H_2 \rightarrow C_nH_{2n+1} + nH_2O \qquad \Delta H_0^{298} < 0 \qquad (3.1)$$
$$nCo + 2nH_2 \rightarrow C_nH_{2n} + nH_2O \qquad \Delta H_0^{298} < 0 \qquad (3.2)$$
$$CO + H_2O \leftrightarrow CO_2 + H_2 \qquad \Delta H_0^{298} < -41 \text{ kJ/mole} \qquad (3.3)$$
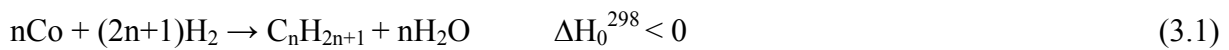
The main reactions in the Fischer-Tropsch synthesis include formation of olefins and paraffins, Eq. (3.1) and (3.2), from synthesis gas. Carbon dioxide is produced in Eq. (3.3), which is known as the water gas shift reaction.

The above mentioned reactions are usually accompanied by side reactions, particularly the formation of alcohols and coke. The side reactions are presented in Eq. (3.4) and (3.5)

$$nCo + 2nH_2 \rightarrow C_nH_{2n+2}O + (n-1) H_2O \qquad \Delta H_0^{298} < 0 \qquad (3.4)$$
$$2 CO \rightarrow C + CO_2 \qquad \Delta H_0^{298} = -170 \text{ kJ/mole} \qquad (3.5)$$

 Reference: [24]

The mechanism of the Fischer-Tropsch synthesis has been unclear and speculative since the discovery of the process in the early 1920's. The specific CO dissociation pathway to form monomers and their kinetic consequences for chain growth are not yet determined. Three different mechanisms have been proposed based on different species as the monomer: the carbide mechanism, the enol mechanism and the CO insertion mechanism. The carbide mechanism was proposed by Fischer and Tropsch, and involves a direct dissociation of CO, resulting in a metal carbide. The carbide is further hydrogenated to CH_x monomers that initiate growth of hydrocarbon chains.[25] In the enol mechanism of Storch *et al*, oxymethylene (HCOH) is responsible for the chain growth. [14] It is assumed that CO adsorbs dissociative on the surface [26] The CO insertion mechanism was proposed by

Pichler and Schultz. In this mechanism, chain growth occurs through the insertion of CO into the metal-methyl bond. [26]

A grand presentation of all these proposed mechanisms would be beyond the scope of this work. However, growth of a hydrocarbon chain occurs, independent of the exact mechanism. The Fischer-Tropsch synthesis proceeds by a stepwise addition of a one-carbon segment derived from CO at the end of an existing chain. An illustration is given in Figure 4.
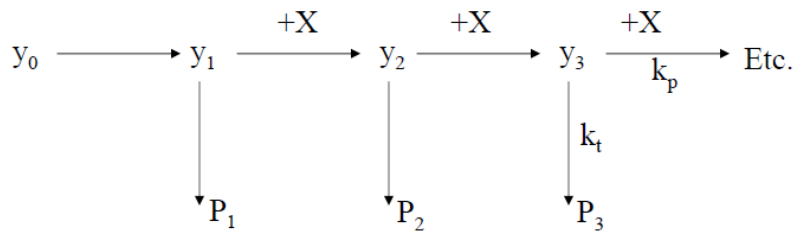
Figure 4: Chain-growth during the Fischer-Tropsch synthesis. Yo → y1 is the initiation step, yn is the growing chain, X is the C1 unit and Pn is the product with n carbon atoms. Kp and kt is the rate constant propagation and termination, respectively. [27]

Figure 4 is a simplified version of the actual reaction network occurring during the Fischer-Tropsch synthesis. Secondary reactions are not included in this scheme. A more detailed scheme is given in Figure 5.
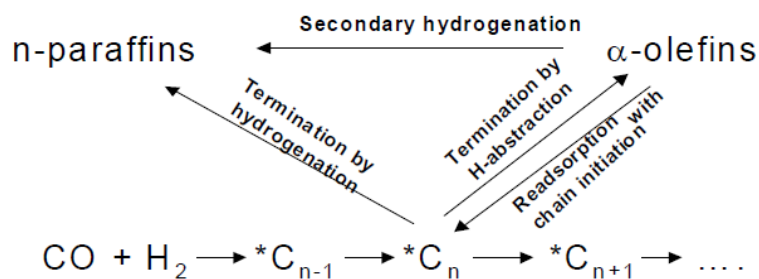
Figure 5: The Fischer-Tropsch reaction network. [27]

A growing chain, $^{*}C_n$, can terminate by hydrogenation to paraffins and by hydrogen abstraction to α-olefins. α-olefins can readsorb on the catalytic surface and initiate surface chains. Secondary hydrogenation of α-olefins competes with readsorption with chain initiation.

Fischer-Tropsch chain propagation and termination have been explained trough the Anderson-Schulz-Flory product distribution. When chain-growth and terminations rates are independent of chain size, the molecular weight distribution of hydrocarbon products is claimed to follow the chain polymerization kinetics model of Anderson, Schulz and Flory. The model assumes that the relative probability of chain growth, α, and chain termination, 1-α, is constant. An illustration of the Anderson, Schulz and Flory model is presented in Figure 6.
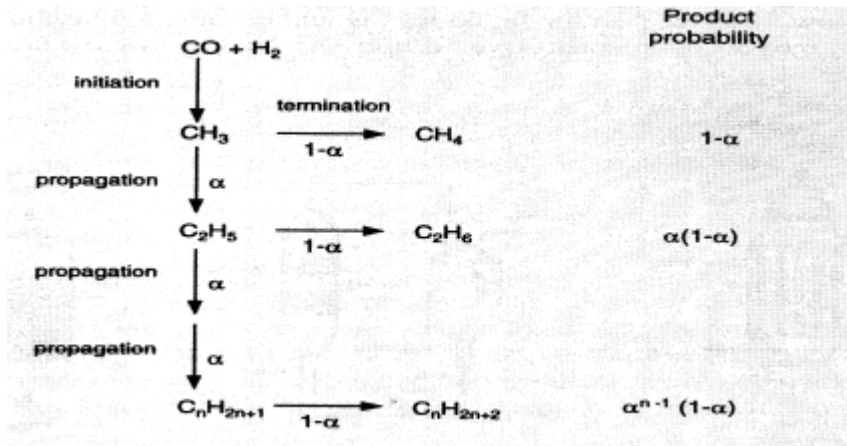
Figure 6: Chain-growth mechanism for the Fischer-Tropsch synthesis with Anderson, Schulz and Flory kinetic. [24]

A mathematic analysis gives the following equation [27]

$$\ln\left(\frac{S}{n}\right) = n\ln(\alpha) + \ln\left[\frac{(1-\alpha)^2}{\alpha}\right] \tag{3.6}$$

where S represent the carbon selectivity. α is the chain-growth probability independent of chain length. Plotting ln(S/n) against n gives a straight line with slope ln(α) The α-value depends on temperature (decreases with increasing temperature), H_2/CO ratio (decreases with increasing hydrogen content), and catalyst.

The kinetics for the Fischer-Tropsch synthesis has been the topic for a numerous research projects. A large number of mechanism and rate determine steps are proposed, but all give Langmuir-Hinshelwood-Hougen- Watson type rate equations. An example is shown in Eq. (3.7)

$$-r_{CO} = \frac{K_1\, p_{CO}^{0.5}\, p_{H2}^{0.5}}{(1 + K_2\, p_{H2}^{0.5} + K_3\, p_{CO}^{0.5})^2} \tag{3.7}$$

K_1 represent the temperature dependent rate constant and K_2 and K_3 are the adsorption constants.

2.1.3   Reactors and catalyst candidates

The Fischer-Tropsch reactions show that the synthesis is highly exothermal. As a consequence, temperature control is essential in the reactor design. There are three different reactor concepts for the Fischer-Tropsch synthesis; tubular fixed bed reactor, fluidized bed reactor and slurry bubble column reactor. A simple sketch of these reactors is given in Figure 7.
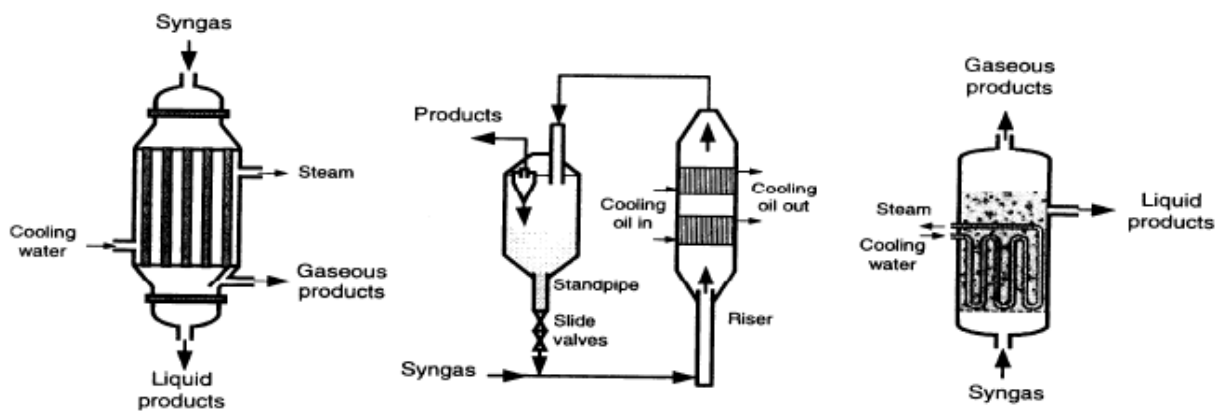
Figure 7: Fixed bed reactor, fluidized bed reactor (riser) and slurry reactor.[24]

All of these reactors are in commercial use and are designed for proper heat management. Temperature control is challenging, and it is almost impossible to have complete isothermicity in a full scale commercial reactor.

The choice of catalyst for the Fischer-Tropsch synthesis depends on a number of factors, such as the price of the active metal, the desired end products and the carbon source for synthesis gas production. In this context the focus, with respect to selectivity, is the formation of wax (C_{5+}) and subsequent potential for diesel production by cracking.

Iron, cobalt, nickel and ruthenium based catalysts have shown a sufficient activity to be considered as commercial catalysts in the Fischer-Tropsch synthesis. Nickel produces too much methane and is of little use in gas-based processes. Ruthenium is an excellent catalyst for wax production, with no water-gas shift. However, the low availability of ruthenium and

high market price makes the use of this element in large-scale applications questionable. This leaves iron and cobalt as the most promising candidates for the Fischer-Tropsch synthesis.

Iron based catalysts gives hydrocarbons and carbon dioxide as products, and have a very good water-gas shift activity. This means that iron is promising for synthesis gas with low H_2/CO ratios, *e.g* from coal or other heavy hydrocarbon feedstock. Cobalt catalysts have a low water-gas-shift activity, and produce hydrocarbons and water as the major products. Cobalt based catalysts can be used when the synthesis gas is produced from natural gas. Only cobalt based catalysts will be considered in this thesis.

2.1.4   Gas chromatography

The Fischer-Tropsch synthesis analysis performed in this work uses a gas chromatography to characterize and quantifies the product mixture. This section gives a description of the gas chromatographic method.

The chromatographic technique is widely used for separation and determination of chemical components present in a mixture. There exist a number of different techniques, such as liquid chromatography, thin layer chromatography and gas chromatography. Chromatography is based on the principle that the substance to be separated is distributed between two phases, a mobile phase and a stationary phase.

Gas chromatography is when the separation is performed with gas as the mobile phase, also known as the carrier gas. The primary purpose with the carrier gas is to transport volatile components through a column. It is important that the carrier gas is pure and inert, so that the gas does not react with the sample or the stationary phase, or contain contaminations that could change the gas's' attribute. Nitrogen, helium and hydrogen are the most common used carrier gases.

The stationary phase is a microscopic layer of high-boiling liquid on an inert solid support, inside a glass or metal column. It is important that the substances used as stationary phase are thermally stable, gives wanted separation and do not react irreversibly with the sample.
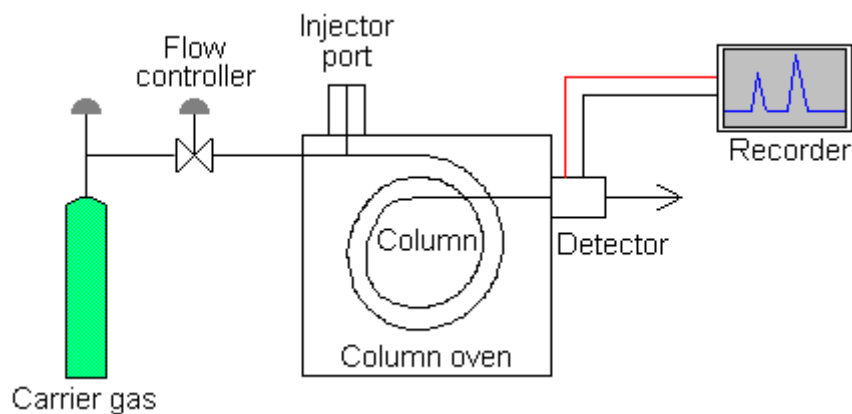
Figure 8: Schematic diagram of a gas chromatograph [28]

A schematic presentation of gas chromatograph is given in Figure 8. The analysis sequence starts with the carrier gas being transported through a flow controller. A reduction valve makes the carrier gas flow through the injector, column and to the detector. The unknown sample is injected into a pre-heated injector, where the sample evaporates and follows the carrier gas into the column. The mixture moves across the column which contains the stationary phase. The gaseous products are separated in the column and introduced to a detector. The detector converts electrical signals that are amplified to drive a recorder. The recorder displays the separation as chromatograms with characteristic peaks for different compounds. The chromatogram peak area is proportional to the amount of the specific component in the mixture.

The interaction with the mobile phase and the stationary phase influences the sample's velocity through the column and thus cause each compound to elute at different times. This is known as the retention time of the compound. The comparison of retention times is what gives the gas chromatography its analytical usefulness. By comparing retention times with known standards makes the identification of components possible.

There are two types of detectors used in gas chromatography; concentration sensitive detectors and weight sensitive detectors. The most common detectors that are used are the thermal conductivity detector (TCD), which is concentration sensitive, and the flame ionization detector (FID), which is weight sensitive. These detectors are described in detail by Greibrokk *et al*. [29]

The peak area for one component in the chromatogram is proportional to the amount of that specific component in the mixture. It is possible to calculate the amount by integrate the area under a specific peak. However, the GC response to different compounds may vary, and peak response factors are needed to get accurate results. This is where the internal standard asserts itself. The molar ratio of a specific component to the internal standard can be calculated by knowing the relative peak area of the internal standard and the component peak. The signal from the analyte is compared with the signal from the internal standard to find out how much analyte is present.

It is difficult to inject samples in the µl range with "good" reproducibility. An internal standard is used as a reference to compensate for the fluctuations in injected amounts. Use of an internal standard can also correct for variations in the chromatographic system during the analysis. The internal standard method for quantitative analysis and the requirements for the internal standard are also described by Greibrokk *et al*. [29]. Nitrogen is used as the internal standard in this thesis.

2.2   Catalyst and support characterisation

This section includes the main principles of hydrogen chemisorption, nitrogen adsorption/desorption and oxygen titration used for catalyst and support characterization.

2.2.1   Adsorption

Gas adsorption on solid surfaces and in pore spaces is a complex phenomenon involving mass and energy interactions and phase changes. A lot of theories have been put forth, where some of them provide the basic framework for later developments. The elementary concepts of adsorption are presented in this section to provide the reader with helpful understanding of the adsorption methods used in this thesis.

Adsorption can be defined as the surface phenomenon of adhesion of species of gas, liquid or dissolved solids to a surface. Gas-surface interactions and reactions on surfaces play an important role in the heterogeneous catalysis. Reactants adsorb on the surface of the catalyst, where at least one of the reactants is dissociated. It is often in the dissociation of a strong bond

that the essence of catalytic action lies. The reaction itself occurs on the surface, and the product desorbs from the surface after the reaction.

An atom or a molecule feels the potential energy set up by the metal atoms in the solid when approaching the surface. The interaction is divided into two regimes; physical adsorption and chemical adsorption.

Physisorption, physical adsorption, is weak interactions, Van der Waals forces, between the adsorbate and the surface. No electrons are shared and there is no chemical bond between adsorbate and surface. The phenomenon is characterized by secondary attractive forces such as dipole-dipole interactions and induced dipoles.[30, 31] During physical adsorption, molecules are not restrained to specific sites which make the molecules able to cover the whole surface. The adsorption process is fully reversible, where equilibrium can be easily achieved since no activation energy is involved. Physical adsorption leads to multilayer adsorption. [32] This forms the basics of the BET isotherm and the surface characterization method called the BET-method. The BET theory begins with the assumption of localized adsorption. The numbers of layers are not limited, and therefore no saturation of the surface with increasing pressure exists. [33] The BET-method is described in Section 3.2.3.

Chemisorption, chemical adsorption, is when molecules or atoms form a chemical bond with the surface upon adsorption. Chemisorption is a much stronger interaction compared to physisorption, involving sharing of electrons between the gas and the solid surface. In chemisorption, the bond between the adsorbate and the adsorbent is often very energetic even the heat of adsorption is low. The process requires activation energy. Physical adsorption takes place on all surfaces provided temperature and pressure conditions are favourable, but chemisorption is localized and occurs only on certain surfaces or surface sites. Under proper condition, physisorption results in multilayer adsorption. Chemisorption, on the other hand, occurs only if the adsorbate makes direct contact with the surface, leading to a single-layer process. Physical adsorption diminished rapidly with temperature elevation, where chemisorption is enhanced by high temperature.[34]
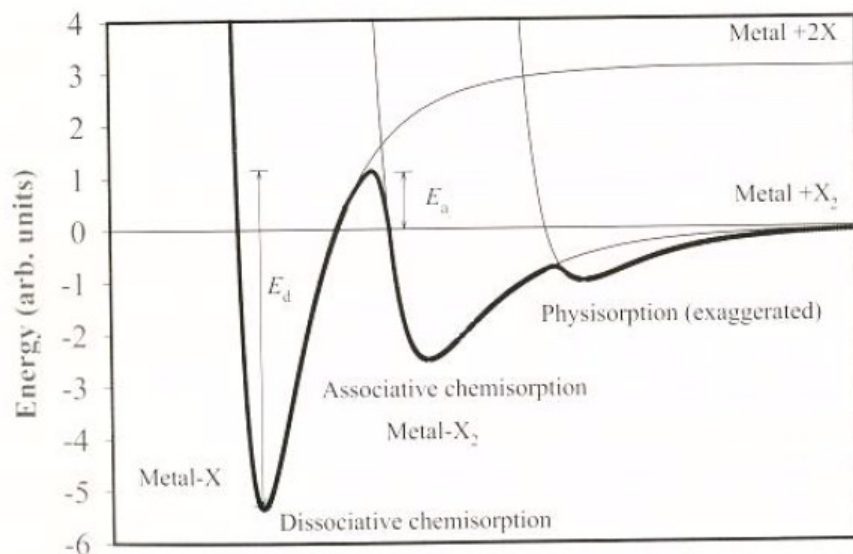
Figure 9: Schematic potential energy diagram along the reaction coordinate indicating the energies of both chemical and physical adsorption [30]

A simplified potential energy diagram for a molecule, X_2, approaching a metal surface is shown in Figure 9. At first the molecule encounters the weak Van der Waals force that leads to physical adsorption. In the next stage the molecule interacts chemically with the surface, leading to associative chemisorption. If the molecule is able to overcome the activation energy barrier, E_a, it may dissociate into two chemisorbed atoms. E_d is the energy required for desorption these atoms again. [30]

Both chemisorption and physisorption may be used to determine the surface area of solid materials. Physical adsorption determines the total surface area of both metal and support. Chemisorption, on the other hand, determines the surface area of the active catalyst i.e. the metal surface of a metal loaded support. [26]

2.2.2 Hydrogen chemisorption

Chemisorption is one of the most applied techniques for determination of catalyst dispersion. This section focuses mainly on the use of hydrogen as adsorbate gas and supported cobalt catalyst as the adsorbent.

The principle with volumetric chemisorption technique of hydrogen is to measure the amount of adsorbed gas as the function of the equilibrium pressure. This gives an adsorption isotherm like the one shown in Figure 10.
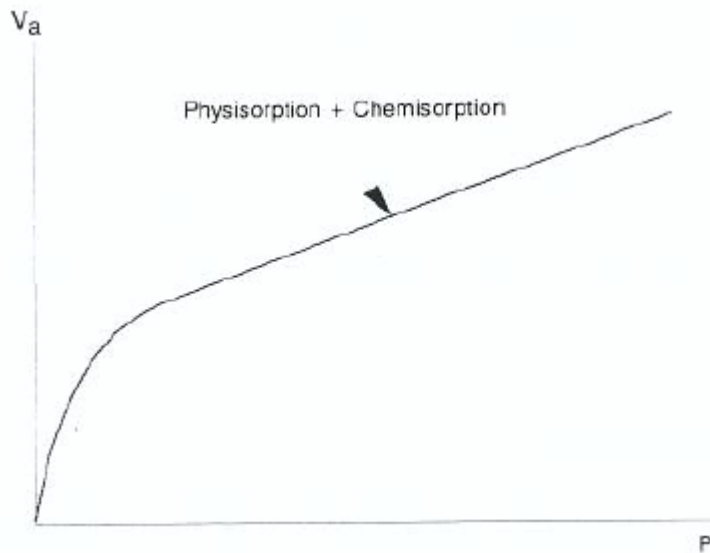
Figure 10: A typical composite isotherm generated by volumetric chemisorption technique. [34]

Figure 10 involves a combination of physisorption and chemisorption. The sample is evacuated after completion of the initial analyses in order to differentiate the chemisorption from the physisorption contribution. This procedure removes only the reversibly adsorbed gas. The analysis is repeated under the same conditions as the initial analyze until the active area of the sample is saturated with chemisorbed molecules. The result of this procedure is illustrated in Figure 11. [34]
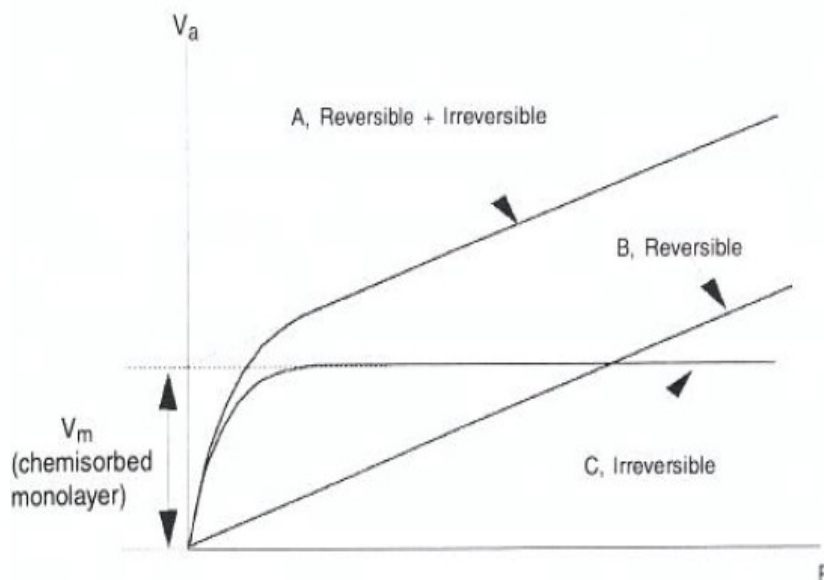
Figure 11: Isotherms generated by the volumetric chemisorption. [34]

In the figures above, V_a represents the adsorbed volume by chemisorption plus physisorption. The adsorbed volume data of the first adsorption isotherm A is a combination of both physical and chemical adsorption, reversible and irreversible respectively. The result from the repeat

analysis where only reversible physisorption occurs is isotherm B. Line C is generated mathematically by subtracting the adsorbed volume data of isotherm B from isotherm A. The difference, indicated as line C, typically conforms to the Langmuir model. This procedure yields the quantity of active gas irreversibly adsorbed by the sample. A description of the Langmuir isotherm is not presented in this thesis. More information about the Langmuir isotherm can be found in the book "*Analytical methods in fine particle technology*" by Webb *et al*. [34]

By expanding a known amount of gas in a fixed volume containing the sample and recording the pressure decrease for several increments of increasing pressure, the isotherm is obtained. There are two ways to determine the volume of adsorbed gas at monolayers, V_m. Either by extending a line tangent to the plateau of the initial adsorption isotherm to zero pressure, or by subtracting the physisorption isotherm from the combined isotherm as described above and then extend a line tangent to the plateau of that isotherm to the y-axis.

Dispersion, D, is a measure of the amount of active metal exposed at the catalytic surface. Dispersion is defined as number of metal atoms on the surface divided by total number of metal atoms. When the amount of gas consumed during chemisorption is available, the dispersion can be calculated by using Eq. (3.8)

$$D = \frac{V_m * M * F}{x} \tag{3.8}$$

where V_m represents the uptake of chemisorbed molecules (mole/ g cat.), M is the molecular weight of the metal, F is the adsorption stoichiometry and x is the weight fraction of the metal in the catalyst. [35] More specifically, F is defined as the number of active sites of the adsorbent covered by one gaseous adsorbate molecule.

In case of chemisorption of hydrogen on supported cobalt catalysts, a stoichiometry of two is used to calculate dispersion. Hydrogen adsorbs dissociatively on metals, M;

$$H_2 + 2M \rightarrow 2M\text{-}H$$
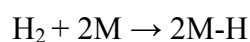
One hydrogen atom per metal surface atom is valid for a number of transition metals, as illustrated in Figure 12.
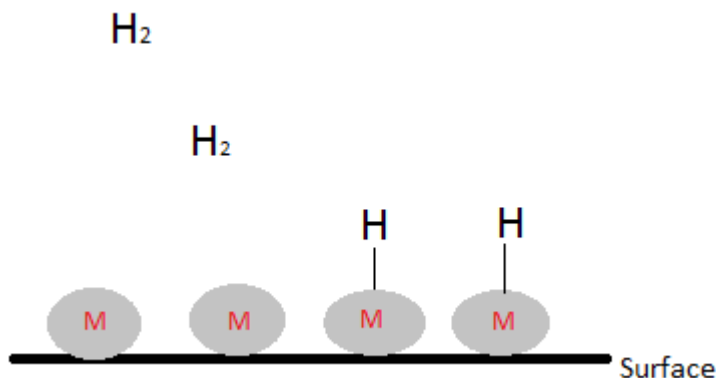
Figure 12: Dissociative adsorption of hydrogen on active sites. [35]

There are some sources of error related to hydrogen chemisorption. Presence of impurities, such as chloride, sulphur, water and metals can alter the gas uptake. Spill over of hydrogen atoms to the support can give H: M >1. It is assumed that rhenium does not adsorb any hydrogen.

2.2.2.1 Cobalt particle size

Cobalt particle sizes are estimated from the cobalt dispersion. For monodisperse spherical particles with a site density of 14.6 atoms/nm2, the relation between cobalt dispersion and cobalt particle diameter is given by Eq. (3.9) [36]

$$d(Co^0) = \frac{96}{D}$$

(3.9)

D is given in percent and d is in nanometers.

2.2.3 Nitrogen adsorption/desorption and the BET-method

In the late 1930's, Brauauer, Emmett and Teller proposed a model for multilayer physisorption for determination of surface area by measuring adsorption/desorption isotherm. They derived an equation that calculates the monolayer coverage of the adsorbate gas. The equation is called the BET-isotherm and is derived from a model that extends the Langmuir isotherm. The method is based on the experimental establishment of the relationship between the pressure of a gas that is in equilibrium with a solid surface and the volume of the gas adsorbed at the particular pressure at the surface.[37]

The BET-isotherm is based on a number of assumptions:

- The rate of adsorption and desorption in any layer are equal
- In the first layer molecules adsorb on equivalent adsorption sites
- ΔH_{ads} for the second and consecutive layers are the same. This adsorption heat is approximately equal to the condensation heat of the gas.
- ΔH_{ads} for the first layer is independent of layer 2 and the consecutive layers.
- The surface is constant during the adsorption.

The BET- technique finds the quantity of gas forming the first layer. Then the covered area is calculated from the number of gas molecules and gas molecules dimensions. The linear form of the BET-equation obtained from an infinite numbers of layers can be shown in Eq. (3.10)

$$\frac{p}{V_a(p_0 - p)} = \frac{1}{V_m C} + \frac{C-1}{V_m C}(\frac{p}{p_0}) \tag{3.10}$$

where

V_a	Total volume of adsorbed gas
V_m	Volume of gas adsorbed in the first monolayer
P	Equilibrium pressure
p_0	Saturation vapour pressure of adsorbed gas at the operating temperatures.
C	Constant

The constant, C, can be estimated as in Eq. (3.11)

$$C \approx \exp(\frac{\Delta H_1^0 - \Delta H_2^0}{RT}) \tag{3.11}$$

Where ΔH_1^0 is the heat of adsorption of the first layer, ΔH_2^0 is the heat of liquefaction of the adsorptive, R is the gas constant and T is the absolute temperature. [34]

A plot of $\frac{p}{V_a(p_0 - p)}$ as a function of $\frac{p}{p_0}$ should yield a straight line (y= ax + b) with intercept $\frac{1}{V_m C}$ (b) and slope $\frac{C-1}{V_m C}$ (a). a and b can be used to evaluate the monolayer capacity, V_m. How to calculate V_m from a and b is expressed in Eq. (3.14)

$$a = \frac{1}{V_m * C} \tag{3.12}$$

$$a = \frac{C-1}{V_m * C} \tag{3.13}$$

$$V_m = \frac{1}{a+b} \tag{3.14}$$

The specific surface area (m^2/g) can be calculated from Eq. (3.15) when the volume of the monolayer (m^3) is recorded.

$$A = \frac{V_m * N_A * \sigma}{V_{ig} * W_m} \tag{3.15}$$

In this equation N_A is the Avogadro's constant, σ is the area occupied by one adsorbed molecule, V_{ig} is the volume of one mole of ideal gas and W_m is the molar weight of the catalyst. [38]

The Barrett, Joyner and Halenda, BJH, method can be used to calculate pore volumes and pore size distribution. In the BJH method, the desorption branch of the isotherm is used. A simplified Kelvin equation is applied as an assumption for the calculations. This method leads to inconsistencies when the pore size approaches molecular dimensions. Earlier studies indicate that the Kelvin equation would underestimate the pore size and should not be extended below a pore size of approximately 7.5 nm. [39]

2.2.4   Oxygen titration

A pulse chemisorption analysis (oxygen titration) makes it possible to determine active surface area, percent metal dispersion and active metal particle size. This is done by applying measured doses of reactant gas to the sample being analyzed. The injected gas will chemically react with each active site until all active sites have reacted. The first few injections may be totally consumed, and as the sample approaches saturation, less gas will be consumed. After reaction has completed, each of the discretely injected gas volumes emerge from the sample tube unchanged. The quantity of molecules chemisorbed is the difference between the total amount of reactant gas injected and the sum amount of that did not react with the active sites of the sample measured by the detector. AutoChem II 2920 used in this thesis has a thermal conductivity detector. [40]
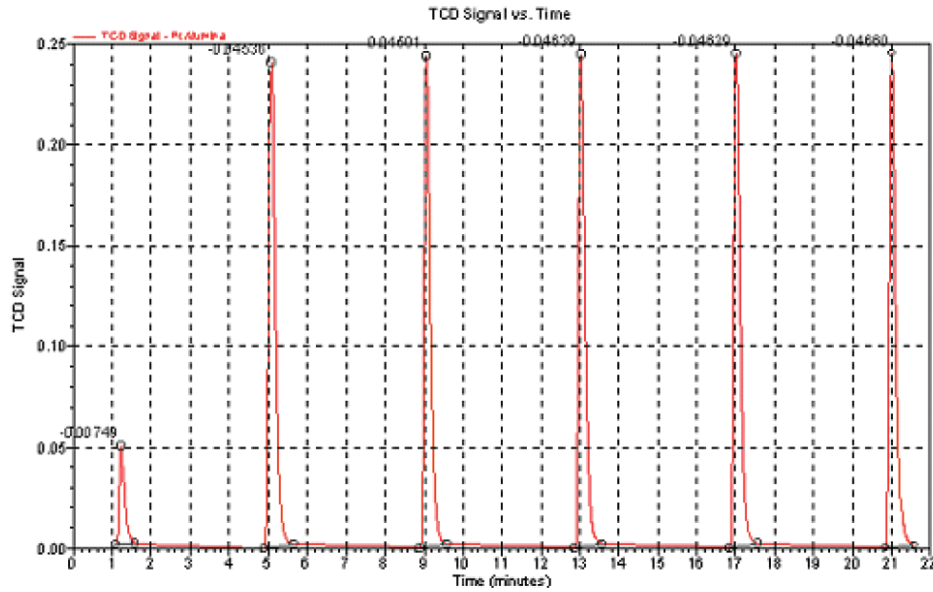
Figure 13: Signals produced by injections of equal volumes of adsorptive gas onto the sample [40]

Figure 13 shows the signals produced by successive injections of equal volumes of adsorptive gas onto the sample. Peaks in the figure represent unabsorbed analysis gas. [40]

2.2.4.1 Degree of reduction

The degree of reduction (DOR) is defined as the ratio between the actual number of oxygen atoms chemisorbed to cobalt and the theoretical number of chemisorbed oxygen atoms to cobalt. Cobalt reacts with oxygen according to Eq. (3.16)

$$2 \text{ Co}^{\text{o}} + 2 \text{ O}_2 \rightarrow \text{Co}_3\text{O}_4 \tag{3.16}$$

The theoretical amount can be calculated from Eq. (3.17), where $n_{Co.teor}$ is given in [moleCo/gcat.]

$$n_{Co.teor.} = \frac{m_{Co}}{Mw_{Co}} = \frac{x_{Co}}{Mw_{Co}} \tag{3.17}$$

In Eq. (3.17), x_{Co} is the weight fraction of the metal in the catalyst and Mw_{Co} is the molecular weight of cobalt.

The actual chemisorbed volume of oxygen can be calculated from Eq. (3.18)

$$n_{O_2 act.} = \frac{V_{O_2}}{V_{i.g}} = \frac{V_{O_2} \, \frac{cm^3}{g.cat}}{22414 \, \frac{cm_{O_2}^3}{mol \, O_2}} \tag{3.18}$$

where V_{O_2} is the cumulative amount given from the instrument and $V_{i.g}$ is the ideal gas volume.

DOR can be found by finding an expression of $n_{Co \, teor.}$ from Eq. (3.17) and the reaction equation. According to the reaction equation, $n_{Co} = \frac{3}{2} n_{O_2}$. DOR can then be calculated by using Eq. (3.19)

$$DOR = \frac{3}{2} * \frac{V_{O_2}}{V_{i.g}} * \frac{Mw_{Co}}{x_{Co}} \tag{3.19}$$

DOR can be used for the correction of the measured cobalt particle size found from the hydrogen chemisorption analysis. The corrected cobalt particle size is found by applying Eq. (3.20)

$$d_{Co} = \frac{96}{D} * DOR \tag{3.20}$$

When the dispersion is measured by hydrogen chemisorption, the amount of chemisorbed hydrogen is proportional with the dispersion. A high calculated dispersion indicates that the cobalt particles are small, as shown in Eq. (3.20). However, it is also possible that small particles give low dispersions. As shown in Figure 14, it is possible that hydrogen atoms are not able to adsorb to the small particles, giving a low calculated dispersion. It is also possible that large particles lead to calculation of high dispersions. If all particles are reduced, then more hydrogen is adsorbed and a high dispersion is calculated.

● Reduced (Co⁰-metal)
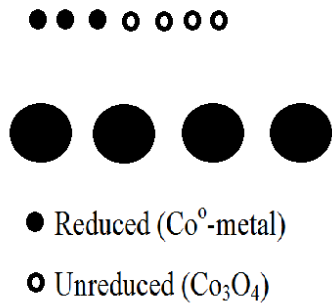
○ Unreduced (Co_3O_4)

Figure 14: Reduced and unreduced cobalt-particles during the hydrogen chemisorption analysis. Covered particles indicate that hydrogen is adsorbed

It is therefore important to correct for the degree of reduction in order to find the correct cobalt metal particle size. An illustration in Figure 15 shows how degree of reduction and Co particle size are related.
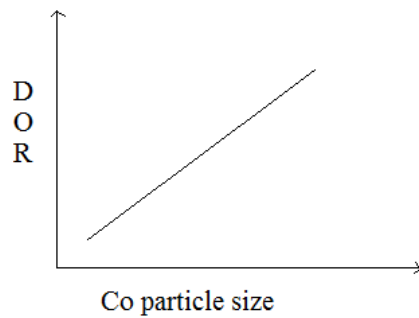
Figure 15: Degree of reduction (DOR) as a function of the cobalt particle size

3   Experimental

This section describes the preparation of the supports, and gives information necessary to reproduce experiments conducted in this project.

Catalyst preparation, nitrogen adsorption/desorption, oxygen titration and chemisorption were conducted at Statoil R&D Centre in Trondheim. The Fischer-Tropsch synthesis was performed in a double fixed bed reactor at The Department of Chemical Engineering at NTNU.

3.1   Catalysts preparation

3.1.1   Metal loading

The support material used in this thesis was nickel-aluminate spinel provided by Statoil R&D. Catalysts containing 12 wt. % cobalt and 0.5 wt. % rhenium on support (20.0 g) were prepared by one-step incipient wetness (co-) impregnation with aqueous solutions of cobalt nitrate hexahydrate, $Co(NO_3)_2 * 6H_2O$ and perrhenic acid, $HReO_4$. Catalysts containing 18 wt.% cobalt and 0.5 wt.% rhenium on the same support (20.0 g) were prepared by using excess impregnation solution of same concentration as for the 12 wt.% Co catalysts.

Incipient wetness (ml/g) was determined by drop-wise water addition to the support until the pores reached full capillary condensation. The purpose of completely filling the pores was to perceive a point where no flowing liquid could be detected. At this point all the water has been absorbed to the support material by surface attractive forces. The water was forced out of the pores by knocking the sample against a solid surface. Calculation made to find the water absorptivity is shown in Appendix A.1.

Impregnation solutions amounts were found according to calculations given in Appendix A.2 and A.3. The mixture was transferred into a glass liner, stirred and placed into an autoclave Parr CSTR (Parr-reactor) for drying. Some catalysts were stirred in a bowl before the mixture was transferred into the glass liner in order to improve the impregnation.

Two catalysts containing 12 wt.% cobalt were dried in an air furnace at 110 ^{o}C for 3 hours. The catalysts were stirred every 15. minutes the first hour and every 30. minutes for the last two hours. One of the catalysts was dried in a glass liner while the other one was dried in a bowl. The intention was that these catalysts would work as standards compared to the other catalysts dried in the Parr-reactor.

Dried and modified catalysts were calcined in a calcination furnace at 300 ^{o}C. The heating rate used for calcination of the support was 150 ^{o}C/h and dwell time was 16 hours.

3.1.2   Drying in an autoclave Parr continuous stirred tank reactor

The catalysts were dried in an autoclave Parr CTSR. The autoclave Parr CTSR is a 450 ml semi-continuous batch reactor. The reactor can tolerate temperatures up to 350 ^{o}C, a pressure of 70 bars, a stirrer rotation of 2000 rpm and a gas flow velocity of 10 NL/min. Temperature, rate of rotation, pressure and gas flows such as N_2, H_2, CO_2 and air can be controlled. It is also possible to extract samples during an experiment without shutting down the reactor. This is done by a liquid sampling valve. A reactor controller is used to control the temperature in the reactor. The control module provides a full three-term proportional-integrated-derivative (PID) control. [8]

The glass liner containing the precursor was placed into the reactor. The two ring sections with bolts were slid into place and positioned so that the drilled shallow socket in the outer surface of one ring section was pointing directly towards the operator. The outer drop band was placed around the two ring section so the cone pointed screw could be tightened towards the socket. The outer drop band is for extra security. Each of the six cap screws was tightened in a criss-cross pattern. The rate of rotation was adjusted by tuning the speed control knob on the front panel. This was done carefully in order to not destroy the impeller.

The temperature was adjusted to the desired temperature by pressing the up and down buttons on the temperature control panel. The **set** button was then pressed to set the temperature in the reactor. A security temperature controller was used to set the maximum temperature in the reactor and would turn off the heat if the reactor reached the maximum temperature.

The majority were dried in an open reactor system. This means that the "gas in" and "gas out" valves had to be open during all experiments, and the liquid sampling valve had to be closed. Three catalysts were dried in a closed reactor system, hydrothermal treated, meaning that all valves had to be closed before the experiment could start.

Since all catalysts are made of cobalt nitrate, NOx will be produced at a certain temperature during the experiment. A gas bubble trap was set up in order to remove the NOx from the outgoing gas. NOx will dissolve in the water and form nitric acid. The contaminated water in the gas bubble trap had to be replaced after each experiment. A flow of nitrogen (5%) was flushed through the system to prevent vacuum in the system and to lead nitrate to the gas bubble trap.

Table 2 gives an overview of the nomenclature used in this thesis.

Table 2: Overview over the nomenclature used in this thesis

12 wt. % Co 0.5 wt.% Re 10 ml H_2O Parr 110 ^{o}C	12.110-x	18 wt. % Co 0.5 wt.% Re 15 ml H_2O Parr 110 ^{o}C	18.110-x
12 wt. % Co 0.5 wt.% Re 10 ml H_2O Parr 150 ^{o}C	12.150-x	18 wt. % Co 0.5 wt.% Re 15 ml H_2O Parr 150 ^{o}C	18.150-x
12 wt. % Co 0.5 wt.% Re 10 ml H_2O Parr 270 ^{o}C	12.270-x	18 wt. % Co 0.5 wt.% Re 15 ml H_2O Parr 270 ^{o}C	18.270-x
Some of the catalysts were treated by a closed or a combination of a closed and open reactor system. These catalysts have a letter C or C/O at the end of the name. C is closed and O is open. These catalysts were made with 12 wt.% Co and 0.5 wt.% Re.			

Names starting with the number 12 means that the catalyst contains 12 wt.% cobalt, and the number 18 refers to 18 wt.% cobalt. The second number in the name corresponds to the set temperature in the Parr-reactor during drying. Based on the name 12.110.x, one knows that

this catalyst contains 12 wt.% cobalt and was supposed to be dried at 110 ^{o}C in the Parr-reactor. It is worth noticing that all catalysts contain 0.5 wt.% rhenium.

Various parameters have been modified in every experiment to see how they affect the catalysts during drying in the reactor. These parameters include temperature, stirring speed and duration. An overview of all catalysts made in this thesis can be seen in Table 3.

Table 3: An overview of all the catalysts dried in the Parr-reactor

Catalyst	Temperature [^{o}C]	Type of liner	Rpm	Duration
12.110-a	110	-	100	3h
12.110-b	110	glass	100	3h
12.110-c	110	glass	100	70 min
12.110-d	110	glass	200	75 min
12.110-e	110	glass	200	50 min
12.110-f	110	teflon	200	3 h
12.110-Closed	110	glass	200	3 h
12.110-h	110	glass	200	3 h
12.150-a	150	glass	200	46 min
12.150-b	150	glass	200	3 h
12.150-closed	150	glass	200	33 min
12.150-d	150	glass	200	1 h
12.270-a	270	glass	200	3 h
12.270-b	270	glass	200	1 h
12.270-c	270	glass	200	1 h
18.110-a	110	glass	200	1 h
18.110-b	110	glass	200	3 h
18.150-a	150	glass	200	3 h
18.150-b	150	glass	200	1 h
18.270-a	270	glass	200	1 h
18.270-b	270	glass	200	3 h
Std.1	110	glass	-	3 h
Std.2	110	bowl	-	3 h
12.110-C/O	110	glass	200	3 h / 1 h

All catalysts presented in Table 3 contained either 12 or 18 wt.% cobalt and 0.5 wt.% rhenium. The temperature column represents the set temperature in the Parr-reactor, and rates per minute, rpm, were either 100 or 200 for all catalysts. Two different liners have been used; a teflon liner and a glass liner. The majority of catalysts were dried in a glass liner, while catalyst 12.110-a was dried in the reactor without any liner and 12.110-f was dried in the teflon liner.

When duration is written as 3 hours, as in the fifth column, this means that the experiment was run for three hours after the temperature had reached the desired set temperature. The same applies for 1h. For other catalysts, where duration is written in minutes, this applies to the duration of the whole experiment.

Three different catalysts were dried in a closed reactor system. Two of these catalysts were dried in the Parr-reactor for three hours and 33minutes, respectively, and then dried in an air furnace at 110 $^{\circ}$C for 1.5 hour. 12.110-C/O was first dried in a closed reactor system for three hours, and then dried in an open reactor system for one hour.

3.2 Hydrogen chemisorption

Hydrogen chemisorption was performed on a Micromeritics ASAP 2020C unit. The catalyst ($\sim$ 0.5g) was loaded into a U-shaped quartz reactor and mounted inside an electrical furnace. Quartz wool was used under and over the catalyst bed to keep the catalyst sample inside the reactor during evaporation. The sample temperature was measured by a thermocouple located approximately the same height as the catalyst sample outside the reactor. The sample was initially dried in vacuum for two hours at 250 $^{\circ}$C before starting the analysis. A vacuum test was performed to prevent any leaks during analysis. The leak test was performed by first evacuating the sample until the pressure was stabilized. Then the vacuum pumps were turned off for one minute. The difference between the pressure before turning off the vacuum pumps and after one minute should not exceed more than 25 μg Hg/min. The temperature analysis program was started when all leaks were excluded.

The sample was initially evacuated at 40 $^{\circ}$C for one hour, and reduced *in situ* in flowing hydrogen for 16 hours at 350 $^{\circ}$C. The temperature was increased by 1 $^{\circ}$C/min from 40 to 350 $^{\circ}$C. After reduction, the sample was evacuated for one hour at 330 $^{\circ}$C and then evacuated for

30 minutes at 100 $^{\circ}$C. The adsorption isotherms were obtained after cooling the samples to 40 $^{\circ}$C. The adsorption isotherm constructed at 40 $^{\circ}$C is based on the adsorbed amount of hydrogen at 11 different pressures in the range 15-500 mmHg. The amount of hydrogen gas required to form a monolayer on the catalyst surface is estimated by extrapolating the straight-line portion of the isotherm to zero pressure. Normally, the eight last points are used for the extrapolation. In order to calculate the cobalt dispersion, it was assumed that two cobalt sites are converted by one cobalt molecule, and that rhenium does not adsorb any hydrogen.

Equation (3.8) was used to calculate the cobalt dispersion, and Equation (3.9) to estimate the cobalt particle size.

3.3   Oxygen titration

The oxygen titration was performed on a Micromeritics AutoChem II 2920 unit. The catalyst sample (0.5 g, 53-90 μm) was first reduced *in situ* under flowing hydrogen for 16 h at 350°C. The temperature was linearly ramped from room temperature to 350°C at a rate of 1°C/min. The sample was then flushed in flowing helium at 350°C for one hour and subsequently heated to 400°C at 1°C/min keeping the same gaseous atmosphere.

At 400 °C, a series of pulses of oxygen were passed through the catalyst bed. By calculate the number of pulses reacting with the sample and the known pulse volume made it possible to find the amount of oxygen consumed by the sample. The degree of reduction was calculated assuming that all cobalt in metallic form was oxidised to Co_3O_4. Any oxidation of Re to Re_2O_7 was not considered in the calculations.

3.4   Nitrogen adsorption/desorption

N_2 adsorption and desorption isotherms were collected for all supports by using a Micrometics TriStar 3000 instrument and the boiling point of liquid nitrogen (-196 $^{\circ}$C) Support (≈0.5 g) was loaded in a sample tube, degassed (250 $^{\circ}$C, 2 hours) and cooled to room temperature before starting the experiment. An isothermal jacket was placed around the sample tube to reduce the temperature gradients in the tube during measurements. A glass rod was placed in each tube to minimize the void.

The surface areas were calculated using the BET-equation (2.2.6). Pore diameters and pore volumes were found from the BJH method. The Micrometrics Tristar 3000 instrument used for nitrogen adsorption/desorption is shown in Figure 16.

Figure 16: To the left is the vacuum drier and to the right the instrument used for the nitrogen adsorption/desorption analysis. [37]

3.5   Fischer-Tropsch synthesis

This section provides the most important aspects regarding experimental procedure for the Fischer-Tropsch synthesis, including apparatus setup and data analysis.

3.5.1   Procedure and apparatus

The Fischer-Tropsch synthesis was run in two parallel fixed-bed reactors made of stainless steel. The reactors were surrounded by an aluminium jacket in order to minimize temperature gradients. An electrical furnace connected to a Eurotherm controller was used to heat the reactors. A schematic illustration of the apparatus is given in Figure 17.
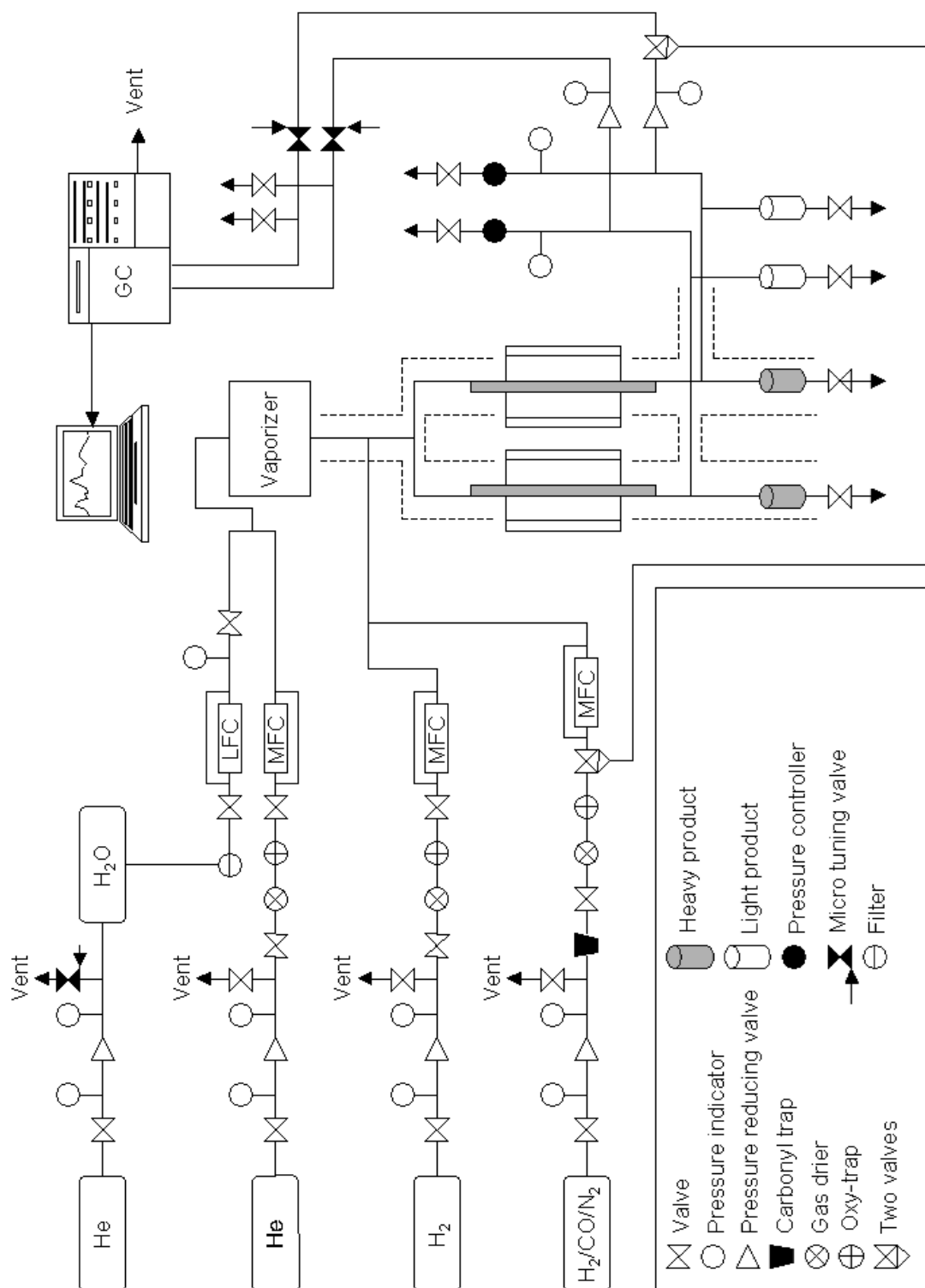
Figure 17: The Fischer-Tropsch apparatus used in this thesis [2]

---

[2] The Fischer-Tropsch apparatus scheme is copied from Bjørn Christian Enger's master thesis from 2005. The rig has since then been modified, but the main features will be the same.

Reactant gases used for this work were pure and no purification was needed, hence gas driers and oxy-traps installed in the FT-synthesis setup used for this work were redundant. Gas flow rates were controlled by mass flow controllers. Reaction conditions are summarized in Table 4.

Table 4: Reaction condition used for all FT-synthesis conducted in this work

Temperature [^{o}C]	210
Pressure [bar]	20
Feed gas ratio [H_2/CO]	2.1

A feed gas analysis was performed before each run to obtain accurate feed gas composition for the Fischer-Tropsch synthesis data analysis. A gas chromatograph equipped with a thermal conductivity detector (TCD) and a flam ionizing detector (FID) unit was used for all gas analyses.

The two fixed-bed reactors were loaded with 1.7 grams of catalyst (53-90 μm) diluted in 15 grams of silicon carbide (SiC). The catalyst had to be diluted with SiC to ensure a proper heat distribution throughout the catalyst bed. The catalyst bed was kept in place by layers of quartz wool.

The rig needed to be examined for any leaks before each experiment. Pressure testing was performed by pressurizing the rig to 20 bar with helium. The rig was left overnight at 20 bar pressure to complete the pressure test. The maximum allowed leak rate was set to be 0.8 bar pressure drop over 10 hours for each reactor. The rig has typically three leaks points: valve sealing, the thermocouple socket and the two valves connecting the reactor to the rig. It is hard to detect the leak within the valves. A leak detector spray can be used to find possible leaks around the thermocouple socket. It is also possible to lower the pressure in the rig followed by a rebuilt with hydrogen. Then a hydrogen detector can be used for the detection.

The catalysts were reduced *in situ* with flowing hydrogen at 350 ^{o}C and 2.0 bar. The temperature was ramped 1 ^{o}C/min and kept at 350 ^{o}C for 16 hours. The reactor was cooled to 170 ^{o}C after 16 hours, and pressurized to 20 bar using helium at 250 Nml/min. The helium flow was turned off and synthesis gas was introduced at 250 Nml/min. The reactor system

was then heated to 200 $^{\circ}$C (1 $^{\circ}$C/min), and finally 0.1 $^{\circ}$C/min to 210 $^{\circ}$C. The temperature profiles were supervised to ensure isothermicity.

3.5.2   Data analysis

Results from the Fischer-Tropsch synthesis were based on gas chromatography of the gas compositions on the inlet and outlet side of the catalyst bed. The amount of data obtained from the GC for each experiment is immense. Data analysis was performed using a pre-programmed excel sheet developed by Bjørn Christian Enger for his PhD thesis in 2007. This section presents a detailed description of the theoretical basis for the calculations preformed in the excel sheet.

The GC uses two different techniques to analyze the gas composition. The TCD detects H_2, N_2, CO, CO_2, CH_4 and H_2O, while the FID can detect hydrocarbon components from CH_4 and heavier. The heaviest hydrocarbon components are separated out of the product stream before the GC analysis in order to avoid condensation of heavier products inside the lines of the setup. No products lighter than C_5 were removed.

An internal standard was incorporated to get quantitative data for each component. A known amount of the internal standard was added to the feed gas as a reference for the quantification. The internal standard is inert to the reactions in the test unit. Nitrogen was used as the internal standard, but helium or argon could just as likely have been used.

Once every hour a sample was injected into the GC. The components in the unknown sample were separated by their different speed of capillary flow through the long column. The GC displays the separation as chromatograms with characteristic peaks for different components, as described in Section 3.1.4.

 The inlet side of the reactor is denoted 0 and the outlet side is denoted 1 in the following derivations. The subscripts i and j ($j = 1$ is CH_4) represents the TCD and FID-detected components, respectively.

The CO conversion, X_{CO}, can be calculated from Eq. (4.1)

$$X_{CO=\frac{F_{CO,0}-F_{CO,1}}{F_{CO,0}}} \tag{4.1}$$

Flow of each component on the inlet side can be written as shown in Equation (4.2)

$$F_{i,0} = x_{i,0} * F_{tot,0} \tag{4.2}$$

The mole fraction ratio between each component and the internal standard, N_2, can be written

$$\alpha_{i,0} = \frac{x_{i,0}}{x_{N_2,0}} \tag{4.3}$$

The response factor is a constant factor that has to be found by calibration. The calibration requires passing exactly known amounts of different gasses through the GC in order to find each response factor. The mole fraction, $\alpha_{i,0}$ is proportional to the relative chromatogram peak area for component i and the peak area of nitrogen, $A_{N2,0}$, detected by the TCD. The proportional constant is the relative response factor, $E_{i,0}$, expressed in Eq. (4.4).

$$E_{i,0} = \frac{\varepsilon_{i,0}}{\varepsilon_{N_2,0}} \tag{4.4}$$

The mole fraction ratio of component i can be written as shown in Eq. (4.5)

$$\alpha_{i,0} = \frac{\varepsilon_{i,0}}{\varepsilon_{N_2,0}} * \frac{A_{i,0}}{A_{N_2,0}} = E_{i,0} * \frac{A_{i,0}}{A_{N_2,0}} \tag{4.5}$$

The mole fraction of component i, $x_{i,0}$ can then be written as

$$x_{i,0} = x_{N_2,0} * \alpha_{i,0} \tag{4.6}$$

To ensure mass balance consistency it is necessary to ensure that

$$\sum_{i=1}^{n} x_{i,0} = \sum_{i=1}^{n} x_{i,1} = 1 \tag{4.7}$$

Combining Eq. (4.3) and (4.7) if follows that

$$\sum_{i=1}^{n} x_{N_2,0} * \alpha_{i,0} = 1$$

(4.8)

Eq. (4.8) may be written as this if nitrogen is component 1

$$\alpha_{i,0} * x_{N_2,0} + \sum_{i=2}^{n} x_{N_2,0} * \alpha_{i,0} = 1$$

(4.9)

Since $\alpha_{N_2,0}=1$, Eq. (4.8) becomes

$$x_{N_2,0} * \left(1 + \sum_{i=2}^{n} \alpha_{i,0}\right) = 1$$

(4.10)

By combining Eq. (4.3) and (4.10) if follows that

$$x_{i,0} = \frac{\alpha_{i,0}}{1 + \sum_{i=2}^{n} \alpha_{i,0}}$$

(4.11)

The mole fractions and the flow rates are closed linked to the total flow rate. The molar flow rates at the reactor inlet for H_2, CO and N_2 can now be determined.

$$F_{i,0} = x_{i,0} * F_{tot,0} = x_{i,0} * \frac{F_{N_2,0}}{x_{N_2,0}}$$

(4.12)

$$F_{i,0} = \alpha_{i,0} * F_{N_2,0}$$

(4.13)

The expression for CO conversion still requires the molar flow rate of CO at the outlet (denoted 1) of the reactor. The derivation of an expression describing the mole fraction ration for a component i to the internal standard on the reactor outlet side is identical to that of the inlet side.

$$\alpha_{i,1} = E_{i,1} \frac{A_{i,1}}{A_{N_2,1}}$$

(4.14)

$$x_{i,1} = \frac{\alpha_{i,1}}{1 + \sum_{i=2}^{n} \alpha_{i,1}}$$

(4.15)

The flow rate of H_2, CO and N_2 can be found from:

$$F_{i,1} = x_{i,1} * F_{tot,1} = x_{i,1} * \frac{x_{N_2,0}}{x_{N_2,1}} * F_{tot,0} \tag{4.16}$$

$F_{N_2,0} = F_{N_2,1}$ because nitrogen is inert during the synthesis.

$$F_{i,1} = \alpha_{i,1} * F_{N_2,0} \tag{4.17}$$

By summarizing the equations above makes it possible to calculate the conversion of CO.

$$X_{CO} = \frac{F_{CO,0} - F_{CO,1}}{F_{CO,0}} = 1 - \frac{A_{CO,1}}{A_{CO,0}} * \frac{A_{N_2,0}}{A_{N_2,1}} \tag{4.18}$$

Selectivity data can be obtained by applying a carbon count strategy/with the concept of a total carbon balance. A different reference is needed to quantify C_{2+} products because the FID detector can't detect nitrogen. Methane is detected by both the TCD and the FID detector and can be used as a reference to calculate the amounts of $C_2 - C_4$. The subscript j describes the FID detected components and n describes the total carbons atoms in that component. $j = 1$ corresponds to methane.

The selectivity towards component j with n carbon atoms in the product gas can be expressed by Eq. (4.19)

$$S_j = n * \frac{F_{j,1} - F_{j,0}}{F_{CO,0} - F_{CO,1}} = n * \frac{F_{j,1} - F_{j,0}}{X_{CO,0} - F_{CO,1}} \tag{4.19}$$

It can be assumed that the feed gas mainly consists of CO, H_2 and N_2. The $F_{j,0}$ becomes 0 and Equation (19) can be written as

$$S_j = n * \frac{F_{j,1}}{X_{CO,0} - F_{CO,1}} \tag{4.20}$$

To get selectivity data from Eq. (4.20), an expression for the calculations of the molar flow rates in the product stream is needed. The mole fraction ratio of component j containing n carbon atoms and the internal standard at the outlet can be found from Eq. (4.21)

$$\alpha_{j,1} = \frac{x_{j,1}}{x_{N_2,1}} = \frac{A'_{j,1}}{A'_{1,1}} * \alpha_{CH_4,1} \tag{4.21}$$

Where n accounts for the response area in proportion to the number of carbon atoms present in compound j. $A'_{j,1}$ represents that the area detected by the FID, hence $A'_{1,1}$ is the CH_4 area detected by the FID. The molar flow rate of product j in the reactor outlet is given as

$$F_{j,1} = \alpha_{j,1} * F_{N_2,0} \tag{4.22}$$

Compositions and flow rate expression for every component is know which make it possible to calculate selectivities and reaction rates.

$$S_j = n * \frac{F_{j,1}}{X_{CO,0} * F_{CO,1}} = \frac{\varepsilon_{CH_4} * A'_{j,1} * A_{CH_4,1} * A_{N_2,0}}{\varepsilon_{CO} * A'_{1,1}(A_{CO,0} * A_{N_2,1} - A_{CO,1} * A_{N_2,0})} \tag{4.23}$$

The selectivity for carbon dioxide can be found from

$$S_{CO_2} = n * \frac{F_{CO_2,1}}{X_{CO,0} * F_{CO,1}} = \frac{\varepsilon_{CO_2} * A_{CO_2,1} * A_{N_2,0}}{\varepsilon_{CO}(A_{CO,0} * A_{N_2,1} - A_{CO,1} * A_{N_2,0})} \tag{4.24}$$

The selectivity towards C_{5+} is defined as the fraction of the carbon atoms present in the feed gas that ends up in a product containing five or more carbon atoms. The selectivity to all C_{5+} components can be calculated from Eq. (4.25)

$$S_{C_{5+}} = 1 - S_{CO_2} - \sum_{j=1}^{4} S_j \tag{4.25}$$

$$S_{C_{5+}} = 1 - \frac{A_{N_2,0}}{\varepsilon_{CO}(A_{CO,0} * A_{N_2,1} - A_{CO,1} * A_{N_2,0})}$$
$$* \left(\varepsilon_{CO_2} * A_{CO_2,1} + \frac{\varepsilon_{CH_4} * A_{CH_4,1}}{A'_{1,1}} * \sum_{j=1}^{4} A'_{j,1} \right) \tag{4.26}$$

Most selectivities to long-chain hydrocarbons in this thesis are calculated by neglecting the formation of carbon dioxide during the FTS. Eq. (4.25) can then be simplified to

$$S_{C_{5+}} = 1 - \sum_{j=1}^{4} S_j \tag{4.27}$$

which can be expressed as

$$S_{C_{5+}} = 1 - \frac{\varepsilon_{CH_4} * A_{CH_4,1} * A_{N_2,0}}{\epsilon_{CO} * A'_{1,1}(A_{CO,0} * A_{N_2,1} - A_{CO,1} * A_{N_2,0})} * \sum_{j=1}^{4} A'_{j,1} \qquad (4.28)$$

The reaction rate based on carbon monoxide consumption is

$$-r_{CO} = \frac{X_{CO} * F_{CO}}{W} = \frac{F_{tot,0} * \varepsilon_{CO} * A_{N_2,0} * \left(\frac{A_{CO,0}}{A_{N_2,0}} - \frac{A_{CO,1}}{A_{N_2,1}}\right)}{W * (\varepsilon_{N_2} * A_{N_2,0} + \varepsilon_{CO} * A_{CO,0} + \varepsilon_{H_2} * A_{H_2,0})} \qquad (4.29)$$

Turn over frequency or specific catalyst activity (TOF) is frequently reported in connection with kinetic experiments. The experiments in this thesis were not specifically tailored to give data in the absence of transport limitations as is usually the case when TOF is reported. TOF can be calculated from Eq. (4.30), and can be used for comparison of data obtained at low and high conversations to determine whether transport limitations are present or not.

$$TOF = \frac{-r_{CO} * M_{CO}}{3600 * x * D} \qquad (4.30)$$

where $-r_{CO}$ is the reaction rate [mol CO/g. Cat. *h], M_{CO} us the molecular weight of cobalt, x is the weight fraction of cobalt on the catalyst and D us the dispersion of the catalyst obtained from volumetric chemisorption of H_2. 3600 is the number of seconds per hour.

4 Results and discussion

This section contains the results obtained in this work, together with some associating explanations and discussions. The key results are presented here while more extensive tables and figures can be found in Appendix B and C. All catalysts presented in this section contain either 12 or 18 wt.% cobalt. All catalyst has been impregnated with rhenium (0.5 wt.%), if nothing else is written in the text.

4.1 Catalyst preparation

The first part of this section presents the catalysts preparation. It is worth knowing that each experiment was devised on the basis of the results obtained from the previous one, which makes it somewhat difficult to present the result in a lucid manner.

It was difficult to reach exact point of incipient wetness for most of the catalysts. A somewhat dry impregnation (not complete capillary condensation) resulted when 12 wt.% Co and 0.5 wt.% Re were prepared. It is believed that this did not cause any substantial effects on the results.

Table 5 gives an overview over all catalysts dried in the Parr reactor, including temperature, rpm, duration, preparation and dryness.

Table 5: Preparation process for the different catalysts prepared in this work

Catalyst	Highest temperature [^{o}C]	Type of liner	rpm	Duration	Comment	Dryness [%]
12.110-a	120	-	100	3h	Cooled to 25°C, without stirring	100
12.110-b	140	glass	100	3h	"	100
12.110-c	115	glass	100	70 min	"	73
12.110-d	130	glass	200	75 min	"	24
12.110-e	155	glass	200	50 min	Cooled to 100°C	100
12.110-f	200	teflon	200	3 h		100
12.110-Closed	140	glass	200	3 h	Closed, Air furnace 1.5h	14
12.110-h	165	glass	200	3 h		100
12.110-d.rep	125	glass	200	75 min	Repetition of 12.110-d	13
12.150-a	180	glass	200	46 min		100
12.150-b	216	glass	200	3 h		100
12.150-closed	170	glass	200	33 min	Closed, Air furnace 1.5h	34
12.150-d	267	glass	200	1 h	Bowl-> glass liner	100
12.270-a	345	glass	200	3 h	Bowl-> glass liner	100
12.270-b	325	glass	200	1 h	Bowl-> glass liner	100
12.270-c	341	glass	200	1 h	Bowl-> glass liner Not calcined	100
18.110-a	114	glass	200	1 h	Air furnace 2 h	33
18.110-b	119	glass	200	3 h	Air furnace 2 h	30
18.150-a	227	glass	200	3 h		100
18.150-b	184	glass	200	1 h		100
18.270-a	274	glass	200	1 h		100
18.270-b.a 18.270-b.b	274	glass	200	3 h	18.270-b.a = Not calcined 18.270-b.b = Calcined	100
Std.1	110	glass	-	3 h	Air furnace 3 h	22
Std.2	110	bowl	-	3 h	Air furnace 3 h	100
12.110-C/O a.a	194	glass	200	3 h / 1 h	Closed (3h) -> open (1h)	24
12.110-C/O a.b	194	glass	200	3 h / 1 h	Closed (3h) -> open (1h) Air furnace 1 h	24

Table 5 gives an overview over the different parameters obtained in the Parr-reactor. The second column contains the set temperature in the reactor, while the third column contains the highest observed temperature during the experiment. Rates per minute, rpm, were either 100 or 200 for all catalysts. When duration is written as 3 hours, this means that the experiment was run for three hours after the temperature had reached set temperature. The same applies for 1h. For other catalysts, where duration is written in minutes, this applies to the duration of the whole experiment. The last column says something about the dryness. More about this is presented in the next section. In the first experiments, the Parr-reactor was cooled to room temperature before the reactor was disconnected. The reactor was disconnected at 100 $^{\circ}$C in the remaining experiments. Some of the catalysts were stirred in a bowl before the mixture was transferred into the liner. It was believed that this would lead to a better impregnation. Extra drying in an air furnace was required for some catalysts.

12.110-d was reproduced, and three catalysts were made to examine how they were affected by drying in a closed reactor system. These were 12.110-Closed, 12.150-Closed and 12.110-C/O. A more detailed explanation about these catalysts can be read in Section 5.1.4.

4.1.1   Drying profile and dryness

One of the aims with this thesis was to investigate if it was possible to use the autoclave Parr-reactor to dry catalysts. Drying profiles of catalysts impregnated with both 12 wt% Co and 18 wt.% Co on support (20g) were made to compare whether the catalysts were completely dry after treatment in the Parr-reactor. These curves were made without addition of rhenium to the catalyst. The catalyst mixtures were transferred into a bowl and dried at 110 $^{\circ}$C in an air furnace for three hours. The mixture was weighted and stirred every 15.minutes the first hour and every 30.minutes the last two hours.

It was possible to calculate the percentage dryness of each catalyst by comparing the weight of the dried catalyst against the drying curves. The majority of the catalysts were dry after treatment in the Parr-reactor, but some catalysts containing 18 wt.% Co and catalysts treated in a closed reactor system had to be further dried in an air furnace. An overview over all catalysts that were not considered dry after ended experiment is presented in Table 6.

Table 6: An overview over all catalysts that were still wet according to the drying curves

Catalyst	Duration- Open/closed	Dryness [%]	Additional drying in air furnace [hours]
12.110-c	70 min – open	73	
12.110-d	75 min – open	24	
12.110-d.rep	75 min – open	13	
12.110-Closed	3 hours – closed	14	1.5 h
12.150-Closed	33 min – closed	34	1.5 h
12.110-C/O a.a 12.110-C/O a.b	3 hours/1 hour – Closed/Open	24	12.110-C/O a.b = 0.5h
Std.1	3 hours –	22	
18.110-a	1 hour – open	33	2 h
18.110-b	3 hour – open	30	2 h

The table shows that particularly catalysts dried at 110 ^{o}C were considered wet compared to the drying curve. According to numbers collected from the table for 12.110-d, 75 minutes of drying in an open reactor system corresponds to a dryness of 24 %. For 12.110-c, 70 minutes in the Parr-reactor corresponds to 70 % dryness. Neither one of these catalysts was further dried in the furnace. The highest temperature observed for 12.110-c was 115 ^{o}C compared to 130 ^{o}C for 12.110-d. Temperature plots for these catalysts shows that 12.110-c has a more stable temperature throughout the experiment. The temperature plots will be discussed in Section 5.1.5. The only noticeable difference between these is the stirring rate. 12.110-c was dried with a lower stirring rate. Still, it is difficult to understand why catalyst 12.110-c was dryer compared to 12.110-d after ended experiment.

All the catalysts treated in a closed reactor system or a combination of closed and open system had to be dried in the air furnace after ended experiment. A part of 12.110-C/O was dry enough to be sifted through the sieve. The other part was too wet, and had to be further dried in the furnace before calcination. 12.110-C/O was divided into two different catalysts because of this; 12.110-C/O a.a and 12.110-C/O a.b (dried in the air furnace).

18.110-a and 18.110-b, both containing 18 wt.% cobalt, had to be dried in the air furnace for two hours. The other 18 wt.% cobalt catalysts were considered dry according to the curve.

Another interesting observation is the drying of Std.1. Apparently, this catalyst contains more water after three hours of drying in the furnace compared Std.2 also dried in the air furnace. Based on this result, it is believed that the shape of the glass liner affects the evaporation of water. The liner has tall walls and small surface in the bottom, compared to the bowl used for the drying of Std.2.

Some of the catalysts had a lower weight after drying in the Parr-reactor compared to the catalysts used for making the drying curve. A lower weight after drying means that more oxide is formed. Oxide is lighter than nitrate. This, indeed, shows that it is possible to dry catalysts by using the Parr-reactor. The measured weights for all catalysts after drying and both drying curves are found in Appendix B.1.

4.1.2   Stirring rate and type of liner

The stirring rate was set to be 100 rpm for all experiments in the first place, but was adjusted on the behalf of the results obtained in the first experiments. Catalyst 12.110-a had a stirring rate of 100 rpm and was cooled down to room temperature before the reactor was opened. The catalyst seemed to be dry, but contained hard lumps. It was impossible to break down some of the lumps into powder. The formation of lumps may be a result of formation of cobalt nitrate salt. Cobalt nitrate hexahydrate is soluble in water and solves into Co^{2+} and NO_3^- ions. Co^{2+} and NO_3^- forms cobalt nitrate salt when water evaporates, and could lead to agglomeration, i.e. lumps.

The dried catalyst had both blue and black colour, which indicates that some of the catalyst was not fully dried (blue colour) and some was calcined (black colour). Normally, cobalt catalysts dried in an air furnace have a purple colour. Figure 18 shows how 12.110-a looked like after the drying.

Figure 18: Sample 12.110-a after three hours at 110 ^{o}C in the Parr-reactor

The figure shows that the lumps are too big to be sifted through the sieve.

Normally, a completed impregnation of cobalt nitrate on support gives a black colour after calcination. The first experiments (12.110-a, 12.110-b and 12.110-c) had a somewhat bluish colour after calcination at 300 ^{o}C, indicating that the cobalt metal was not evenly impregnated to the supports. The stirring rate was adjusted to 200 rpm for the remaining experiments in order to achieve more evenly impregnation.

Most of the experiments were devised on the behalf of the results obtained from the previous one. The first experiments were cooled down to room temperature before the reactor was disconnected from the reactor system. It appeared that these catalysts contained a lot of agglomerate, and it was difficult to clean the glass liner because of black coating formed by the catalyst during the experiment. It was believed that this was caused by the formation of cobalt nitrate salt. The reactor was disconnected at 100 ^{o}C in the remaining experiments in order to avoid black coating and lumps. The stirring rotation was the same during both

experiment and cooling. Unfortunately, a higher stirring rate and disconnecting at 100°C did not lead to less agglomeration and coating.

A teflon liner was tested to see if the black coating caused by drying could be avoided, and to make the cleaning easier. The teflon liner can withstand a maximum of 250 °C, but did not lead to less coating. It was more difficult to clean the teflon liner compared to the glass liner, and the teflon liner was only used for drying of 12.110-f.

4.1.3   Duration

Duration was in the first place set to be three hours after reaching the desired set temperature. This was the same duration as for drying in an air furnace at 110 °C. Observed temperatures and temperature behaviour varied in each experiment, yet the set temperature was the same. The observed trend for all experiments was that the temperature increased rapidly to 100-120 °C in the beginning. The temperature was stable at ~ 110 °C for some minutes before it decreased and further increased to set temperature. From the literature one knows that water will evaporate at 1atm and 100 °C, so it was believed that most of the water was evaporated when the temperature decreased from 100-120 °C to less than 100 °C in the reactor. This hypothesis resulted in a lower drying duration for some samples; they were dried until the temperature drop occurred. The intention was to compare these samples with the others that were dried for three hours. More about temperature behaviour in the Parr-reactor is presented in Section 5.1.5.

4.1.4   Closed reactor system

Only three different catalysts were hydrothermal treated in a closed reactor system or a combination of closed and open reactor system. All three catalysts were impregnated with 12 wt.% Co and 0.5 wt.% Re.

12.110-Closed was dried in a closed reactor system for three hours at 110 °C and 1 atm. The catalyst was still wet after three hours, and had to be further dried in an air furnace for 1.5 hours before calcination.

The intention was to dry 12.150-Closed for three hours at 150 °C in the Parr-reactor, but a leakage was discovered after 33 minutes. The coupling and the top of the reactor were

covered with a yellow nitrate layer, and the reactor had to be disconnected. The highest pressure observed during this experiment was 2 bar. The catalyst was still wet and had to be dried in the furnace for 1.5 hour. Only three catalysts were hydrothermally treated before the leakage was discovered. No more catalysts were treated in a closed reactor system due to high probability that another leakage might occur.

A combination of both closed and open reactor system was investigated in order to determine the effect. Catalyst 12.110-C/O was run with closed conditions for three hours at 110 ^{o}C before the valves was opened for one hour. After the experiment the catalyst had both blue and black colour, indicating that some of the catalyst was calcined. The catalyst was tried sieved at 212 μm, but almost half of the catalyst was too wet to be sifted through and had to be dried in the furnace. 12.110-C/O was separated into two different catalysts, 12.110-C/O a.a and 12.110-C/O a.b, according to whether it was dried in the air furnace or not. The colour after 30 minutes in the air furnace was purple for 12.110-C/O a.b compared to a more bluish colour for 12.110-C/O a.a. A blue colour indicated that the catalyst was still wet, (24 % dryness) but it was possible to sieve it. Both catalysts were calcined separately at 300 ^{o}C.

4.1.5   The temperature effect

This section describes the temperature behaviour in the Parr-reactor. The temperature in the reactor was registered manually and at random intervals during each experiment. The heating jacket was removed if the temperature in the reactor became too high. The heating jacket was off until the reactor approached set temperature.

4.1.5.1   110°C

Table 7 displays the highest observed temperature during each experiment when the set temperature was 110 ^{o}C. The table includes catalysts containing both 12 and 18 wt.% Co.

Table 7: An overview over the highest observed temperature during drying for catalysts with a set temperature of 110 ^{o}C

Catalyst	Highest observed temperature [^{o}C]
12.110-a	120
12.110-b	140
12.110-c	115
12.110-d	130
12.110-e	155
12.110-f (Teflon)	200
12.110-Closed	140
12.110-h	165
12.110-d.rep	125
12.110-C/O a.a	194
12.110-C/O a.b	194
18.110-a	114
18.110-b	119

Table 7 shows that 12.110-f and 12.110-C/O a.a reached the highest temperatures compared to the other catalysts dried at 110 ^{o}C. According to the table, it can be seen that catalysts containing 12 wt.% Co reached higher temperatures during the drying compared to catalysts containing 18 wt.% cobalt. This could be a result of the different solution amounts used for impregnation. 12 wt.% Co catalysts contain enough water to achieve full capillary condensation, while catalyst containing 18 wt.% Co have a surplus of water. The water will be kept in the support material by surface attractive forces, and requires a certain amount of energy to make the evaporation possible. Likely, more energy is required to evaporate water kept in the pores of the support material versus excess water outside the pores. This could indicate that the water in the catalysts containing 18 wt.% Co evaporates more easily compared to 12 wt.% Co catalysts, and makes the temperature in the reactor more stable. This can be seen in Figure 19, where the black line represent 18.110-a. In addition, the Parr-reactor is designed for hydrothermal treatment, and with so little amount of water presence in the catalyst makes temperature control rather difficult. 12.110-Closed and 12.110-C/O, both treated in a closed or a combination of closed and open reactor system, are not included in this figure.
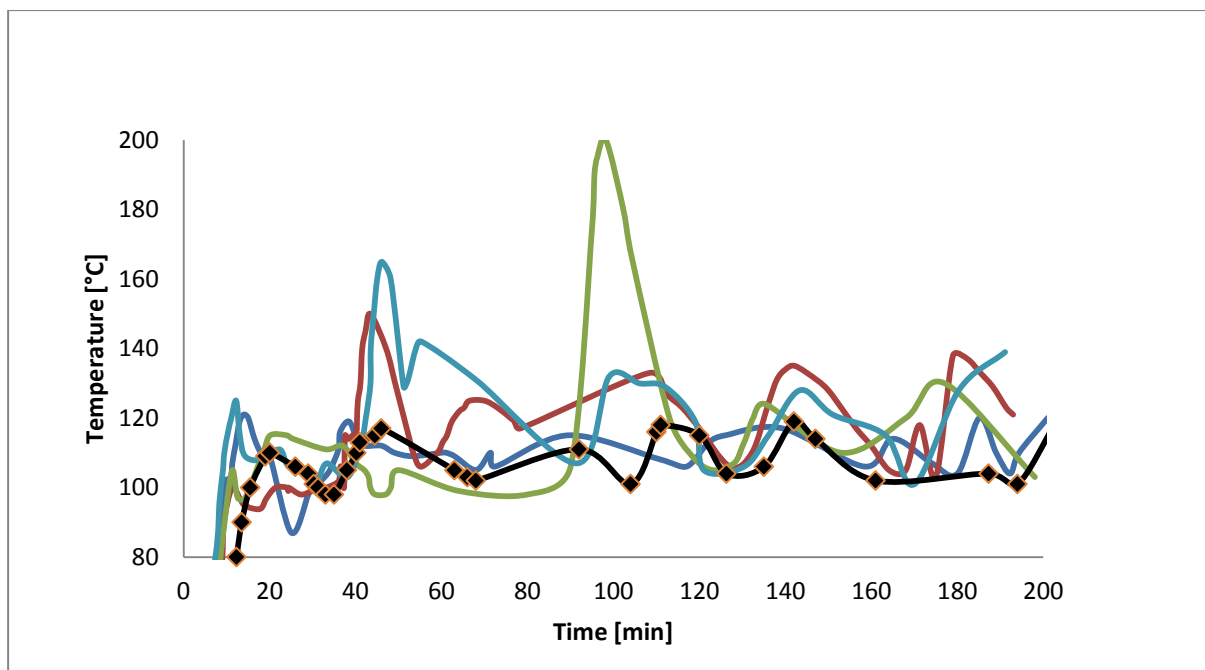
Figure 19: Observed temperatures during experiments for catalysts with a set temperature of 110 °C

Mainly three peaks can be observed in Figure 19. A lot of thoughts have been put in forth to find an explanation for this temperature behaviour. It is believed that the first temperature peak is when water evaporates. The phase transition from liquid to gas requires a lot of energy, and when water evaporates from the catalyst surface it will cool down the rest of the catalyst due to the amount of water it loses. In order to compensate for the heat loss, the heating jacket has to supply with more heat to maintain the set temperature. This leads to an overshoot in temperature.

The second peak could be evaporation of water in the pores. This water is presumably more stable that it would be as pure water and will probably require more energy to evaporate.

The third peak could be nitrate decomposition. A study made by Mansour [41] showed that cobalt nitrate hexahydrate decomposes in four steps. First, melting at about 75 °C, then dehydration between 80-170 °C, where cobalt nitrate monohydrate is formed. The third step is dehydration and decomposition of the monohydrate into unstable intermediate structure. This structure contains $Co(NO_3)_2$, CoO, Co_2O_4. The final step is decomposition into Co_3O_4 at about 240 °C. It has also been reported in the literature by El-Shobaky *et al* [42] that cobalt nitrate hexahydrate impregnated on alumina support decomposes at lower temperatures than cobalt nitrate hexahydrate itself. However, in this thesis, nitrate is already in the solution. The

possible nitrate decomposition in this case could be the final step in Monsour's study, i.e. decomposition into Co_3O_4.

The temperature plots for catalysts dried for one hour with a set temperature of 110 ^{o}C shows the same trend as for the plot in Figure 19. This temperature plot is found in Appendix B.2.

4.1.5.2   150 ^{o}C
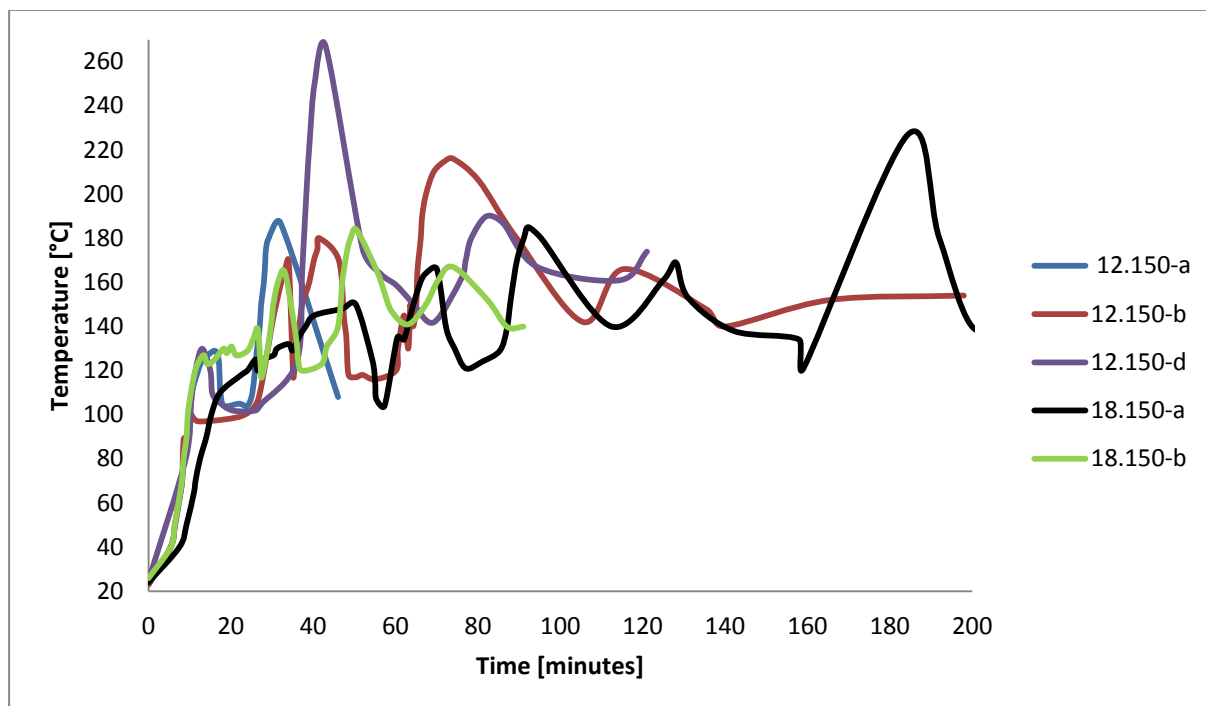
Figure 20: Observed temperatures during experiments for catalysts with a cobalt loading of 12 wt% and a set temperature of 150°C

Figure 20 presents temperature plotted against time for catalysts dried at 150 ^{o}C in the Parr-reactor. It is also possible to locate the same peaks that were identified in the previous chapter for the catalysts dried for three hours. It was believed that it would be easier to maintain a constant set temperature when the set temperature increased from 110 to 150 ^{o}C. The figure shows that the recorded temperatures still increased and decreased with time, with almost equal peak heights as seen in previous section.

Table showing the highest observed temperature in each experiment and other temperature plots can be seen in Appendix B.2.
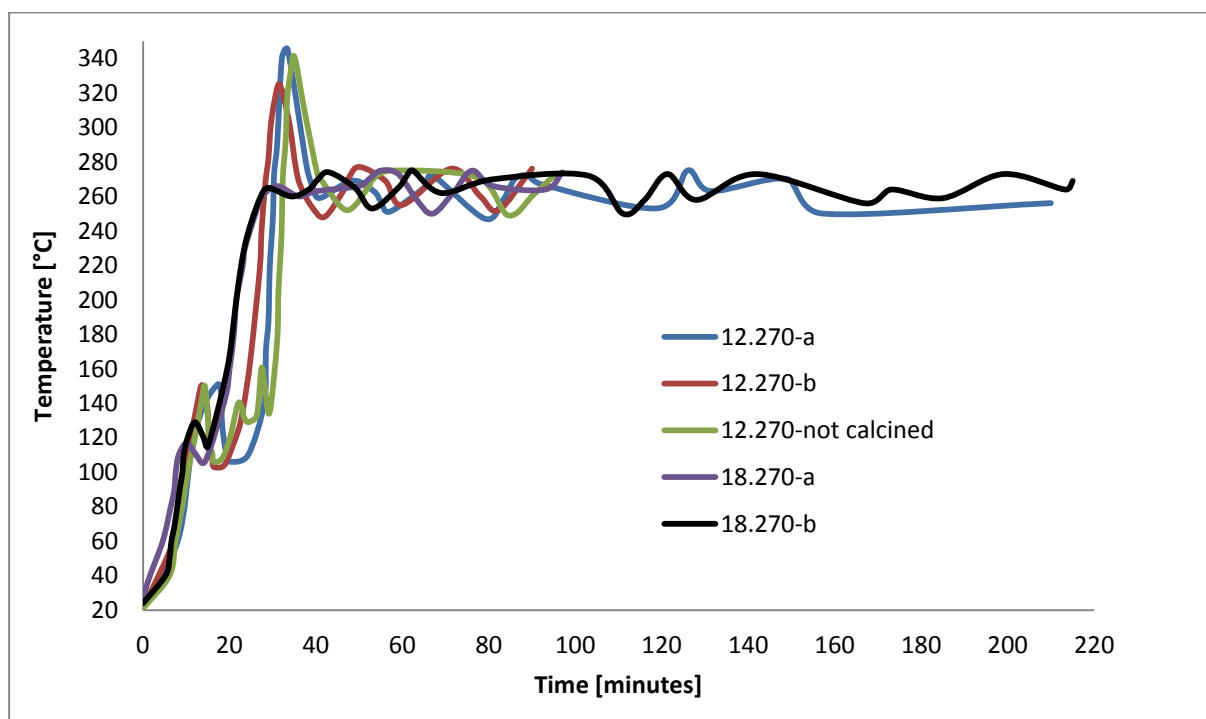
Figure 21: Observed temperatures during experiments for catalysts with a set temperature of 270°C.

Figure 21 shows temperature plotted against time for catalysts dried at 270 °C in the Parr-reactor. It is also possible to see the same temperature trends in this figure as in the previous ones. The first temperature drop occurs at 120 °C, which enhances the belief that it is free water that evaporates in the first peak. The temperature reached set temperature after evaporation.

It has been shown that it is difficult to maintain a constant set temperature during each experiment due to evaporation of water and fluctuating temperature. When water evaporates, the temperature in the reactor decreases, and the heating jacket has to produce more heat to maintain the set temperature. This leads to overshoot in temperature, especially for catalysts dried at 110 °C.

Since the temperature measurements were recorded manually and it was hard to maintain a constant set temperature in the reactor, one needed to be constantly aware about the temperature increase after the evaporations. This applies particularly to catalysts treated at 110 °C. If the temperature got too high the heating jacket had to be taken off in order to

remove heat. This was also done manually. Most of the water was removed after the first evaporation, which means that the reactor contained almost dried powder after this. The reactor and the reactor's controller are not designed to treat powder, which enhances the difficulty to maintain a good temperature control. However, it would have been interesting to run support powder (not impregnated with cobalt and rhenium) in the Parr-reactor in order to record the temperature behaviour during the run.

4.2   Catalyst characterisation

This section presents the result obtained from the characterisation work. Equal temperatures and durations are considered for the catalysts being compared in this section. There will be different temperature behaviour for all catalysts, so the highest observed temperature has been used as starting point for the comparisons.

4.2.1   Nitrogen adsorption/desorption

Results from nitrogen adsorption/desorption were retrieved from calculations carried out by the Micromeritics Tristar 3000 software program. The computer algorithm that forms the basis for the method (BJH) used to calculate the pore sizes and pore volumes frequently leads to inconsistencies when carried out on low surface area materials. The result of this is calculation of a too large volume of small pores. However, it was observed from the pore sizes distribution plots that all of the distributions converged to zero pore volume at both start and end of the size interval. The size interval ranges from $1.7 - 300$ nm.

There are some uncertainties related to the usage of nitrogen adsorption/desorption. The heat of adsorption is not necessary the same at the whole surface and some trace amounts of other substances may occur. This could modify the adsorption properties of the surface. The BET theory does not account for capillary condensation, and it can be negligible when the BET-isotherm is performed in the pressure range of $0 < \frac{p}{p_0} < 0.3$. This pressure range also ensures multilayer adsorption.

The experimental factor is ± 5 for surface area [m^2/g], ± 0.14 for the pore diameter [cm^3/g] and ± 0.5 for the pore volumes [nm]. The uncertainty is based on three independent runs for catalyst 12.150-d. Experimental error may be due to human factors. It is also worth knowing

that only a small fraction of the total sample is being characterized, and the surface area for the rest of the sample is not necessarily the same. This is one of the reasons that the calculated surface area is given with no decimals.

Most of the nitrogen adsorption/desorption results are presented ongoing in the next tables. The tables are divided into different parts, in order to make it easier for the reader to see the impact of the various parameter(s) that has been altered during each experiment. All of the results are presented in Appendix C.1.

Table 8: An overview over some of the results obtained for the nitrogen adsorption/desorption analysis

Catalyst	Surface area [m^2/g]	Pore volume [cm^3/g]	Pore size [nm]
12.110-Closed	56	0.19	11.9
12.110-d.rep	54	0.19	12.1
Support	*53*	*0.26*	*13.9*
Std.1	52	0.19	12.4
12.110-d	49	0.18	11.9
12.110-b	47	0.18	12.2
12.270-a	47	0.19	12.8
12.110-a	45	0.16	12.1
12.150-a	45	0.17	12.2
18.110-a	42	0.15	11.4
18.270-b.a	13	0.06	14.5
18.270-b.b	31	0.12	12.3

Table 8 presents some of the results from the nitrogen adsorption/desorption analysis. For most catalysts, impregnation leads to a slight decrease in surface area and pore volume. The reduction in pore volume and surface area upon impregnation might be due to cobalt oxide particles taking up space in the porous support structure. The pores are blocked by cobalt oxide particles. The change is in the same range and direction for most of the catalysts prepared in this thesis, except 12.110-Closed and 12.110-d. These catalysts have a higher surface area compared to the support. However, there will be some uncertainties associated with the BET-method, which makes the results relatively equal. Exception is the results for 18.270-b.a, which has not been calcined after drying. A very low surface area and pore volume have been measured for catalyst 18.270-b.a. This could indicate that the catalyst surface contains un-decomposed nitrate particles or water. If water and/or nitrate still are

present on the catalyst surface, this could lead to an overestimation of the pore size, i.e. small pores will not be counted, and an underestimation of the surface area. This observation can be confirmed by comparing the measure surface area and pore volume with 18.270-b.b (calcined) made in the same batch. 18.270-b.b has a much higher surface area and pore volume compared to 18.270-b.a.

4.2.1.1 The temperature effect
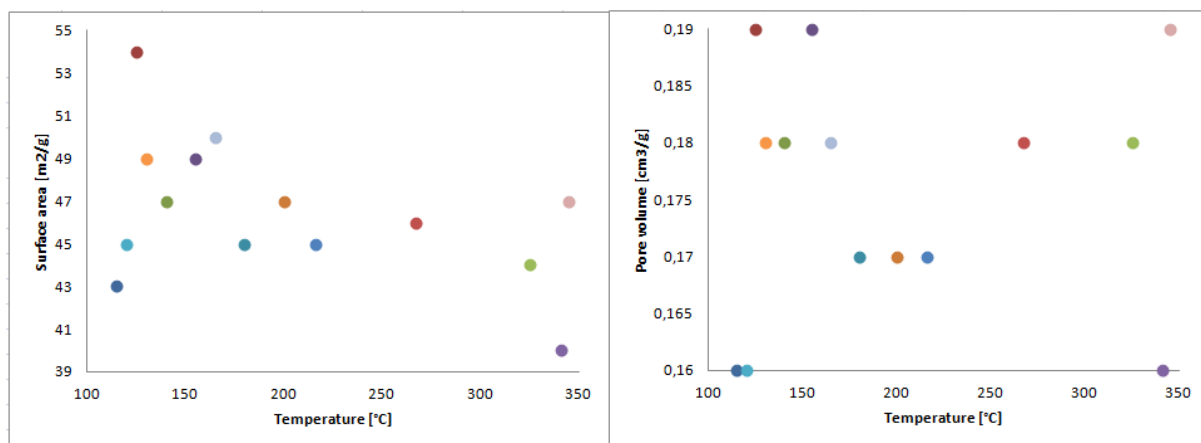
Figure 22: Result from nitrogen adsorption/desorption - The temperature effect

Figure 22 shows some of the nitrogen adsorption/desorption results obtained for catalysts impregnated with 12 wt.% cobalt. Catalysts treaded in a closed reactor system are not included in this figure. The x-axis in the figure represents the highest temperature observed during each experiment. It is possible to observe a connection between temperature and surface area from the figure. Apparently, higher temperatures lead to a decrease in surface area. The high temperature treatment could have led to a collapse in pore structure. However, the majority of catalysts were calcined after treatment in the Parr-reactor. The temperature behaviour observed for each experiment in the Parr-reactor shows that the temperature increases and decreases ongoing. It is possible that the sudden temperature increase causes clogging of pores, especially for catalysts dried with a high temperature. The same trend can be observed for catalysts containing 18 wt.% Co, shown in Appendix C.1.2.

It is also worth knowing that other parameters could have influenced the results, not only the highest observed temperature during the experiment. However, these results provide an indication of how an increase in temperature affects the catalyst.

Apparently, no correlation between the temperature change and pore volume can be seen in the figure.

4.2.1.2 Effect of treatment in the Parr-reactor

Table 9: Result from nitrogen adsorption/desorption - The effect of treatment in the Parr-reactor

Catalyst	H. temp. – duration – rpm	Surface area [m²/g]	Pore volume [cm³/g]	Pore size [nm]
Std.1	110 – 3h -	52	0.19	12.4
Std.2	110 – 3h -	42	0.16	11.3
12.110-c	115 – 70min.- 100	43	0.16	12.2
12.110-a	120 – 3h - 100	45	0.16	12.1
12.110-d.rep	125 – 75min. -200	54	0.19	12.1
12.110-d	130 – 75 min - 200	49	0.18	11.9

Results obtained from the nitrogen adsorption/desorption analysis in Table 9 shows that there is a slight difference in both surface area and pore volume between Std.1 and Std.2. Both catalysts have been dried in the air furnace at 110 $^{\circ}$C for three hours. It appears that the surface area is lower for Std.2, dried in a bowl, compared to Std.1, dried in the glass liner. It was believed that the result would have been opposite. It was a lot easier to obtain a homogenized mixture with stirring in the bowl compared to the glass liner. The glass liner wall was taller than the length of the glass wand used for the stirring, which made it difficult to obtain a proper stirring. In addition, the bowl has a higher surface accessible for the diffusion to the air.

Three catalysts treated in the Parr-reactor are compared against Std.1 and Std.2 in order to investigate the effect of treatment in the Parr-reactor. These three were the only 12 wt % Co catalysts dried with a temperature that did not exceed 130 $^{\circ}$C. The results from the nitrogen adsorption/desorption show that both surface area and pore volume for Std.1 is equal to 12.110-d.rep and 12.110-d, and Std.2 is equal to 12.110-c and 12.110-a. The measure pore sizes for the catalysts are also similar. Why Std.2, 12.110-c and 12.110-a have the same surface area and pore volume is uncertain. It can be due to different conditions during drying in the Parr-reactor, or it could be caused by human errors during the catalyst synthesis.

According to Table 6 in Section 5.1.1, 12.110-d.rep, 12.110-d and Std.1contained water after ended drying. As mention earlier, surface area may decrease when water still is present in the pores. It is believed that all this water has been evaporated before the analysis began, since the surface area and pore volume for these catalysts are higher compared to Std.2, 12.110-c and 12.110-a.

Figure 23 shows the correlation between measure surface area and dryness given in percentage.
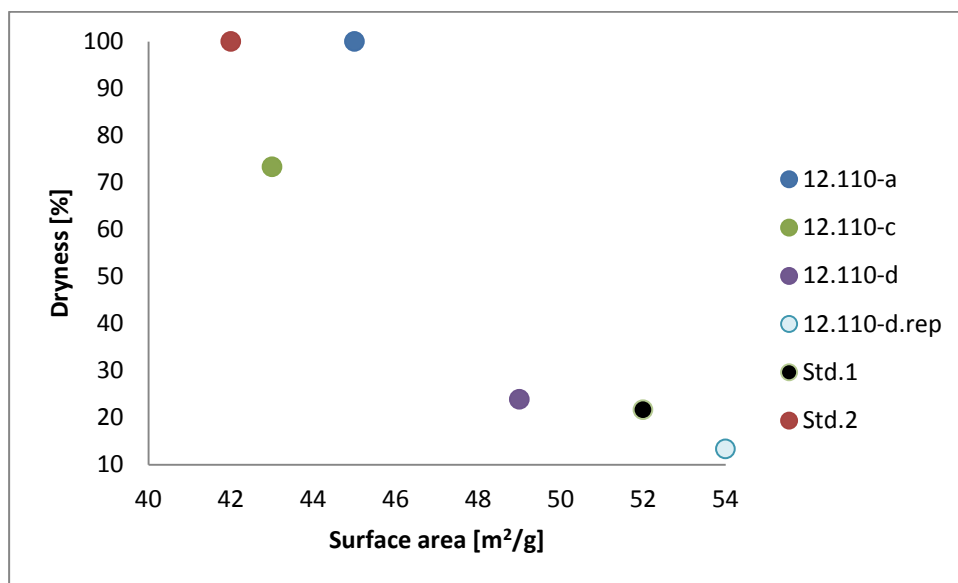
Figure 23: Dryness as a function of surface area for some of the catalysts

Apparently, "dry" catalysts have a lower surface area compared to the "wet" catalysts. This indicates that water still presence in the catalyst before calcination could affect the catalyst surface. Indeed, more results are needed to gain a fully explanation about this statement.

Table 10: Result from nitrogen adsorption/desorption - The calcination effect

	Catalyst	**Surface area [m^2/g]**	**Pore volume [cm^3/g]**	**Pore size [nm]**
Calcined	18.270-b.b	31	0.12	12.3
Not calcined	18.270-b.a	13	0.06	14.5
Calcined	12.270-a	47	0.19	12.8
Calcined	12.270-b	44	0.18	12.7
Not calcined	12.270-c	42	0.17	12.8

Catalyst 18.270-b. was divided into two parts after treatment in the Parr-reactor, where one part was further calcined at 300 °C for 16 hours (18.270-b.b). The nitrogen adsorption/desorption results in Table 10 shows that 18.270-b.a has a lower surface area and pore volume compared to 18.270-b.b (calcined). The reduction in pore volume and surface area could be a result of water and/or nitrate present on the surface, as explained earlier.

One of the aims with this thesis was to investigate the possibility of using the Parr-reactor for calcination. According to Table 10, 12.270-c and 12.270-b, both dried for one hour in the Parr-reactor at 270 °C, contain the same surface area and pore volume. These catalysts are not made in the same batch, as for 18.270-b.a and 18.270-b.b. In addition, 12.270-a, dried for three hours in the reactor, also have the same surface area and pore volume. This could indicate that it is possible to use the Parr-reactor for calcination. Since 18.270-b.a contained a significant lower surface area compared to the calcined 18.270-b.b catalyst, more data is needed to state this theory.

Table 11: Result from nitrogen adsorption/desorption – Effect of extra cobalt loading

Catalyst	Surface area [m^2/g]	Pore volume [cm^3/g]	Pore size [nm]
12.110-h	50	0.18	12.2
18.110-b	38	0.14	12.2
12.110-d.rep	54	0.19	12.1
18.110-b	42	0.15	11.4
12.150-b	45	0.17	12.9
18.150-a	32	0.12	13.8

The results in Table 11 indicate that addition of extra cobalt to the support leads to a decrease in both surface area and pore volume. Same duration and temperature are emphasized for the comparison in Table 11. The reduction in pore volume and surface area could be a result of pore blocking by the extra cobalt added. Borg *et al* [43] measured surface areas for γ-alumina supports impregnated with 12- and 18 wt% Co, respectively. They observed that the surface area decreased with extra cobalt loading to the catalyst.

All of the results obtained from the nitrogen adsorption/desorption analysis are given in Appendix C.1.

4.2.2   Hydrogen chemisorption

Dispersion together with metallic surface area were retrieved from calculation performed by Micromeritics ASAP 2020 software program. The results are found from the total hydrogen uptake by extrapolating the linear parts of the adsorption isotherms to zero pressure as described in Section 3.2.2. The cobalt metal particle size, Eq. (3.9), is calculated from the dispersion, and one calculation example is given in Appendix A.4. Eq. (3.9) is not entirely valid depending on how the cobalt phases are dispersed. The degree of reduction may have a significant effect on the actual average particle diameter. The cobalt metal particle size for some of the catalysts has been corrected by the result from the oxygen titration analysis. Results from this analysis are given in Section 5.2.4.
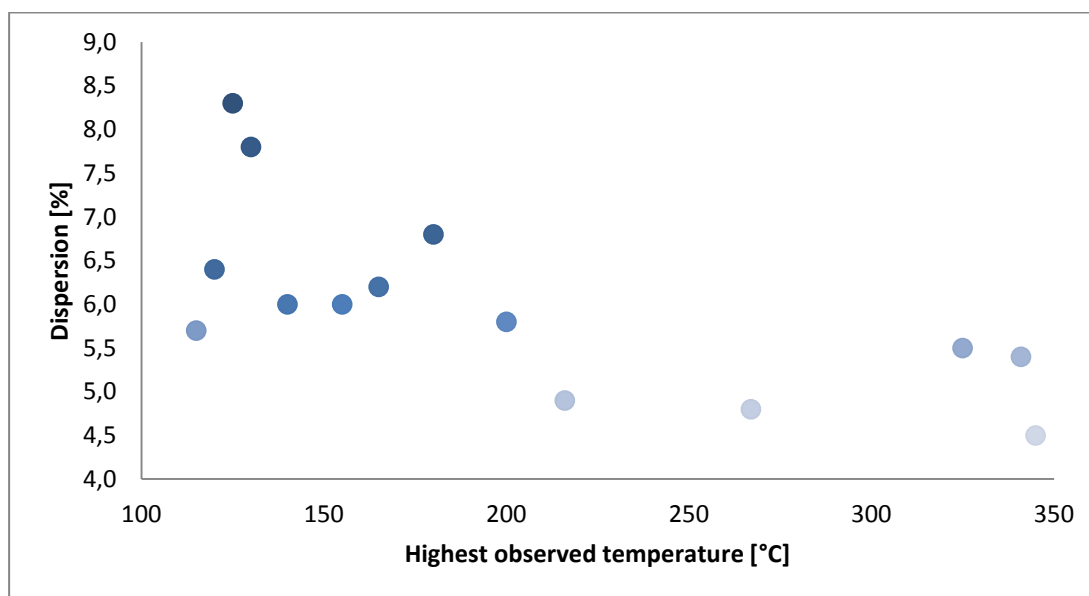
Figure 24: Result from hydrogen chemisorption - The temperature effect

Figure 24 displays the highest temperature observed during the experiment against dispersion. All these catalysts contain 12 wt.% Co, and catalysts treated in a closed reactor system are not included in this figure. It appears that optimal cobalt dispersion is achieved around 100 to 150 ^{o}C. There are small differences in measured dispersions when the temperature exceeds 200 ^{o}C. Results from the nitrogen adsorption/desorption showed that there was a trend between temperature and surface area. It was observed that higher temperatures led to a decrease in surface area. The dispersion results in Figure 24 could be explained by this observation.

The figure shows that low drying temperature in the reactor is promising, but is not suitable for calcination

Borg *et al* [5] observed a decrease in cobalt dispersion with increasing calcination temperature, and found two possible explanations: crystallite-growth and lower reducibility of cobalt. Presence of water and nitrogen oxides in a combination of high temperatures favours crystallite-growth. Presence of water in the catalyst after drying has been observed earlier in this thesis. For further work, it would be interesting to investigate if Borg's explanations agree with the result in this thesis.

The same result is observed for catalysts loaded with 18 wt.% cobalt. The temperature plot for these catalysts is presented in Appendix C.2.1.

4.2.2.2 Effect of treatment in the Parr-reactor

Table 12: Result from hydrogen chemisorption - The effect of treatment in the Parr-reactor

Catalyst	Dispersion [%]	Surface area [m²/g sample]	Cobalt metal particle size [nm]
Std.1	7.8	6.29	12.3
Std.2	8.3	6.75	11.6
12.110-c	5.7	4.65	16.8
12.110-a	6.4	5.16	15.0
12.110-d.rep	8.3	6.70	11.6
12.110-d	7.8	6.36	12.3

Table 12 presents some of the results obtained from the hydrogen chemisorption analysis. The effect of drying in the Parr-reactor appears to be a decrease in dispersion for 12.110-c and 12.110-a. However, equal dispersions are observed for 12.110-d and Std.1, and for 12.110-d.rep and Std.2.

A lower surface area was measured for both 12.110-c and 12.110-a compared to the others. This could have resulted in lower dispersions, as seen in Table X. On the other hand, the surface area for Std.2 was almost the same as for 12.110-c and 12.110-a, but the dispersion is higher.

In addition, the results from the nitrogen adsorption/desorption analysis showed that Std. 1 had a higher surface area compared to Std.2. A poorer drying was registered for Std.1 compared to Std.2, due to usage of glass liner for drying of Std.1 compared to a bowl for drying of Std.2. It is worth noticing that the cobalt metal particle size characteristics presented in this table and in the rest of this section were not corrected for degree of reduction.

Apparently, water still present in the catalyst after drying seems to affect the catalyst properties. It has already been observed that catalysts containing water after drying have a higher surface area compared to dry catalysts.
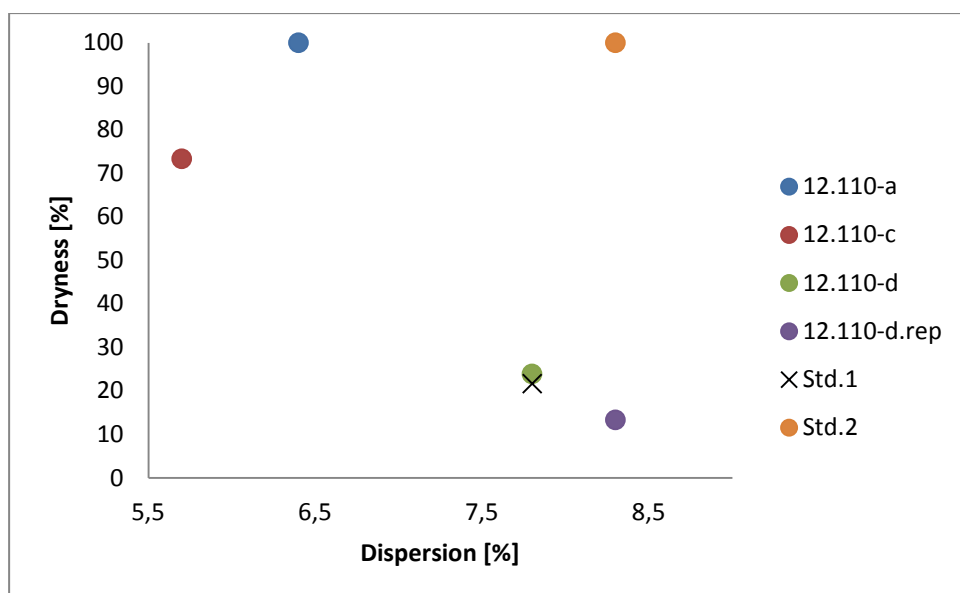
Figure 25: Dryness as a function of dispersion for some of the catalysts

In Figure 25, the "wet" catalysts have a higher dispersion, thus lower calculated cobalt particle sizes, compared to the dry catalysts, except Std.2. This result indicates that water still present in the catalyst after drying affects the catalyst characteristic in a positive way. Still, more experiments need to be carried out to state this.

4.2.2.3   Calcination effect

Table 13: Result from hydrogen chemisorption - The calcination effect after drying

	Catalyst	Dispersion [%]	Surface area [m²/g sample]	Cobalt metal particle size [nm]
Calcined	18.270-b.b	5.2	6.31	18.5
Not calcined	18.270-b.a	5.1	6.17	18.8
Calcined	12.270-a	4.5	3.67	21.3
Calcined	12.270-b	5.5	4.44	17.5
Not calcined	12.270-c	5.4	4.41	17.8

It appears that the dispersion is unchanged for catalyst calcined after drying in the Parr-reactor compare to catalyst not calcined, as indicated in Table 13. Results from the nitrogen adsorption/desorption analysis showed that there was a noticeable difference in surface areas between 18.270-b.a and 18.270-b.b. 18.270-b.a (not calcined) contained a lower surface area compared to 18.270-b.b. This was probably caused by water and/or nitrate still present in

18.270-b.a after drying. On the other hand, the result in the table shows that the dispersion is equal and no good explanation has been found.

12.270-a has a lower dispersion compare to the two other catalysts containing 12 wt.% cobalt. Since the surface areas for these three catalysts were the same, this result may be caused by different unnoticeable conditions during drying. Table 13 shows that the dispersions are similar or higher for the catalysts not calcined compared to those which are calcined. More experiments need to be investigated to yield a conclusion upon the calcination effect.

4.2.2.4   Effect of addition of extra cobalt loading

Table 14: Result from hydrogen chemisorption - The effect upon extra addition of cobalt

Catalyst	Dispersion [%]	Surface area [m^2/g sample]	Particle size [nm]
12.110-h	6.2	5.07	15.5
18.110-b	5.5	6.65	17.5
12.110-d.rep	8.3	6.7	11.6
18.110-a	5.6	6.8	17.1
12.150-b	4.9	3.96	19.6
18.150-b	4.8	5.8	20.0
12.270-b	5.5	4.44	17.5
12.270-b.b	5.2	6.31	18.5

A decrease in dispersion for catalysts containing 18 wt.% cobalt treated at 110 ^{o}C can be observed in Table 14. The measured surface area for the support used in this thesis was 53m^2/g, and there will be limitations of how much cobalt that can interact with the surface. The dispersion is almost unchanged for catalysts dried at temperatures higher than 150 ^{o}C. This may be due to large cobalt particles.

4.2.2.5 Effect of closed reactor system

Table 15: Result from hydrogen chemisorption - The effect of closed reactor system

Catalyst	Dispersion [%]	Surface area [m^2/g sample]	Particle size [nm]
12.110-h	6.2	5.07	15.5
12.110-Closed	8.9	7.18	10.8
12.150-a	6.8	5.53	14.1
12.150-Closed	5.9	4.80	16.3
12.110-C/O a.a	5.6	4.58	17.1
12.110-C/O a.b	7.7	6.25	12.5

Apparently, treating catalysts in a closed reactor system leads to an increase or decrease in dispersion, as shown in Table 15. 12.110-Closed, run for three hours in the Parr-reactor, has a higher dispersion compared to 12.110-h, treated in an open system. However, 12.150-Closed has a lower dispersion compared to 12.150-a, treated in an open system. The low dispersion for 12.150-closed could be a result of nitrate formation during the experiment. The nitrate formation might have caused sintering of the cobalt crystallites, or changed the cobalt oxide phase to a less active cobalt phase. The figure shows that hydrothermal treatment, treatment in a closed reactor system, is promising for making good catalysts.

All of the results obtained from the hydrogen chemisorption analysis are given in Appendix C.2.

Some of the results presented in the previous sections show that it is difficult to explain why the results are as they are. It is also difficult to say what exactly that affects these results. It could be the temperature or stirring rate, but it could also be something else that is not observed or registered during the treatment in the Parr-reactor. It should be mention that it is not only one parameter that will affect the treatment in the Parr-reactor, but the whole system. This makes the comparison of the different parameters difficult. However, these results provide an indication of how the different parameters effects affect the catalyst synthesis.

In this thesis, only the end product was investigated. For further work, it might be appropriate to extract samples during drying in the Parr-reactor in order to gain a better understanding about what is happening during the drying. It most also be noticed that the results are only based on nitrogen adsorption/desorption and hydrogen chemisorption characterization. It might be useful to use other characterization methods in order to be able to get some answers to the unsolved observations.

4.2.2.6   Cobalt particle size

The cobalt particle size is calculated from Eq. (3.9) in Section 3.2.2.1. The cobalt particle size is a function of the dispersion, where the particle size increases with decreasing dispersion. The particle sizes of the catalysts made in this thesis ranges from 11 nm until 21 nm, which is defined as large cobalt particles according to [12].

In supported cobalt catalysts the reducibility of the cobalt species will often depend on the extent of the metal support interactions. Reduction temperatures of the cobalt species depend on the nature and the amount of other cations in the catalyst. It is important to notice that the dispersion data and the cobalt metal particle size presented in this chapter were not corrected for degree of reduction.

4.2.3 Combining the results obtained from nitrogen adsorption/desorption analysis and hydrogen chemisorption.
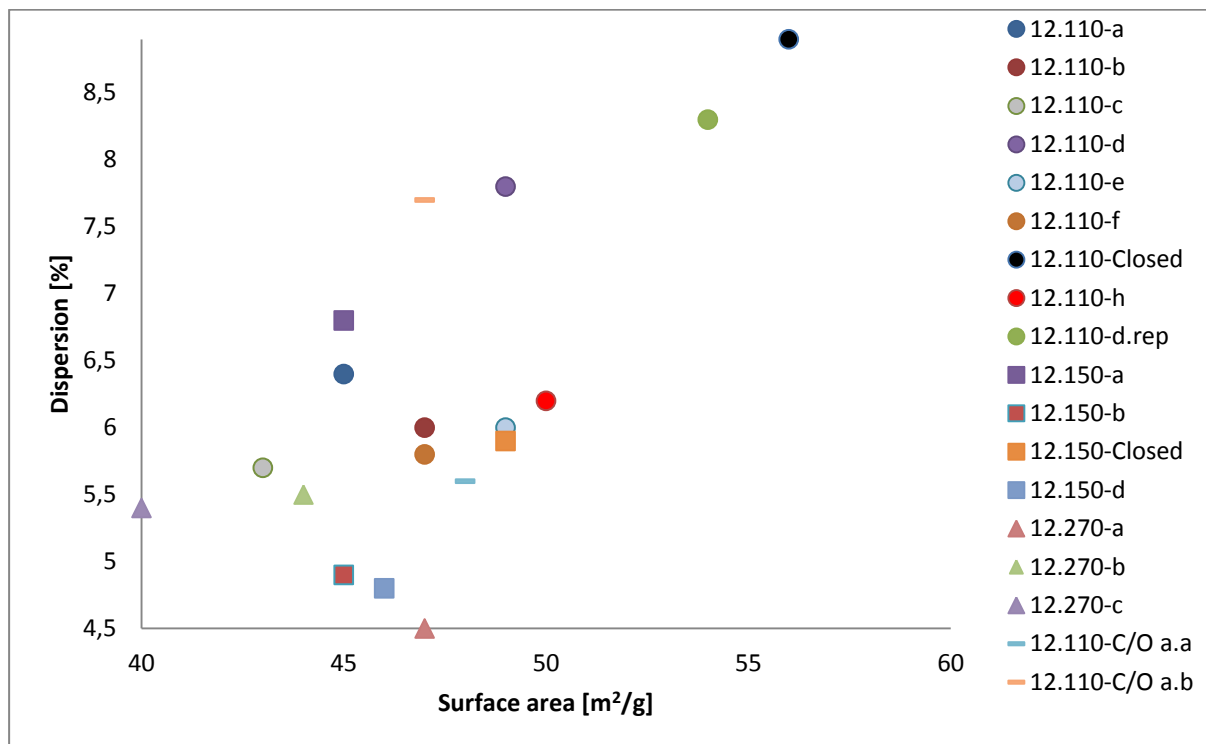
Figure 26: The results obtained from both nitrogen adsorption/desorption and hydrogen chemisorption analysis for catalysts containing 12 wt.% cobalt

Dispersion is plotted against measured surface area in Figure 26. Catalysts with a set temperature of 110 ^{o}C, 150 ^{o}C and 270 ^{o}C are shown as circles, squares and triangles, respectively. The figure shows that the highest cobalt dispersion is obtained in catalyst 12.110-Closed, which also has the highest measured surface area. There is normally a correlation between the surface area and the dispersion, where larger surface areas enhance the possibility of catalytic reaction. It is possible to observe the trend in dispersion with increasing surface area for the catalysts dried with a set temperature of 110 ^{o}C. This does not apply 12.110-C/O a.a versus a.b, as discussed earlier.

On the other hand, the dispersions are more random for measured surface areas in the rage of 44 – 50 m^2/g. This could indicate that the measured dispersions in this range are not affected by the surface area, or other parameters could play a role.
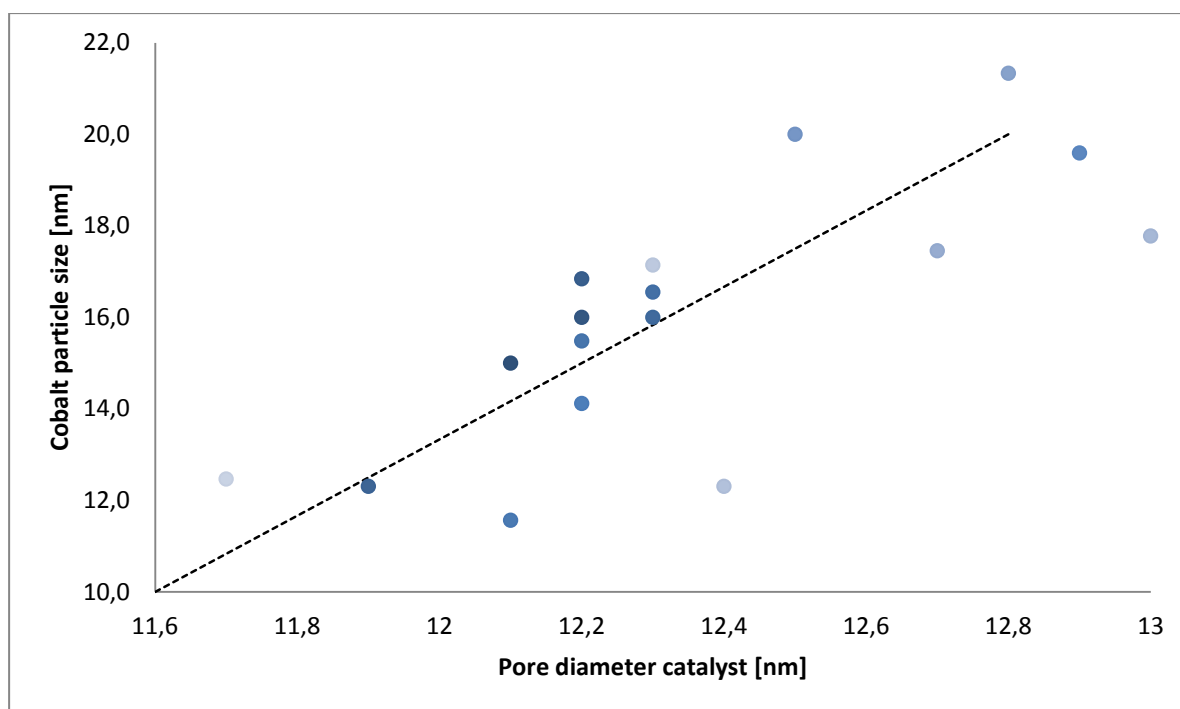
Figure 27: Effect on the catalyst pore diameter on the cobalt particle size calculated from hydrogen chemisorption data

Figure 27 shows that the individual cobalt particle size (calculated from hydrogen chemisorption) followed the pore size of the catalyst. The figure only include catalysts with a cobalt loading of 12 wt.%. The cobalt particle size is not corrected for degree of reduction. However, it is believed that the same trend is obtained if the degree of reduction is considered. The figure indicates that cobalt particle size depends on the pore diameter of the support.

4.2.3.1   Comparison of 12.110-d and 12.110-d.rep

The incentive for making another 12.110-d catalyst was to investigate if it was possible to reproduce the same catalyst with same properties. The experiment was performed with the same conditions and performance as for the first 12.110-d sample. Results obtained from the nitrogen adsorption/desorption and hydrogen chemisorption shows that the surface areas are almost the same, but a slight difference in dispersion can be observed. The difference in dispersion for 12.110-d and 12.110-d.rep is 7.8 % and 8.3 %, respectively. 12.110-d was dried exactly the way 12.110-d was dried. If the heating jacket was taken off after 50 minutes during the drying of 12.110-d, then the heating jacket was taken off at that time during drying of 12.110-d.rep, and so on. These results show that it is possible to reproduce the same

catalyst by maintaining the same drying conditions and parameters. One could almost think that the rest of the experiment dried at almost the same temperature, with same duration time and stirring rate would give similar results. This indicates that more investigations are required to find answer to all the unsolved questions.

4.2.4 Degree of reduction

Oxygen titration was performed by a Micromeritics AutoChem II 2920 unit, and the results were retrieved from calculations carried out by instrument's software program. Calculation of the degree of reduction from oxygen titration data assumes stoichiometric oxidation of Co^o to Co_3O_4. The results are presented in Table 16.

Table 16: Hydrogen chemisorption and oxygen titration data

Catalyst	Dispersion [%]	$d\ (Co^0)_{uncorr}$ [nm]	Cumulative quantity [cm^3/g STP]	Degree of reduction [%]	$d\ (Co^0)_{corr}$ [nm]
12.110-Closed	8.9	10.8	20.7	68	7.4
Std.1	7.8	12.3	18.1	59	7.3
12.110-d.rep	8.3	11.6	19.7	65	7.5
Std.2	8.3	11.6	20.1	66	7.6
12.150-a	6.8	14.1	16.6	55	7.7

The degree of reduction measured using oxygen titration ranged from 59 to 68 percent, as shown in Table 16. The lowest and highest value was obtained for Std.1 and 12.110-Closed, respectively. A high degree of reduction, or a high metal fraction, increases the number of cobalt atoms likely to participate in the reactions, though the dispersion is of course determining the actual cobalt metal surface area. As presented earlier in this thesis, the size of the cobalt particle will influence the Fischer-Tropsch activity and the selectivity towards C_{5+}. A too low particle size gives a low FT activity. However, a cobalt particle size of 8-10 nm or more increases the activity.

According to [44] cobalt-support interactions depends on cobalt particle size. It is expected that larger particle sizes result in weaker metal-support interactions, which again leads to a high degree of reduction of cobalt species. In this case, the catalyst with the largest particle size has the lowest degree of reduction.

4.3   Fischer-Tropsch synthesis

Fischer-Tropsch catalytic performance data were obtained in an isothermal dual fixed-bed reactor at 20 bar, 210 $^{\circ}$C and a H_2/CO rate of 2.1. The main source of error for the synthesis was attributed to temperature variations in the catalyst bed. The temperature varied with $\approx 1^{\circ}$C throughout the bed, and the average bed temperature deviated from 210 $^{\circ}$C with no more than ±0.5 $^{\circ}$C. The difference between two fixed-bed reactors was found to be within $\pm$ 1% in CO conversion. This error was found by running a standard catalyst in both beds.

The space velocity was adjusted to give an estimated CO conversion level of 50 %. This was done because C_{5+} selectivity strongly depends on conversion. The Fischer-Tropsch reaction yield water as a product, and an increase in CO conversion leads to a rise in C_{5+} selectivity due to an elevated amount of water present at the catalyst surface.[21] It is therefore important to compare C_{5+} selectivity at the same conversion level.

Due to the large number of samples, Fischer-Tropsch synthesis was only run for a selection of catalysts. Std.1. and Std.2 were run in the synthesis for the comparison between these two and catalysts dried in the Parr-reactor. 12.110-Closed and 12.110-d.rep were chosen because they had the highest cobalt dispersions. 12.150-a was chosen to investigate how the temperature increase during drying affects the Fischer-Tropsch results. All catalysts obtained 50 % CO conversion. In addition, all catalysts, without 12.150-a, reached 25 % or higher CO conversion with a syngas flow of 250 Nml/min. The results are presented in Table 17.

Table 17: Results obtained from the Fischer-Tropsch synthesis after 48 hours on stream

Catalyst	Dispersion [%]	Surface area [m²/g]	Degree of reduction [%]	CO conversion [%]	C_{5+} selectivity [%]	TOF * 10^{-2} [s^{-1}]	Rate * 10^{-2} [molCO/g*h]	d(Co⁰)corr. [nm]
12.110-Closed	8.9	56	68	51	83.6	5.30	3.46	7.4
Std.2	8.3	42	66	51	84.0	4.95	3.02	7.6
12.110-d.rep	8.3	54	65	52	83.5	5.71	3.48	7.5
Std.1	7.8	52	59	50	83.5	5.33	3.04	7.3
12.150-a	6.8	45	55	53	83.4	4.50	2.24	7.7

Table 17 shows the initial data obtained after 48 hours on stream. All catalysts display similar TOF values, as shown in Table 17. The TOF values are based on hydrogen chemisorption

results, and it is believed that the dispersion results are reliable. It can be seen that TOF does not change to any large extent, as expected.
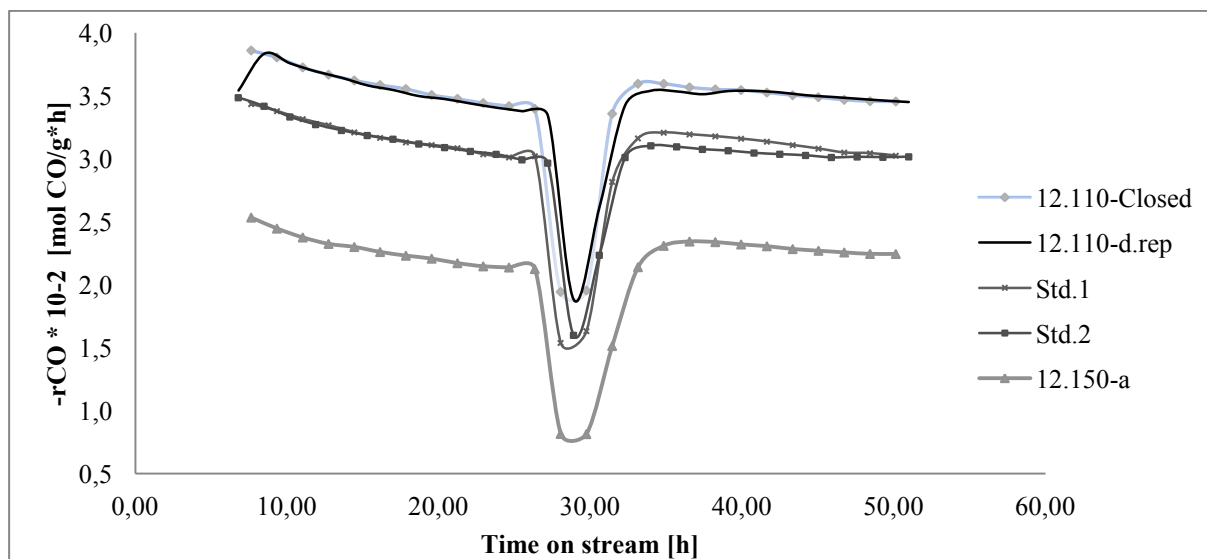
4.3.1 Catalytic activity

Figure 28: Rate as a function of time on stream for the different catalysts tested

The activity results in Figure 28 are as expected. All catalysts run in the FTS have almost the same dispersion, and results obtained from the oxygen titration measurement indicate that the degree of reduction for all catalysts was equal. 12.150-a has a lower activity due to a lower dispersion (and degree of reduction). The decrease in rate after 30 hours on stream is caused by adjustment of the syngas flow in order to reach 50 % CO conversion. It was assumed that there were no transport restrictions imposed by pore sizes in either experiments.

From the literature, it is found that higher CO conversion apparently leads to a more rapid deactivation.[14] In this case the deactivation happens more rapidly in the beginning. It is believed that the deactivating rate flattens out after a certain time and reaches steady-state. The figure shows that the CO conversion for 12.110-d.rep is almost constant between 34 to 50 hours on stream.

Deactivation of the catalysts may be a result of cluster growth by diffusion. This will lead to fewer active sites. Another possibility could be deactivation by dissociative adsorption of CO. This will lead to carbon deposits, which may block the available pores and lead to a decrease in adsorption capacity. Deactivation could also happen by reoxidation of the highly dispersed

phase experiencing strong support interactions or by loss of active metal leaving with the product stream.

4.3.2 Selectivity

Figure 29: Effect of the CO conversion on the C_{5+} selectivity for the catalysts at 210 ^{o}C, 20 bar and $H_2/CO = 2.1$

Figure 29 displays the trend of increased C_{5+} selectivity due to an increase in CO conversion. More water will be formed by the Fischer-Tropsch reaction with an increase in CO conversion. It is known that the water concentration level is important for the C_{5+} selectivity, and a rise in C_{5+} selectivity may be due to an elevated amount of water present at the catalyst surface.[21] In this work, the experimental conversion was almost identical for all the catalysts.

Figure 30: C$_{5+}$ selectivity as a function of time on stream for the different catalysts tested

Figure 30 shows that the C$_{5+}$ selectivity for all catalysts decreases with time on stream. As mentioned earlier, the flow rate of each experiment was the same in the beginning for all experiment, leading to a lower CO conversion for 12.150-a compared to the rest. The flow rate was adjusted to reach 50 % CO conversion after 30 hours on stream. According to the characterization results, the catalysts are very much alike. This is verified in the figure.

FTS results shows that all catalysts were active during the synthesis and managed to reach a high C$_{5+}$ selectivity. Catalysts dried at 110 ^{o}C in the Parr-reactor shows a slight higher activity compared to the two catalysts dried in the air furnace and 12.150-a, dried at 150 ^{o}C. Apparently, catalyst preparation in the Parr-reactor has the potential of making good FT catalysts. However, a better temperature control during drying in the reactor is required. It has been shown that treatment in a closed reactor system is able to enhance the catalyst properties, and more catalysts need to be hydrothermal treatment in order to state this effect. If the leakage was not discovered, then more experiments could have been run in a closed reactor system.

5   Further work

It has been shown that it was difficult to maintain a good temperature control during drying in the Parr-reactor. The temperature control in the Parr-reactor has to be optimized if any of these experiments are going to be repeated. A possible scenario could be to run only the support material in the reactor in order to record the temperature behaviour. This could give an indication of how the temperature behaves during drying of a solid catalyst, and will make the comparison easier. In addition, evaporation of pure water in the Parr-reactor could give an indication about the temperature behaviour during the evaporation.

It has been indicated that catalysts containing water after drying have higher surface areas and dispersions compared to dry catalysts. In this thesis, higher dispersions and surface areas could be a result of different reactor conditions during drying and not only present of water. More investigations are needed in order to determine the whole effect.

There could be an indication that catalysts treated in a closed reactor system contain better catalyst properties. It would have been interesting to treat more catalysts in a closed reactor system at different temperatures and durations.

6   Conclusion

The effect of performing catalysts synthesis in an autoclave continuous stirred tank reactor has been studied at different conditions. The intention was to dry each catalyst in the reactor for three hours and with a stirring rate of 100 rates per minutes. The stirring rate was adjusted to 200 rpm, and duration varied within 30 minutes to three hours during drying in the reactor.

It was difficult to maintain a constant set temperature in the reactor, due to evaporation of water and decomposition of nitrate. Apparently, catalysts not considered dry after drying contained a higher surface area and higher dispersion compared to "dry" catalysts. The majority of catalysts were dry after treatment in the reactor.

It was somewhat difficult to interpret the results based on one particular parameter in the reactor, because the whole reactor system affects the catalyst during drying. However, the results provide an indication of how the different parameters affect the catalysts.

A decrease in both surface area and dispersion were observed upon higher drying temperatures in the reactor. A low drying temperature in the reactor is promising, but is not suitable for calcination. A decrease in both surface area and dispersion was found when 18 wt.% was added to the catalyst.

Three catalysts were dried in a closed or a combination of a closed and open reactor system. One of these catalysts had the highest dispersion and surface area. Treatment in a closed reactor system is promising for making catalysts with good properties.

Two catalysts were dried with exact same drying procedure. The results from the characterisation showed that it was possible to reproduce this catalyst.

A total of five catalysts were run in the Fischer-Tropsch synthesis. The results obtained from the Fischer-Tropsch synthesis shows that all catalysts were active during the synthesis and managed to reach a high C_{5+} selectivity. This shows that it was possible to use an autoclave continuous stirred tank reactor for preparing active Fischer-Tropsch catalysts.

References

1. Borg, Ø., et al., *Fischer–Tropsch synthesis over< i> γ</i>-alumina-supported cobalt catalysts: Effect of support variables.* Journal of Catalysis, 2007. **248**(1): p. 89-100.

2. Van de Loosdrecht, J., et al., *Calcination of Co-based Fischer–Tropsch synthesis catalysts.* Topics in Catalysis, 2003. **26**(1): p. 121-127.

3. Lee, S.Y. and R. Aris, *The distribution of active ingredients in supported catalysts prepared by impregnation.* Catalysis Reviews Science and Engineering, 1985. **27**(2): p. 207-340.

4. Kowalski, S.J., *Toward a thermodynamics and mechanics of drying processes.* Chemical engineering science, 2000. **55**(7): p. 1289-1304.

5. Borg, Ø., et al., *Effect of calcination atmosphere and temperature on γ-Al 2 O 3 supported cobalt Fischer-Tropsch catalysts.* Topics in Catalysis, 2007. **45**(1): p. 39-43.

6. ExxonMobil, *Preparation og high activity cobalt catalysts, the catalyst and their use.* 2010: US. p. WO 2010/011333.

7. ExxonMobil, *Hydrolytical decomposing intermediate material.* 2009: US. p. WO 2010/011333.

8. Company, P.I. *Stirred Reactor & Pressure Vessels homepage.* 2012 22.05.2012]; Available from: http://www.parrinst.com/.

9. Suchanek, W.L., *Hydrothermal Synthesis of Alpha Alumina (α-Al2O3) Powders: Study of the Processing Variables and Growth Mechanisms.* Journal of the American Ceramic Society, 2010. **93**(2): p. 399-412.

10. Zhang, J., et al., *Chemical treatment of [gamma]-Al2O3 and its influence on the properties of Co-based catalysts for Fischer-Tropsch synthesis.* Applied Catalysis A: General, 2003. **243**(1): p. 121-133.

11. Yoshimura, M. and K. Byrappa, *Hydrothermal processing of materials: past, present and future.* Journal of Materials Science, 2008. **43**(7): p. 2085-2103.

12. van Breejen, J.p., *Cobalt Particle Size Effects in Catalysis.* Doctorial Thesis 2010. **University Utrecht**.

13. Bezemer, G.L., et al., *Cobalt particle size effects in the Fischer-Tropsch reaction studied with carbon nanofiber supported catalysts.* Journal of the American Chemical Society, 2006. **128**(12): p. 3956-3964.

14.   Borg, Ø., *Role of Alumina Support in Cobalt Fischer-Tropsch Synthesis.* Doctorial Thesis, 2007.

15.   Moodley, D.J., *On the deactivation of cobalt-based Fischer–Tropsch synthesis catalysts.* Thesis, 2008(november).

16.   Wang, W.J. and Y.W. Chen, *Influence of metal loading on the reducibility and hydrogenation activity of cobalt/alumina catalysts.* Applied catalysis, 1991. **77**(2): p. 223-233.

17.   Morales, F. and B.M. Weckhuysen, *Promotion effects in co-based Fischer-Tropsch catalysis.* Catalysis, 2006. **19**: p. 1-40.

18.   Li, J., et al., *Fischer-Tropsch synthesis: effect of small amounts of boron, ruthenium and rhenium on Co/TiO2 catalysts.* Applied Catalysis A: General, 2002. **223**(1-2): p. 195-203.

19.   Storsæter, S., et al., *Study of the effect of water on Fischer–Tropsch synthesis over supported cobalt catalysts.* Journal of Catalysis, 2005. **231**(2): p. 405-419.

20.   Bertole, C.J., C.A. Mims, and G. Kiss, *Support and rhenium effects on the intrinsic site activity and methane selectivity of cobalt Fischer–Tropsch catalysts.* Journal of Catalysis, 2004. **221**(1): p. 191-203.

21.   Borg, Ø., et al., *The Effect of Water on the Activity and Selectivity for γ-Alumina Supported Cobalt Fischer–Tropsch Catalysts with Different Pore Sizes.* Catalysis letters, 2006. **107**(1): p. 95-102.

22.   Fischer, N., *Preparation of nano and ångstøm sized cobalt ensembles and their performance in the Fischer-Tropsch synthesis.* Doctorial Thesis, 2011.

23.   Wang, X., *Advanced natural gas engineering*. 2009, Gulf publishing company: Houston Texas. p. 262-283.

24.   Moilijn, J.A., M. Makkee, and A. van Diepen, *Chemical Process Technology*. 2008: Chichester: John Wiley & Sons Ltd.

25.   Ojeda, M., et al., *CO activation pathways and the mechanism of Fischer–Tropsch synthesis.* Journal of Catalysis, 2010. **272**(2): p. 287-297.

26.   Holmen, A., *Heterogen katalyse*. 2010, Trondheim: IKP NTNU.

27.   Rønning, M. *Fischer-Tropsch synthesis kinetics*. in *Lecture notes in TKP4155*. 2010.

28.   University, S.H. *Gas Chromatography*.   05.06.2012]; Available from: http://teaching.shu.ac.uk/hwb/chemistry/tutorials/.

29.   Greibrokk, T., et al., *KROMATOGRAFI, seperasjon og deteksjon*. 3 ed. 1994, Oslo: Universitetsforlaget.

30.   Niemantsverdriet, J.W. and I. Chorkendorf, *Consepts of Modern Catalysis and Kinetics*. 2 ed. 2007: WILEY-VCH.

31.   Øye, G. *Van der Waals forces*. 2010: TKP 4115.

32.   Ramachandran, V.S. and J.J. Beaudoin, *Handbook of analytical techniques in concrete science and technology*. 2001: William Andrew Publishing/Noyes.

33.   Hiementz, P.C. and R. Rajagopala, *Principles of Colloid and Surface Chemistry*. 3 ed. 1997, New York: Marcel Dekker Inc., .

34.   Webb, P.A. and C. Orr, *Analytical methods in fine particle technology*. 1 ed. 1997, Norcross: Micrometerics instrument corporation.

35.   Rønning, M. *Kinetics 1: Adsorption*. in *lecture notes in TKP4155*. 2010.

36.   Jones, R.D. and C.H. Bartholomew, *Improved Flow Technique for Measurement of Hydrogen Chemisorption on Metal Catalysts*. Applied Catalysis, 1988. **39**: p. 77 - 88.

37.   Blekkan, E.A. *Basics*. in *Lecture notes in TKP 4515*. 2011.

38.   Øye, G. *Adsorption at gas-solid interfaces*. in *lecture notes in TKP 4115,*. 2011.

39.   Yang, R.T., *Adsorbents: Fundamentals and applications*. 2003: John Wiley & sons. Inc.

40.   Micromeritics. *AutoChem II 2920 TECHNIQUE Pulse Chemisorption Analysis*. 2012 15.05.2012]; Available from: http://www.micromeritics.com/Repository/Files/Autochem%20II%202920%20technique%20Pulse%20Chemisorption%20analysis.pdf

41.   Mansour, S.A.A., *Spectrothermal studies on the decomposition course of cobalt oxysalts Part II. Cobalt nitrate hexahydrate*. Materials chemistry and physics, 1994. **36**(3-4): p. 317-323.

42.   El-Shobaky, G.A., G.A. Fagal, and A.M. Dessouki, Egyptian J. Chem, 1988. **41**: p. 317.

43.   Borg, Ø., et al., *Identification of cobalt species during temperature programmed reduction of Fischer-Tropsch catalysts*. Studies in surface science and catalysis, 2007. **163**: p. 255-272.

44.   de la Osa, A., et al., *FTS fuels production over different Co/SiC catalysts.* Catalysis Today, 2012.

Appendix

Appendix A: Calculations

A.1 Water absorptivity

When metals are impregnated upon a support by the incipient wetness method, a mixture of metal nitrate dissolved in water is thoroughly homogenized with the sample being impregnated. Water absorptivity (ml/g) is a measure on how much amount of water is needed to obtain the point of incipient wetness. The water absorptivity is found by weighing out a small amount of support (minimum 2 grams) in a bowl and adding water drop wise until total capillary condensation is achieved. The total amount of water needed to reach the incipient wetness point for a given support can be calculated from Eq. (A.1.1)

$$m_{H_2O} = \left(\frac{m_{H_2O_{abs.}}}{m_s}\right) * m_s \tag{A.1.1}$$

where
$m_{H_2O_{abs.}}$ is the weight of water needed to achieve the point of incipient wetness
m_s is the weight of the support
$\frac{m_{H_2O_{abs.}}}{m_s}$ is measured water absorptivity

A.2 Metal nitrate hydrate needed for impregnation

Eq. (A.2.1) was used in order to determine the amount of metal hydrate needed to obtain the desired weight fraction of that specific metal in the support.

$$m_{metal\ nitrate\ hydrate} = \frac{x_{metal}}{1-x_{metal}} * \frac{Mw_{metal\ nitrate\ hydrate}}{Mw_{metal}} * m_s \tag{A.2.1}$$

$m_{metal\ nitrate\ hydrate}$ is the weight if the metal nitrate needed to obtained the desired weight fraction of the metal, x_{metal}. Mw_{metal} and $Mw_{metal\ nitrate\ hydrate}$ is the molecular mass of the metal and metal nitrate hydrate, respectively. m_s is the weight of the support being impregnated.

The needed amount of $Co(NO_3)_2*6\ H_2O$ to a support (20g) to reach a loading of 12 wt% cobalt can be seen in Eq. (A.2.2)

$$m_{Mg(NO_3)_2*6H_2O} = \frac{0.12}{0.88} * \frac{292.03\frac{g}{mole}}{58.93\frac{g}{mole}} * 20g = 13.51g \tag{A.2.2}$$

21.67 g of $Co(NO_3)_2*6\ H_2O$ has to be weighed out in order to reach 18 wt.% cobalt loading.

A.3 Perrhenic acid needed for impregnation

Eq. (A.3.1) is applied to determine the amount of perrhenic acid (75-85 %) needed to obtain a catalyst loading of 0.5 wt.% rhenium.

$$m_{HReO_4} = \frac{x_{Re}}{(1-x_{Re})*0.775} * \frac{Mw_{perrhenic\ acid}}{Mw_{rhenium}} * m_S \qquad (A.3.1)$$

where m_{HReO_4} is the weight fraction of perrhenic acid needed to obtain the desired weight fraction of rhenium, x_{Re}. $Mw_{rhenium}$ and $Mw_{perrhenic\ acid}$ are the molecular mass of rhenium and perrhenic acid, respectively. m_s is the weight of the support being impregnated.

The amount of perrhenic acid needed to have a loading of 0.5 wt.% for a support weighing 20 grams is shown in Eq. (A.3.2)

$$m_{HReO_4} = \frac{0.005}{(1-0.005)*0.775} * \frac{251.21\frac{g}{mole}}{186.2\frac{g}{mole}} * 20g = 0.189g \qquad (A.3.2)$$

Table A.1 gives an overview over the molecular masses needed in the catalyst preparation procedure.

Table A.1: Relevant molecular masses used for the catalyst preparation

Compound	Molecular weight [g/mole]
Cobalt, Co	58.93
Rhenium, Re	186.2
$Co(NO_3)_2 * 6\ H_2O$	251.21
$HReO_4$	251.21

A.4 Cobalt metal particle size from hydrogen chemisorption

Cobalt metal particle sizes were estimated from the cobalt dispersion. The relation between cobalt dispersion and cobalt metal particle diameter for monodisperse spherical particles with a site density of 14.6 atoms/nm^2 is given by Eq. (A.4.1)

$$d(Co^0) = \frac{96}{D} \tag{A.4.1}$$

where d is the calculated cobalt metal particle diameter given in nm and D is the dispersion (%).

The cobalt metal particle size for the catalyst Std.1 with a dispersion of 7.8 % is

$$d(Co^0) = \frac{96}{7.8} = 12 \; nm$$

Calculated cobalt particle size for each catalyst is shown in Appendix C.

A.5 Cobalt metal particle size from oxygen titration

The degree of reduction is found by using the Eq. (A.5.1), as described in Section 3.2.4.1.

$$DOR = \frac{3}{2} * \frac{V_{O_2}}{V_{i.g}} * \frac{Mw_{Co}}{x_{Co}} \tag{A.5.1}$$

where V_{O_2} is the cumulative amount given from the instrument and $V_{i.g}$ is the ideal gas volume. Mw_{Co} is the molecular weight of cobalt and x_{Co} is the weight fraction of Co in the catalyst.

Cobalt metal particle size for some of the catalysts was corrected for degree of reduction. The corrected particle size was calculated after Eq. (A.5.2)

$$d_{Co} = \frac{96}{D} * DOR \tag{A.5.2}$$

where d is the calculated cobalt metal particle diameter given in nm, D is the dispersion(%) and DOR is the degree of reduction (%).

Calculated corrected cobalt metal particle sizes and the degree of reduction for the measured catalysts are presented in Table A.5.

Table A.5: The calculated cobalt metal particle size corrected by the degree of reduction from oxygen titration

Catalyst	Dispersion [%]	Cumulative amount [cm³/g STP]	Degree of reduction [%]	$d(Co^0)_{corr.}$ [nm]
Std.1	7.8	18.1	59	7.3
Std.2	8.3	20.1	66	7.6
12.110-d rep	8.3	19.7	65	7.5
12.110-Closed	8.9	20.7	68	7.4
12.150-a	6.8	16.6	55	7.7

The calculated degree of reduction for Std.1 is

$$DOR = \frac{3}{2} * \frac{18.1 \ \frac{cm^3}{g \ STP}}{22414 \ \frac{cm^3}{mole \ STP}} * \frac{58.93 \ \frac{g}{mole}}{0.12} * 100 \ \% = 59 \ \%$$

The corrected cobalt particle size for Std.1 becomes

$$d_{Co} = \frac{96}{7.8} * 0.59 = 7.3 \ nm$$

Appendix B: Additional results from the catalyst preparation

B.1   Temperature profile and drying curves

12 wt.% Co and 18 wt.% Co were impregnated on support (20g) and dried in an air furnace for three hours. The catalyst mixtures were weighted and stirred every 15.minutes the first hour and every 30.minutes the last two hours. The weight was then plotted against time. These curves are presented in Figure B.1.1 and B.1.2.
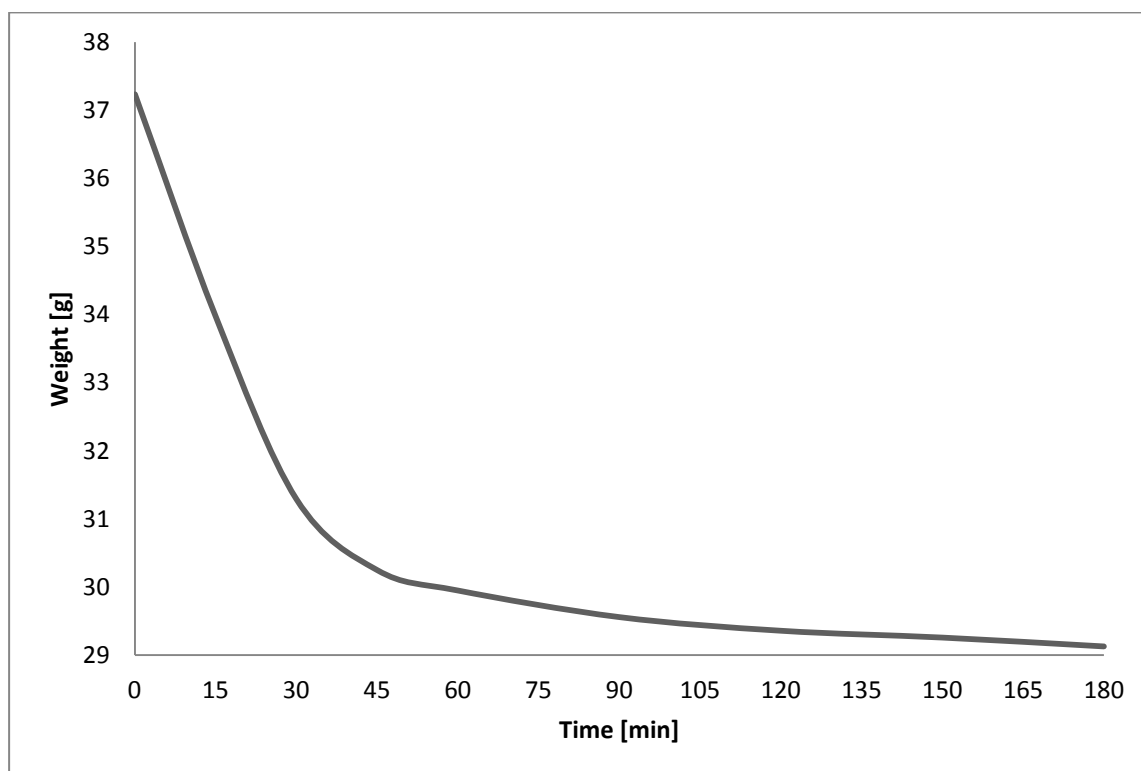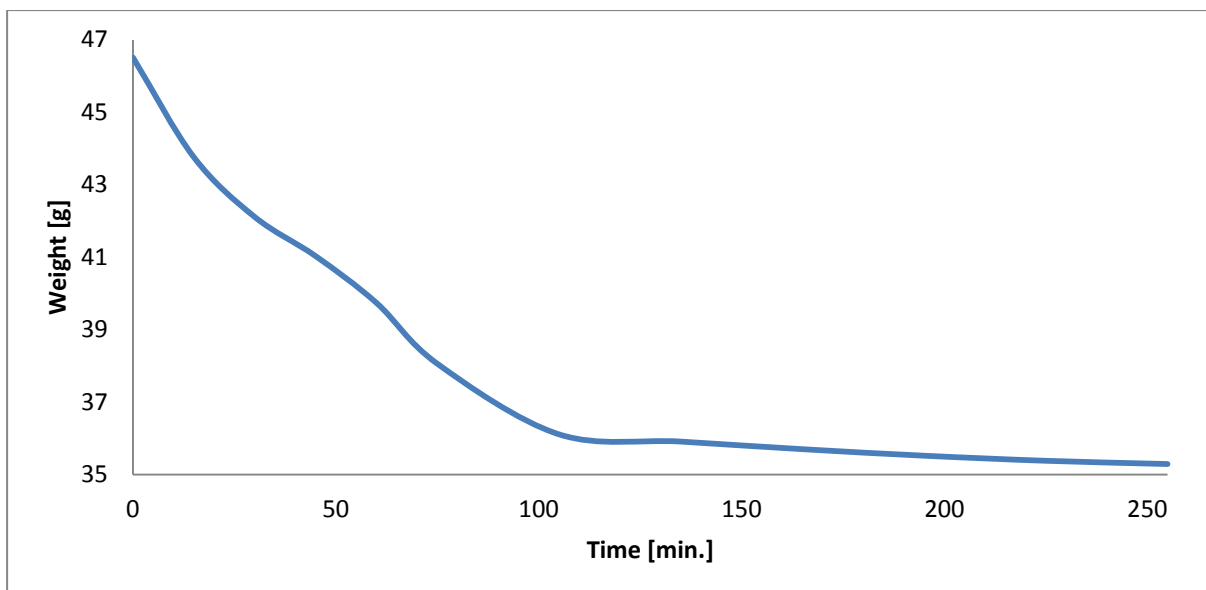

Figure B.1.1: Drying curve for 12 wt.% cobalt obtained from three hours in an air furnace for three hours

Figure B.1.2: Drying curve for 18 wt.% cobalt obtained from three hours in an air furnace for three hours

Table B.1.1 and B.1.2 display the weight after drying in the Parr-reactor of the catalyst containing 12 wt.% and 18 wt.% cobalt, respectively.

Table B.1.1: Overview over the measure weight after drying for catalysts impregnated with 12 wt.% cobalt and 0.5 wt.%

Catalysts	Weight after drying	Weight corresponding to number of minutes in the air furnace [min]	Dryness [%]
Catalyst dried for making the drying curves	29.13		100
12.110-c	29.32	132	73
12.110-d	30.38	43	24
12.110-d.rep	32.31	24	13
12.110-e	29.02		100
12.110-f	28.04		100
12.110-Closed	32.09	26	14
12.110-h	28.81		100
12.150-a	28.48		100
12.150-b	25.89		100
12.150-Closed	29.93	62	34
12.150-d	25.85		100
12.270-b	24.65		100
12.270-c	24.11		
12.110-C/O	30.30	44	24
Std.1	30.68	39	22

Table B.1.2: Overview over the measure weight after drying for catalysts impregnated with 18 wt.% cobalt and 0.5 wt.%

Catalysts	Weight after drying	Weight corresponding to number of minutes in the air furnace [min]	Dryness [%]
Catalyst dried for making the drying curves	35.29	60	33
18.110-a	39.73	54	30
18.110-b	40.24		
18.150-a	27.0		100
18.150-b	29.74		100
18.270-a	27.96		100
18.270-b	28.40		100

B.2   Temperature profiles during drying in the Parr-reactor

The temperature in the reactor was registered manually and at random intervals during each experiment. This appendix presents the observed temperature during all experiment together with extensive tables. The catalysts are organized after the desired set temperature during drying, i.e. 110, 150 and 270 ^{o}C.

B.2.1   110 ^{o}C

Observed temperatures for catalysts dried for less than 3 hours are shown in Figure B.2.1. The black line represent 18.110-a, containing 18 wt.% cobalt and 0.5 wt.% rhenium.
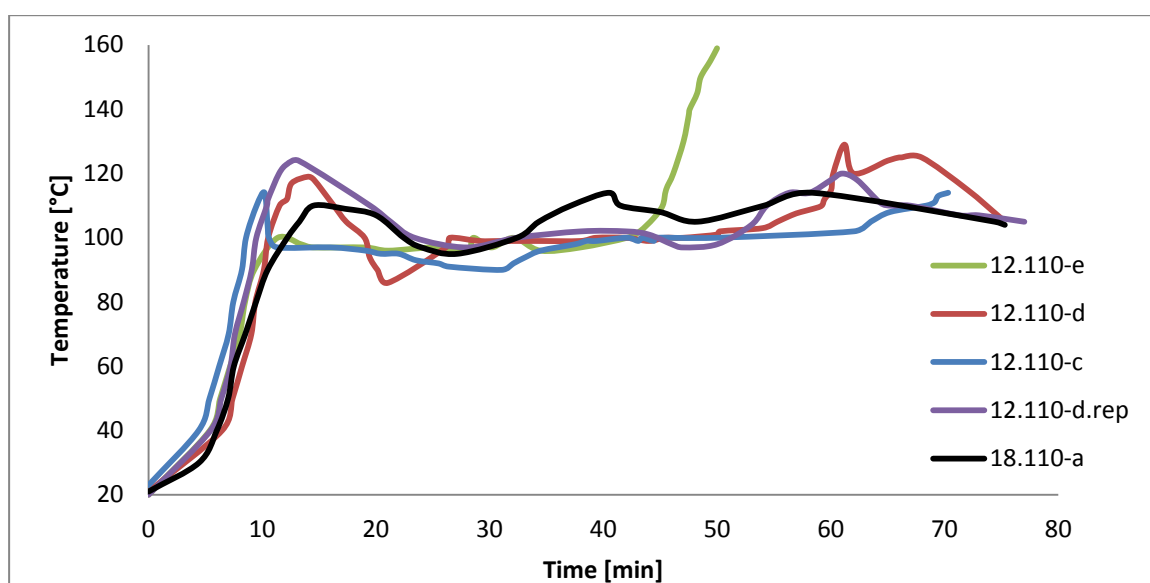

Figure B.2.1.1: Observed temperatures during experiments for catalysts with a set temperature of 110 ^{o}C run for less than three hours

Observed temperatures for catalysts dried for 3 hours are shown in Figure B.2.1.2. The black line represent 18.110-b, containing 18 wt.% cobalt and 0.5 wt.% rhenium.
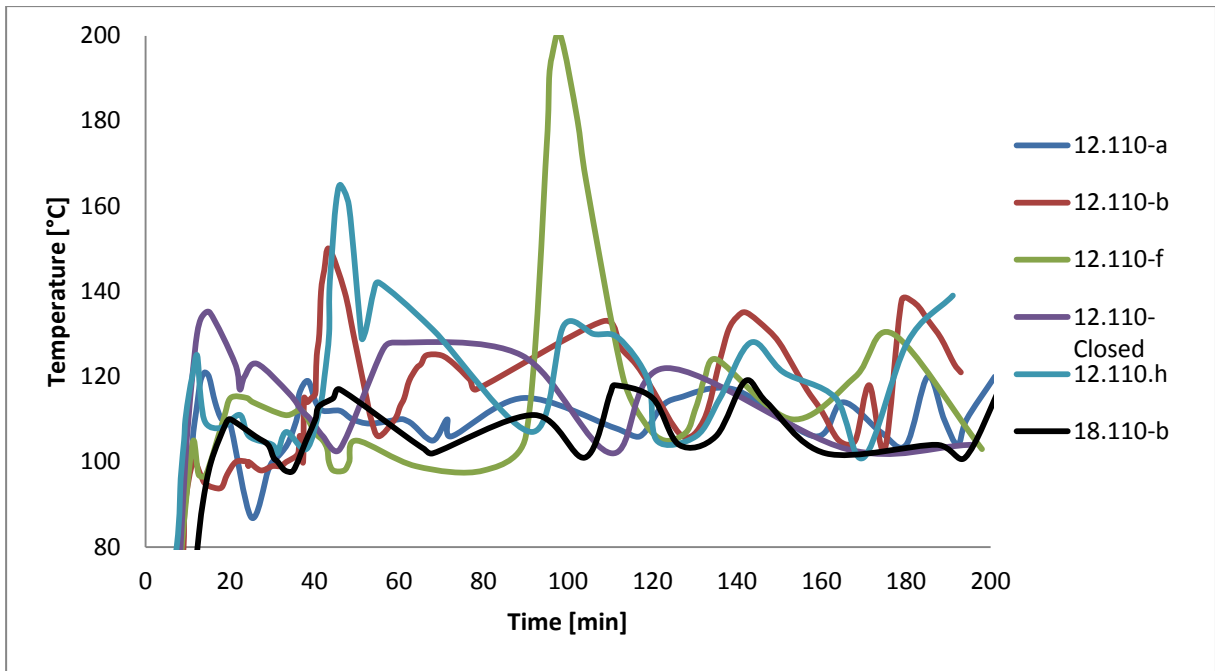
Figure B.2.1.2: Observed temperatures during experiments for catalysts with a set temperature of 110 °C run for three hours

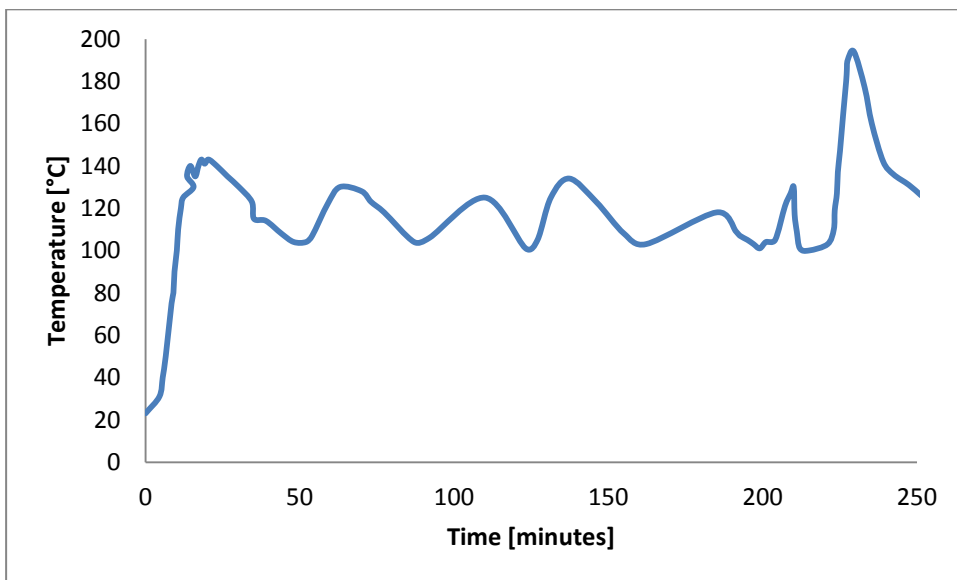Figure B.2.1.3 shows the registered temperature behaviour in the Parr-reactor for catalyst 12.110-C/O.

Figure B.2.1.3: Observed temperatures during drying of 12.110-C/O

Table B.2.2. displays the highest observed temperatures for catalysts dried in the Parr-reactor with a set temperature of 150 ℃.

Table B.2.2: An overview over the highest observed temperature during drying for catalysts with a set temperature of 150 ℃

Catalyst	Highest observed temperature [℃]
12.150-a	180
12.150-b	216
12.150-Closed	170
12.150-d	267
18.150-a	227
18.150-b	184

The temperature behaviour for these catalysts during drying is shown in Figure B.2.2.

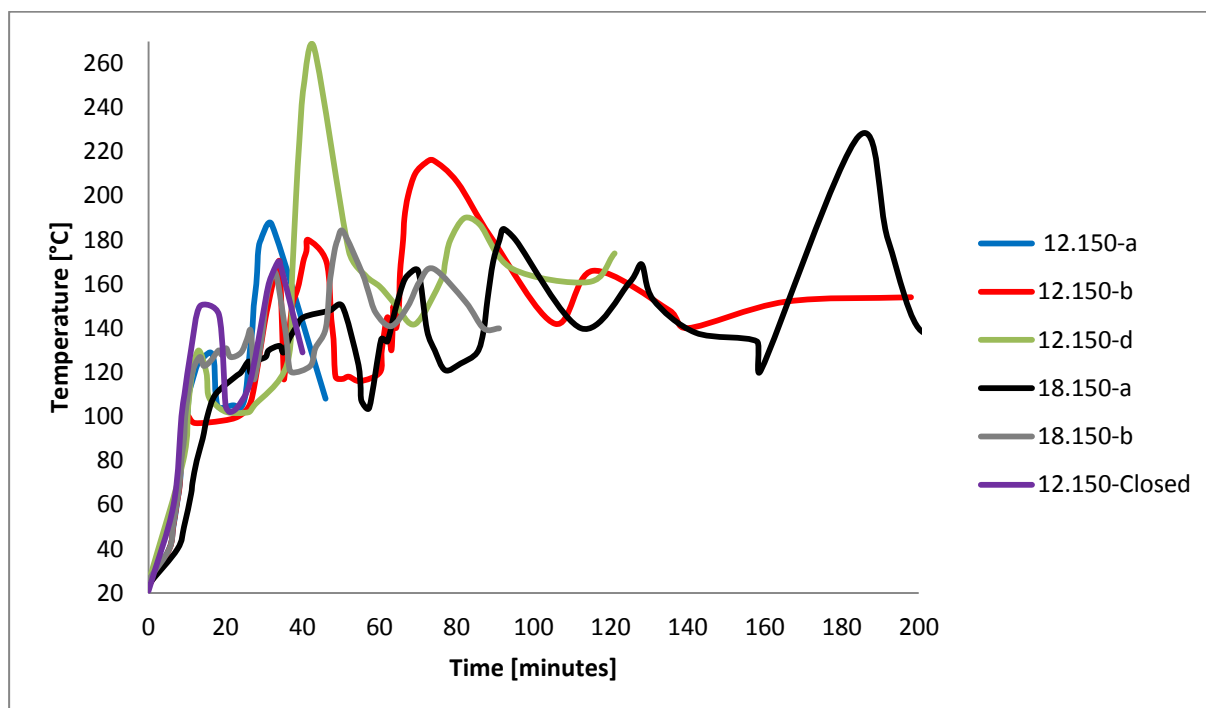**Figure B.2.2.: Observed temperatures during experiments for catalysts with a set temperature of 150 ℃**

B.2.3   270 °C

A table based on highest observed temperatures for catalysts dried in the Parr-reactor with a set temperature of 270 °C are shown in Table B.2.3.

Table B.2.3: An overview over the highest observed temperature during drying for catalysts with a set temperature of 270 °C

Catalyst	Highest observed temperature [°C]
12.270-a	345
12.270-b	325
12.270-c	341
18.270-a	274
18.270-b.a	274
18.270-b.b	274

The temperature behaviour for these catalysts during drying is shown in Figure B.2.3.

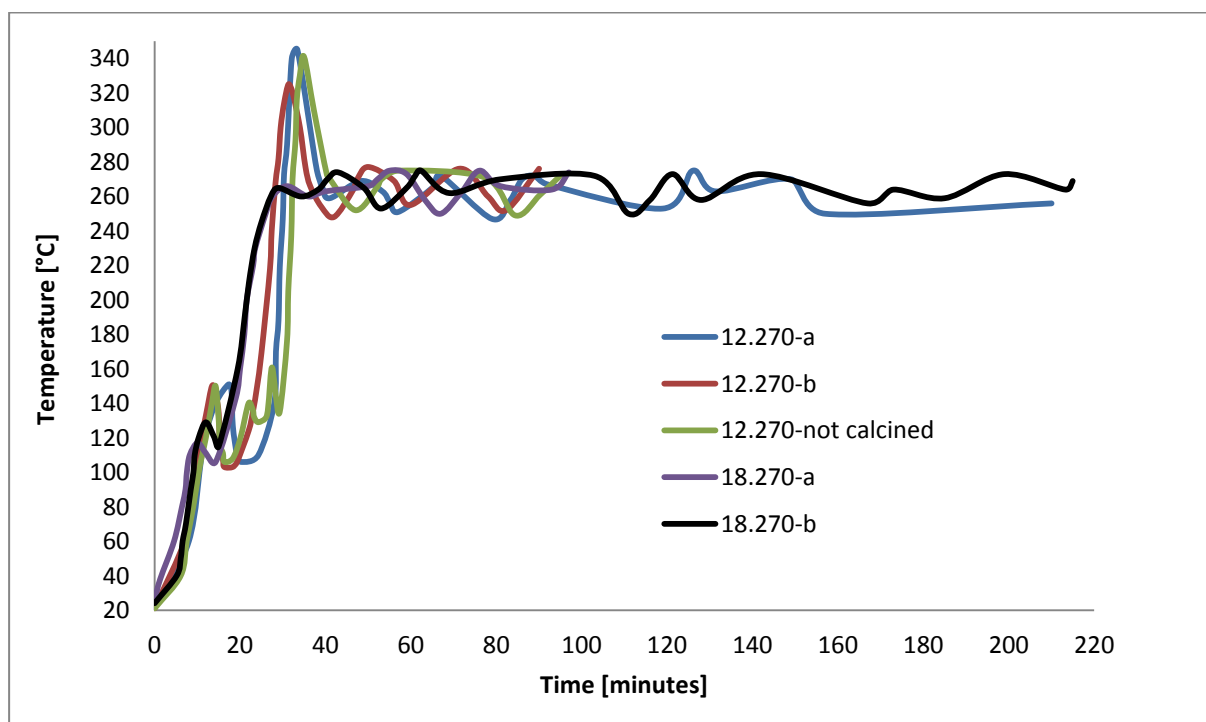**Figure B.2.3: Observed temperatures during experiments for catalysts with a set temperature of 270 °C**

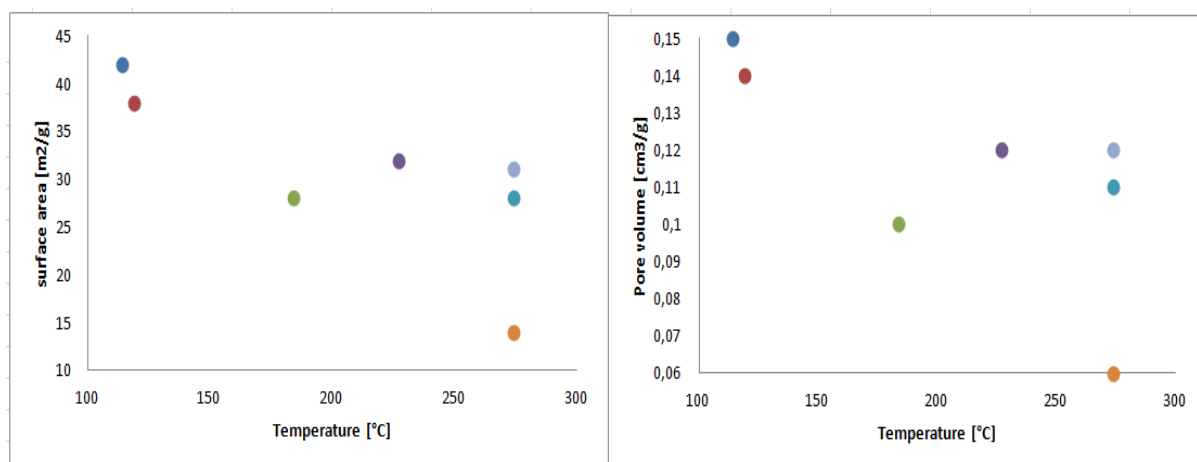# Appendix C: (Additional) results from the catalyst characterization

C.1 Nitrogen adsorption/desorption analysis

Results from the nitrogen adsorption/desorption analysis are shown in Table C.1.

Table C.1: An overview over the result obtained from the nitrogen adsorption/desorption analysis

Catalyst	Surface area [m^2/g]	Pore volume [cm^3/g]	Pore size [nm]
12.110-a	45	0.16	12.1
12.110-b	47	0.18	12.2
12.110-c	43	0.16	12.2
12.110-d	49	0.18	11.9
12.110-d.rep	54	0.19	12.1
12.110-e	49	0.19	12.3
12.110-f	47	0.17	12.3
12.110-Closed	56	0.19	11.9
12.110-h	50	0.18	12.2
12.150-a	45	0.17	12.2
12.150-b	45	0.17	12.9
12.150-Closed	49	0.18	11.8
12.150-d	46	0.18	12.6
12.270-a	47	0.19	12.8
12.270-b	44	0.18	12.7
12.270-c	42	0.17	12.8
18.110-a	42	0.15	11.4
18.110-b	38	0.14	12.1
18.150-a	32	0.12	13.8
18.150-b	28	0.10	11.5
18.270-a	28	0.11	12.1
18.270-b.a	14	0.06	14.5
18.270-b.b	31	0.12	12.3
Std.1	52	0.19	12.4
Std.2	42	0.16	11.3
12.110-C/O a.a	48	0.17	12.3
12.110-C/O a.b	47	0.17	11.7
Support	53	0.26	13.9

C.1.2 The temperature effect

Figure C.1.2: Result from nitrogen adsorption/desorption - The temperature effect II

Figure C.1.2 shows the results from nitrogen desorption/desorption for catalysts containing 18 wt% Co. A connection between temperature and surface area can be observed in the figure. Apparently, higher temperatures lead to a decrease in surface area. Also a decrease in pore volume can be observed upon higher temperature.

C.2 Additional hydrogen chemisorption results

Results from the hydrogen chemisorption analysis are shown in Table C.2.

Table C.2: An overview over the result obtained from hydrogen chemisorption

| Catalyst	Dispersion [%]	Surface area (m^2/g sample)	Cobalt particle size [nm]
12.110-a	6.4	5.16	15
12.110-b	6.0	4.89	16
12.110-c	5.7	4.65	17
12.110-d	7.8	6.36	12
12.110-d.rep	8.3	6.70	12
12.110-e	6.0	4.88	16
12.110-f	5.8	4.70	17
12.110-Closed	8.9	7.18	11
12.110-h	6.2	5.07	16
12.150-a	6.8	5.53	14
12.150-b	4.9	3.96	20
12.150-Closed	5.9	4.80	16
12.150-d	4.8	3.93	20
12.270-a	4.5	3.67	21
12.270-b	5.5	4.44	18
12.270-c	5.4	4.41	18
18.110-a	5.6	6.76	17
18.110-b	5.5	6.65	18
18.150-a	4.8	5.8	20
18.150-b	5.5	6.65	18
18.270-a	4.9	6.0	20
18.270-b.a	5.1	6.17	19
18.270-b.b	5.2	6.31	19
Std.1	7.8	6.29	12
Std.2	8.3	6.70	12
12.110-C/O-a.a	5.6	4.58	17
12.110-C/O-a.b	7.7	6.25	13
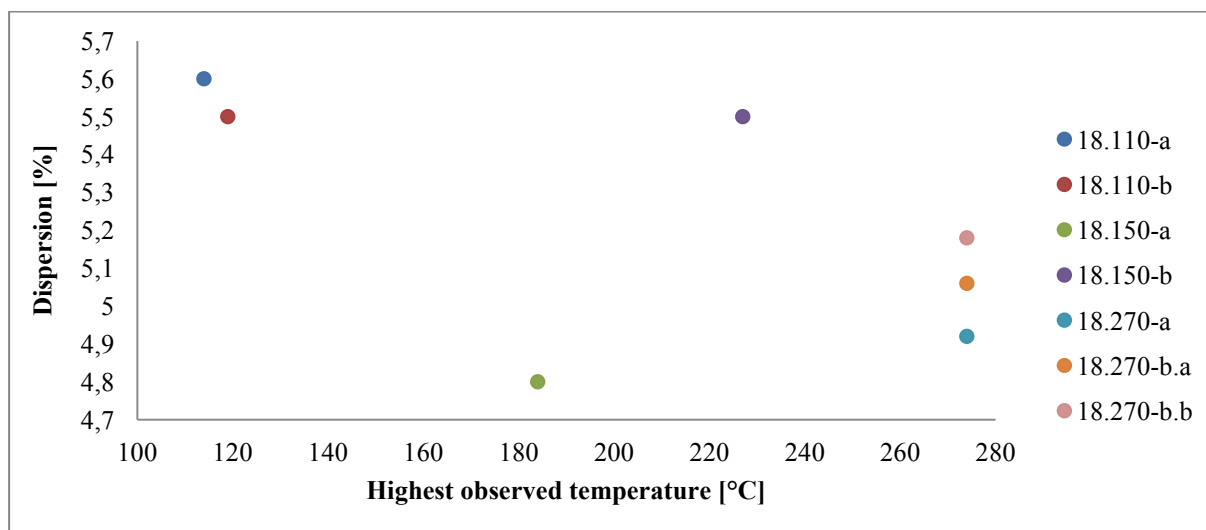
Figure C.2.1: Result from hydrogen chemisorption - The temperature effect II

Figure C.2.1 shows the results from hydrogen chemisorption for catalysts containing 18 wt% Co.

C.3 Addition results from the combination of nitrogen adsorption/desorption and hydrogen chemisorption analysis.
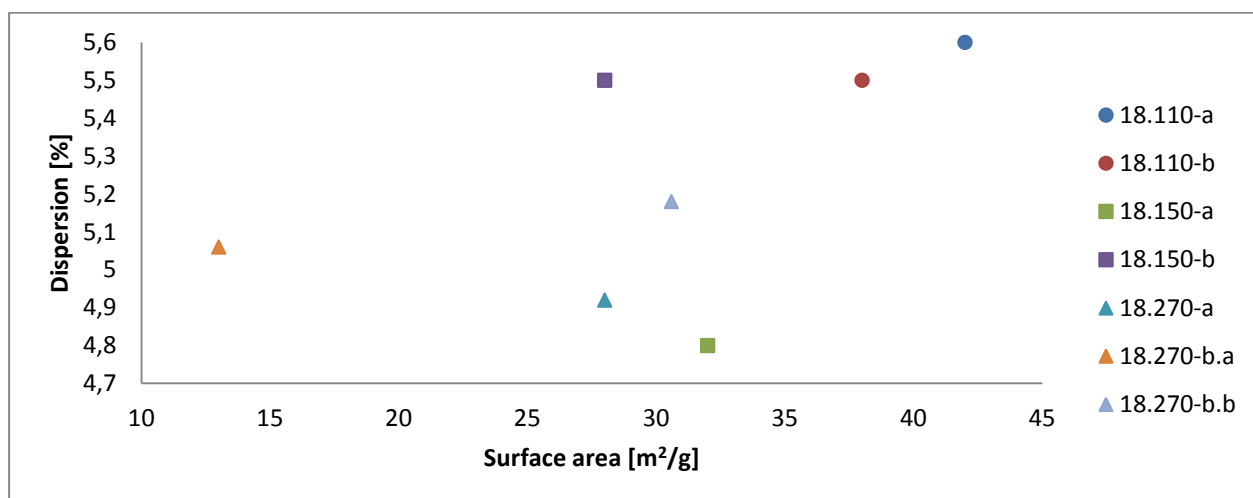
Figure C.3.1: Results obtained from both nitrogen adsorption/desorption and hydrogen chemisorption analysis for catalysts containing 18 wt.% Co and 0.5 wt.% Re

Dispersion plotted against measure surface areas for catalysts containing 18 wt.% cobalt and 0.5 wt.% rhenium are displayed in Figure C.3.1.

Figure C.3.2 shows the calculated cobalt particle size from hydrogen chemisorption plotted against pore diameter.
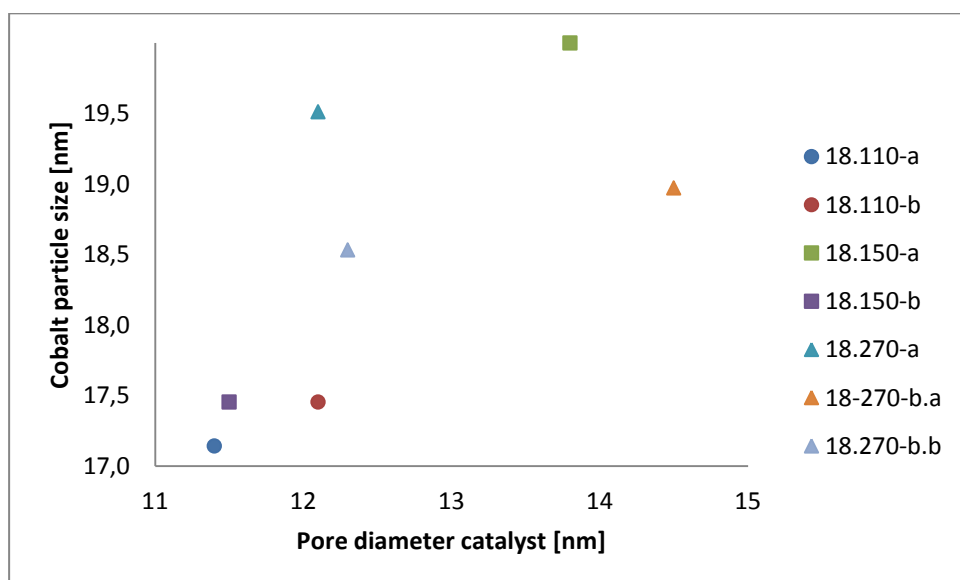
Figure C.3.2: Effect on the catalyst pore diameter on the cobalt particle size calculated from hydrogen chemisorption data

.

Appendix D: Risk Assessment

NTNU		Risikovurdering	Nummer	Dato
HMS	Hazardous activity identification process	HMS-avd.	HMSRV2601	
		Godkjent av	Side	Erstatter

Unit: _Kjemisk prosessteknologi_   **Date:** 30.01.2012

Line manager: _Øyvind Gregersen_

Participants in the identification process (including their function): Nina Tung Gymild, Master student

Short description of the main activity/main process: Catalyst preparation and catalyst testing in Fischer-Tropsch synthesis

ID no.	Activity/process	Responsible person	Laws, regulations etc.	Existing documentation	Existing safety measures	Comment
1	Crushing of catalyst/support	NTG	The working environment act	Safety data sheet	Provide appropriate protection from fines,	Avoid inhalation of fines
2					use fume hood	
3	Impregnation	NTG	The working environment act	Safety data sheet	Lab coat, glasses, gloves, use in fume	Avoid skin contact and ingestion
4					hood	

No.	Process	NTG	Act	Document	PPE	Safety note
5	Surface area measurement	NTG	The working environment act	Safety data sheet	Glasses, special gloves	Avoid skin contact. Avoid inhalation. Liquid nitrogen
6	Calsination	NTG	The working environment act		Glasses	Avoid touching hot surfaces
7	Hydrothermal treatment	NTG	The working environment act	Safety sheet on apparatus	Glasses, gloves, special gloves	Avoid touching hot surfaces, high pressure
8	Dispersion measurement	NTG	The working environment act	Safety data sheet	Glasses, gloves	Avoid skin contact. Avoid inhalation.
10	Fischer-Tropsch syntesis	NTG	The working environment act	Apparatus card	Vents and gas detectors/alarms	Leave area if alarms og off
11	Fischer-Tropsch syntesis	NTG	The working environment act	Apparatus card	Emergency stop button	
12	Fischer-Tropsch syntesis	NTG	The working environment act	Apparatus card	Heat resistant gloves	
13	Fischer-Tropsch syntesis	NTG	The working environment act	Apparatus card	Pressure gauges	Be sure whether equipment is pressurized

Risk assessment

	Utarbeidet av	Nummer	Dato
	HMS-avd.	HMSRV260 3	04.02.201 1
	Godkjent av	Side	Erstatter
		2	

Unit: _Kjemisk prosessteknologi_   **Date:** 30.01.201

Line manager: _Øyvind Gregersen_

Participants in the identification process (including their function): _Nina Tung Gymild, Master student_

Signatures: NTG

ID no.	Activity from the identification process form	Potential undesirable incident/strain	Likelihood:	Consequence:				Risk value	Comments/status Suggested measures
			Likelihood (1-5)	Human (A-E)	Environment (A-E)	Economy / material (A-E)	Reputation (A-E)	Human	
1	Crushing of catalyst/support	Inhalation of fines	2	A	A	A	A	2A	
2									
3	Impregnation	Skin contact inhalation/ingestion of magnesium nitrate or aluminium nitrate	1	B	A	A	A	1B	
4									

5	Surface area measurement	frostbite	3	B	A	A	A	A	3A	
6	Calcination	Burns	1	A	A	A	A	A	1A	
7	Hydrothermal treatment	too high pressures, burns	2	A	A	A	A	A	2A	
8	Dispersion measurement		1	A	A	A	A	A	1A	
10	Fischer–Tropsch synthesis	Flammable and toxic gases	1	B	A	A	A	B	B1	
11	Fischer–Tropsch synthesis	Contact with electricity		A	A	A	A	A	A1	
12	Fischer–Tropsch synthesis	Contact with hot surfaces		A	A	A	A	A	A3	Gloves
13	Fischer–Tropsch synthesis	Equipment under high pressure		B	A	A	A	A	B2	

Likelihood, e.g.:

1. Minimal
2. Low
3. Medium
4. High
5. Very high

Consequence, e.g.:

A. Safe
B. Relatively safe
C. Dangerous
D. Critical
E. Very critical

Risk value (each one to be estimated separately):
Human = Likelihood x Human Consequence
Environmental = Likelihood x Environmental consequence
Financial/material = Likelihood x Consequence for Economy/materiel

Potential undesirable incident/strain

Identify possible incidents and conditions that may lead to situations that pose a hazard to people, the environment and any material/equipment involved.

Criteria for the assessment of likelihood and consequence in relation to fieldwork

Each activity is assessed according to a worst-case scenario. Likelihood and consequence are to be assessed separately for each potential undesirable incident. Before starting on the quantification, the participants should agree what they understand by assessment criteria:

Likelihood	Minimal 1	Low 2	Medium 3	High 4	Very high 5
	Once every 50 years or less	Once every 10 years or less	Once a year or less	Once a month or less	Once a week

Consequence				
E Very critical	May produce fatality/ies	Very prolonged, non-reversible damage	Shutdown of work >1 year.	
D Critical	Permanent injury, may produce serious serious health damage/sickness	Prolonged damage. Long recovery time.	Shutdown of work 0.5-1 year.	
C Dangerous	Serious personal injury	Minor damage. Long recovery time	Shutdown of work < 1 month	
B Relatively safe	Injury that requires medical treatment	Minor damage. Short recovery time	Shutdown of work < 1week	
A Safe	Injury that requires first aid	Insignificant damage. Short recovery time	Shutdown of work < 1day	

The unit makes its own decision as to whether opting to fill in or not consequences for economy/material, for example it the unit is going to use particularly valuable equipment. It is up to the individual unit to choose the assessment criteria for this column

Risk = Likelihood x Consequence

Please calculate the risk value for "Human", "Environment" and, if chosen, "Economy/material", separately.

About the column **"Comments/status, suggested preventative and corrective measures":**
Measures can impact on likelihood and consequences. Priorities measures both that can prevent the incident from occurring; in other words, likelihood-reducing measures are to be priorities above greater emergency preparedness, i.e. consequence-reduction measures.